National Library of Canada
Acquisitions and Bibliographic Services Branch
395 Wellington Street
Ottawa, Ontario
K1A 0N4

Bibliothèque nationale du Canada
Direction des acquisitions et des services bibliographiques
395, rue Wellington
Ottawa (Ontario)
K1A 0N4

Your file / Votre référence

Our file / Notre référence

NOTICE

The quality of this microform is heavily dependent upon the quality of the original thesis submitted for microfilming. Every effort has been made to ensure the highest quality of reproduction possible.

If pages are missing, contact the university which granted the degree.

Some pages may have indistinct print especially if the original pages were typed with a poor typewriter ribbon or if the university sent us an inferior photocopy.

Reproduction in full or in part of this microform is governed by the Canadian Copyright Act, R.S.C. 1970, c. C-30, and subsequent amendments.

AVIS

La qualité de cette microforme dépend grandement de la qualité de la thèse soumise au microfilmage. Nous avons tout fait pour assurer une qualité supérieure de reproduction.

S'il manque des pages, veuillez communiquer avec l'université qui a conféré le grade.

La qualité d'impression de certaines pages peut laisser à désirer, surtout si les pages originales ont été dactylographiées à l'aide d'un ruban usé ou si l'université nous a fait parvenir une photocopie de qualité inférieure.

La reproduction, même partielle, de cette microforme est soumise à la Loi canadienne sur le droit d'auteur, SRC 1970, c. C-30, et ses amendements subséquents.

Canada

UNIVERSITY OF ALBERTA

FRICTIONAL FORCES IN BRACKET AND ARCHWIRE INTERACTIONS

BY

DARREN NEIL TKACH

©

A thesis submitted to the Faculty of Graduate Studies and Research in partial fulfilment of the requirements for the degree of MASTER OF SCIENCE

IN

CLINICAL SCIENCES (ORTHODONTICS)

DEPARTMENT OF DENTISTRY

EDMONTON, ALBERTA

FALL 1993

National Library of Canada
Acquisitions and Bibliographic Services Branch
395 Wellington Street
Ottawa, Ontario
K1A 0N4

Bibliothèque nationale du Canada
Direction des acquisitions et des services bibliographiques
395, rue Wellington
Ottawa (Ontario)
K1A 0N4

Your file Votre référence

Our file Notre référence

The author has granted an irrevocable non-exclusive licence allowing the National Library of Canada to reproduce, loan, distribute or sell copies of his/her thesis by any means and in any form or format, making this thesis available to interested persons.

L'auteur a accordé une licence irrévocable et non exclusive permettant à la Bibliothèque nationale du Canada de reproduire, prêter, distribuer ou vendre des copies de sa thèse de quelque manière et sous quelque forme que ce soit pour mettre des exemplaires de cette thèse à la disposition des personnes intéressées.

The author retains ownership of the copyright in his/her thesis. Neither the thesis nor substantial extracts from it may be printed or otherwise reproduced without his/her permission.

L'auteur conserve la propriété du droit d'auteur qui protège sa thèse. Ni la thèse ni des extraits substantiels de celle-ci ne doivent être imprimés ou autrement reproduits sans son autorisation.

ISBN 0-315-88408-8

Canada

UNIVERSITY OF ALBERTA

RELEASE FORM

NAME OF AUTHOR: Darren Neil Tkach

TITLE OF THESIS: Frictional Forces in Bracket and Archwire Interactions

DEGREE: Master of Science in Clinical Sciences (Orthodontics)

YEAR THIS DEGREE GRANTED: 1993

Permission is hereby granted to the University of Alberta Library to reproduce single copies of this thesis and to lend or sell such copies for private, scholarly or scientific research purposes only.

The author reserves all other publication and all other rights in association with the copyright in the thesis, and except as hereinbefore provided neither the thesis or any substantial portion thereof may be printed or otherwise reproduced in any material form whatever without the author's prior written permission.

280 Coachwood Point W.
Lethbridge, Alberta
T1K 6A2

DATE: September 02, 1993

UNIVERSITY OF ALBERTA

FACULTY OF GRADUATE STUDIES AND RESEARCH

The undersigned certify that they have read, and recommended to the Faculty of Graduate Studies and Research for acceptance, a thesis entitled FRICTIONAL FORCES IN BRACKET AND ARCHWIRE INTERACTIONS submitted by DARREN NEIL TKACH in partial fulfilment of the requirements for the degree of MASTER OF SCIENCE in CLINICAL SCIENCES (ORTHODONTICS).

Dr. P.W. Major

Dr. K.E. Glover

Dr. M.G. Faulkner

Dr. A.W. Lipsett

DATE: September 02, 1993

Dedication

I would like to dedicate this work to those individuals with whom I spent too little time during its completion: my wife, Jan; my son, Stephen; and my daughter, Rachel,

and to Vic and Ruby, my parents.

Abstract

The purpose of this investigation was to determine and compare frictional coefficients for various pairings of orthodontic bracket and archwire materials. This study determined the surface roughness of these archwires and related it to the frictional coefficients. The study examined electron micrographs of the brackets and archwires to provide an appreciation of microscopic surface characteristics.

The testing protocol involved sliding an archwire sample along a bracket sample while simultaneously measuring the force required to produce the sliding. This protocol repeated the sliding trials under conditions of varying load, contact area, lubrication, and with samples from several manufacturers. Nondestructive surface roughness testing provided information pertaining to archwire surface roughness.

The results indicated that frictional coefficients vary significantly depending on the archwire and bracket material, with titanium alloyed archwires and ceramic brackets offering increased friction compared to stainless steel alloyed archwires and stainless steel brackets. Varying loads had little effect on frictional coefficients. The effects of lubrication were variable, with the results showing some increased as well as decreased frictional coefficients. Smaller contact areas resulted in smaller frictional coefficients. Frictional coefficients varied widely when comparing similar materials from different manufacturers.

Acknowledgements

Many individuals deserve special recognition for the roles they played in the realization of this thesis, and my clinical orthodontic education. I would like to acknowledge the following:

My thesis committee chairman, Paul Major, and committee members Ken Glover and Gary Faulkner, for their time, knowledge and guidance;

Mechanical Engineering technical support personnel Mr T. Villet, and Mr. A. Muir and staff, for their knowledge and tireless assistance;

Statistician Terry Taerum, for direction through a bewildering array of statistics;

Electron Microscopist Dr. M. Chen, for time spent to create countless micrographs;

Orthodontic clinical staff members Dr. R. Mullen, Dr. M. Pawliuk, Dr. R. Haryett, and Dr. S. Alimchandani, for their invaluable contributions to my understanding of orthodontics,

Orthodontic support staff members Carol Gervais, Brigitte Klemp, Margaret McGillicuddy, and Maureen Dmytrash for their assistance and patience.

Table of Contents

Chapter 1		Introduction and Literature Review	1
	A.	Orthodontic Concerns	1
	B.	Overview of Friction	3
	C.	Review of Orthodontic Literature	6
	D.	Statement of Problem	12
	E.	Purpose of Study	12
	F.	Research Questions	13
	G.	Hypotheses	14
Chapter 2		Materials and Methods	18
	A.	Materials	
		1. Bracket and Archwire Test Samples	18
		2. Testing Apparatus	22
		3. Materials for Electron Micrograph Study	24
		4. Materials for Surface Roughness Study	24
	B.	Method	
		1. Method Utilized for Friction Testing	25
		2. Method Utilized for the Surface Roughness Study	30
		3. Method Utilized for Microscope Study	31
		4. Method Error	32
Chapter 3		Results	
	A.	Frictional Coefficient Testing	33
	B.	Surface Roughness Testing	50
	C.	Scanning Electron Micrographs	53
	D.	Method Error	53

Chapter 4		Discussion	54
	A.	Frictional Coefficients	54
		1. Normal Force	55
		2. Area of Contact	56
		3. Archwire and Bracket Type	57
		4. Dynamic verses Static Friction	60
		5. Lubrication	60
		6. Manufacturer Differences	62
	B.	Archwire Surface Roughness Relative to Frictional Coefficients	63
	C.	Archwire and Bracket Surface Roughness	64
	D.	Method Error	65
	E.	Clinical Implications	65
	F.	Limitations	67
	G.	Discussion of Hypotheses	68
Chapter 5		Conclusions	70
	A.	Suggestions for Further Study	71
		1. Other Sources of Friction	71
		2. Ion Implantation	71
Bibliography			74
Appendix A		Overview of Tribology	80
	A.	Historical Aspects of Friction	80
	B.	Surface Characteristics of Solids	82
	C.	Surface Interactions and Contact Mechanics	85
	D.	Frictional Interactions	91
	E.	Lubrication	99

Appendix B	Plates of Bracket and Archwire Samples	104
A.	Plates of Bracket Samples	104
B.	Plates of Archwire Samples	114
C.	Plates of Testing Apparatus	121
Appendix C	Statistical Analysis	123
A.	Results of Statistical Analysis	123
Appendix D	Frictional Force Calculation	158

List of Tables

		Page
Table 2.1	Description of Archwire Materials..	19
Table 2.2	Description of Bracket Materials..	20
Table 2.3	Description of Frictional Coefficient Experimental Variables..	28
Table 2.4	Description of Surface Roughness Experimental Variables..	29
Table 2.5	Identification Code for SEM Study..	31
Table 3.1	Frequencies - Dynamic and Static Frictional Coefficients for Varying Normal Forces (ceramic bracket,flat wire, unlubricated)..	37
Table 3.2	SNK Multiple Comparisons for Varying Normal Force (ceramic bracket, flat wire unlubricated)..	37
Table 3.3	Frequencies - Dynamic and Static Frictional Coefficients for Varying Normal Forces (steel bracket,flat wire, unlubricated)..	39
Table 3.4	SNK Multiple Comparisons for Varying Normal Force (steel bracket, flat wire unlubricated)..	39
Table 3.5	Frequencies - Static Frictional Coefficients for Various Archwires against Ceramic Bracket, Lubricated and Unlubricated (flat wire)..	41
Table 3.6	SNK Comparisons of Static Frictional Coefficients, Lubricated and Unlubricated, for Various Archwire Types (ceramic bracket, flat wire)..	41
Table 3.7	Frequencies - Static Frictional Coefficients for Various Archwires against Steel Bracket, Lubricated and Unlubricated (flat wire)..	43
Table 3.8	SNK Comparisons of Static Frictional Coefficients, Lubricated and Unlubricated, for Various Archwire Types (steel bracket, flat wire)..	43
Table 3.9	Frequencies - Static Frictional Coefficients for Various Archwire Types and Configurations against Ceramic bracket (unlubricated)..	45

Table 3.10	SNK Comparisons of Static Frictional Coefficients, Flat and Round Archwires, for Various Archwire Types (ceramic bracket, unlubricated)..	45
Table 3.11	Frequencies - Static Frictional Coefficients for Various Archwire Types and Configurations against Steel bracket (unlubricated)..	47
Table 3.12	SNK Comparisons of Static Frictional Coefficients, Flat and Round Archwires, for Various Archwire Types (steel bracket, unlubricated)..	47
Table 3.13	SNK Comparisons of Static Frictional Coefficients for Various Archwire Types against Ceramic and Steel Bracket (flat wire, unlubricated)..	48
Table 3.14	Frequencies - Static Frictional Coefficients for Various Archwire Types against Ceramic and Steel Bracket (flat wire, unlubricated)..	49
Table 3.15	Frequencies - Surface Roughness Values, in Micro-inches, for Various Archwire Types..	52
Table 3.16	SNK Comparisons of Surface Roughness for Various Archwire Types..	52
Table 3.17	Frequencies for Method Error Test..	53
Table 4.1	Force Losses due to Friction for Various Bracket-Archwire Combinations..	67
Table C.1	Frequencies - Dynamic and Static Frictional Coefficients for Varying Companies (ceramic bracket, flat wire, unlubricated)..	124
Table C.2	Frequencies - Dynamic and Static Frictional Coefficients for Varying Companies (steel bracket, flat wire, unlubricated)..	125
Table C.3	Frequencies - Dynamic and Static Frictional Coefficients under Varying Normal Forces (ceramic bracket, flat wire, unlubricated)..	126
Table C.4	SNK Multiple Comparisons of Frictional Coefficients for Varying Normal Force (ceramic bracket, flat wire, unlubricated)..	127
Table C.5	SNK Multiple Comparisons of Frictional Coefficients for Varying Normal Force (steel bracket, flat wire, unlubricated)..	127

Table C.6	Frequencies - Dynamic and Static Frictional Coefficients under Varying Normal Forces (steel bracket, flat wire, unlubricated)..	128
Table C.7	Frequencies - Dynamic Frictional Coefficients for Various Archwire Types, both Lubricated and Unlubricated (ceramic bracket, flat wire)..	130
Table C.8	Frequencies - Dynamic Frictional Coefficients for Various Archwire Types, both Lubricated and Unlubricated (steel bracket, flat wire)..	131
Table C.9	Frequencies - Static Frictional Coefficients for Heat Treatable Archwire on Varying Bracket Type (flat wire, unlubricated)..	133
Table C.10	Frequencies - Static Frictional Coefficients for NiTi Archwire on Varying Bracket Type (flat wire, unlubricated)..	134
Table C.11	Frequencies - Static Frictional Coefficients for Steel Archwire on Varying Bracket Type (flat wire, unlubricated)..	135
Table C.12	Frequencies - Static Frictional Coefficients for TMA Archwire on Varying Bracket Type (flat wire, unlubricated)..	136
Table C.13	SNK Comparisons Static of Frictional Coefficients for Heat Treatable Archwire against Various Ceramic and Steel Brackets (flat wire unlubricated)..	137
Table C.14	SNK Comparisons of Static Frictional Coefficients for NiTi Archwire against Various Ceramic and Steel Brackets (flat wire unlubricated)..	137
Table C.15	SNK Comparisons of Static Frictional Coefficients for Steel Archwire against Various Ceramic and Steel Brackets (flat wire unlubricated)..	138
Table C.16	One-way ANOVA Comparing Static Frictional Coefficients for TMA Archwire against Ceramic and Steel Brackets (flat wire, unlubricated)..	138
Table C.17	Frequencies - Static Frictional Coefficients for Various Archwire Types and Configurations (ceramic bracket, lubricated)..	140
Table C.18	Frequencies - Static Frictional Coefficients for Various Archwire Types and Configurations (steel bracket, lubricated)..	141

Table C.19	Frequencies - Static Frictional Coefficients for NiTi Archwire against Ceramic and Steel Brackets (flat wire, unlubricated)..	143
Table C.20	Frequencies - Static Frictional Coefficients for NiTi Archwire against Ceramic and Steel Brackets (flat wire, lubricated)..	144
Table C.21	One-way ANOVA of Static Frictional Coefficients for NiTi Archwire against A Company Ceramic and Steel Brackets (flat wire, unlubricated)..	145
Table C.22	One-way ANOVA of Static Frictional Coefficients for NiTi Archwire against A Company Ceramic and Steel Brackets (flat wire, lubricated)..	145
Table C.23	Frequencies - Static Frictional Coefficients for Various Archwires against Ceramic and Steel Bracket (Cerum, flat wire, unlubricated)..	146
Table C.24	Frequencies - Static Frictional Coefficients for Various Archwires against Ceramic and Steel Bracket (Cerum, flat wire, lubricated)..	147
Table C.25	SNK Comparisons of Frictional Coefficients for Various Archwires against Ceramic and Steel Brackets (Cerum, flat wire unlubricated)..	148
Table C.26	SNK Comparisons of Frictional Coefficients for Various Archwires against Ceramic and Steel Brackets (Cerum, flat wire lubricated)..	148
Table C.27	Frequencies - Static Frictional Coefficients for Various Archwires against Steel Bracket (Dentaurum, flat wire, unlubricated)..	149
Table C.28	Frequencies - Static Frictional Coefficients for Various Archwires against Steel Bracket (Dentaurum, flat wire, lubricated)..	150
Table C.29	One-way ANOVA of Static Frictional Coefficients for Dentaurum Steel Bracket against Steel and NiTi Archwires (flat wire, unlubricated)..	151

Table C.30 One-way ANOVA of Static Frictional Coefficients for Dentaurum Steel Bracket against Steel and NiTi Archwires (flat wire, lubricated).. 151
Table C.31 Frequencies - Static Frictional Coefficients for Various Archwires against Ceramic and Steel Bracket (Ormco, flat wire, unlubricated)..152
Table C.32 Frequencies - Static Frictional Coefficients for Various Archwires against Ceramic and Steel Bracket (Ormco, flat wire, lubricated).. 153
Table C.33 SNK Comparisons of Frictional Coefficients for Various Archwires against Ceramic and Steel Brackets (Ormco, flat wire unlubricated)..154
Table C.34 SNK Comparisons of Frictional Coefficients for Various Archwires against Ceramic and Steel Brackets (Ormco, flat wire lubricated).. 154
Table C.35 Frequencies - Static Frictional Coefficients for Various Archwires against Ceramic and Steel Bracket (RMO, flat wire, unlubricated).. 155
Table C.36 Frequencies - Static Frictional Coefficients for Various Archwires against Ceramic and Steel Bracket (RMO, flat wire, lubricated).. 156
Table C.37 SNK Comparisons of Frictional Coefficients for Various Archwires against Ceramic and Steel Brackets (RMO, flat wire unlubricated).. 157
Table C.38 SNK Comparisons of Frictional Coefficients for Various Archwires against Ceramic and Steel Brackets (RMO, flat wire lubricated).. 157

List of Figures

		Page
Fig. 1.1	Forces Encountered during Sliding..	3
Fig. 1.2	Bracket-Archwire Contact during Sliding..	5
Fig. 2.1	Friction Testing Apparatus: Stage Details..	21
Fig. 2.2	Friction Testing Apparatus..	23
Fig. 3.1	Representative Tracing Produced by Recording Equipment..	34
Fig. 3.2	Boxplot of Frictional Coefficient by Normal Force by Type of Friction for Ceramic Bracket (flat wire, unlubricated)..	36
Fig. 3.3	Boxplot of Frictional Coefficients by Normal Force by Type of Friction for Steel Bracket (flat wire, unlubricated)..	38
Fig. 3.4	Boxplot of Static Frictional Coefficients by Wire Type by Lubrication Mode for Ceramic Bracket (flat wire)..	40
Fig. 3.5	Boxplot of Static Frictional Coefficients by Wire Type by Lubrication Mode for Stainless Steel Bracket (flat wire)..	42
Fig. 3.6	Boxplot of Static Frictional Coefficients by Wire Type by Wire Configuration for Ceramic Bracket (unlubricated)..	44
Fig. 3.7	Boxplot of Static Frictional Coefficients by Wire Type by Wire Configuration for Steel Bracket (unlubricated)..	46
Fig. 3.8	Boxplot of Static Frictional Coefficients by Wire Type by Bracket Type (flat wire, unlubricated)..	49
Fig. 3.9	Scatter Diagram for Static Frictional Coefficients and Archwire Surface Roughness..	50
Fig. 3.10	Boxplot of Archwire Surface Roughness by Wire Type..	51
Fig. A.1	Surface Topography..	83
Fig. A.2	Theoretical Metal Surface..	84
Fig. A.3	Apparent and Real Area of Contact..	86
Fig. A.4	Junctional Growth Phenomenon..	90

Fig. A.5	Forces Encountered during Tangential Sliding..	93
Fig. A.6	Contact Under Boundary Lubrication..	101
Fig. C.1	Boxplot of Frictional Coefficient by Company by Type of Friction for Ceramic Bracket (flat wire, unlubricated)..	124
Fig. C.2	Boxplot of Frictional Coefficient by Company by Type of Friction for Steel Bracket (flat wire, unlubricated)..	125
Fig. C.3	Boxplot of Frictional Coefficient by Load by Type of Friction for Ceramic Bracket (flat wire, unlubricated)..	126
Fig. C.4	Boxplot of Frictional Coefficient by Company by Type of Friction for Steel Bracket (flat wire, unlubricated)..	128
Fig. C.5	Boxplot of Dynamic Frictional Coefficient by Wire Type by Lubrication for Ceramic Bracket (flat wire)..	130
Fig. C.6	Boxplot of Dynamic Frictional Coefficient by Wire Type by Lubrication for Steel Bracket (flat wire)..	131
Fig. C.7	Boxplot of Static Frictional Coefficient by Company by Bracket Type for Heat Treatable Flat Wire (unlubricated)..	133
Fig. C.8	Boxplot of Static Frictional Coefficient by Company by Bracket Type for NiTi Flat Wire (unlubricated)..	134
Fig. C.9	Boxplot of Static Frictional Coefficient by Company by Bracket Type for Steel Flat Wire (unlubricated)..	135
Fig. C.10	Boxplot of Static Frictional Coefficient by Company by Bracket Type for TMA Flat Wire (unlubricated)..	136
Fig. C.11	Boxplot of Static Frictional Coefficient by Wire Type by Wire Configuration for Ceramic Bracket (lubricated)..	140
Fig. C.12	Boxplot of Static Frictional Coefficient by Wire Type by Wire Configuration for Steel Bracket (lubricated)..	141
Fig. C.13	Boxplot of Static Frictional Coefficient by Bracket Type by Wire Type for A Company (flat wire, unlubricated)..	143
Fig. C.14	Boxplot of Static Frictional Coefficient by Bracket Type by Wire Type for A Company (flat wire, lubricated)..	144

Fig. C.15	Boxplot of Static Frictional Coefficient by Bracket Type by Wire Type for Cerum (flat wire, unlubricated)..	146
Fig. C.16	Boxplot of Static Frictional Coefficient by Bracket Type by Wire Type for Cerum (flat wire, lubricated)..	147
Fig. C.17	Boxplot of Static Frictional Coefficient by Bracket Type by Wire Type for Dentaurum (flat wire, unlubricated)..	149
Fig. C.18	Boxplot of Static Frictional Coefficient by Bracket Type by Wire Type for Dentaurum (flat wire, lubricated)..	150
Fig. C.19	Boxplot of Static Frictional Coefficient by Bracket Type by Wire Type for Ormco (flat wire, unlubricated)..	152
Fig. C.20	Boxplot of Static Frictional Coefficient by Bracket Type by Wire Type for Ormco (flat wire, lubricated)..	153
Fig. C.21	Boxplot of Static Frictional Coefficient by Bracket Type by Wire Type for RMO (flat wire, unlubricated)..	155
Fig. C.22	Boxplot of Static Frictional Coefficient by Bracket Type by Wire Type for RMO (flat wire, lubricated)..	156
Fig. D.1	Situation Before Force Application in the Case of Premolar Extraction..	158
Fig. D.2	Situation After Force Application in the Case of Premolar Extraction..	158
Fig. D.3	Schematic Diagram of Archwire Behaviour During Canine Retraction..	159
Fig. D.4	Cross-section of Hypothetical Archwire Material..	161
Fig. D.5	Forces Experienced by a Bracket During Simulated Canine Retraction..	162

List of Plates

	Page
Plate 1 Micrograph of Cerum Stainless Steel Bracket Slot (B1)..	105
Plate 2 Micrograph of Cerum Stainless Steel Bracket Base (B1)..	105
Plate 3 Micrograph of Cerum Ceramic Bracket Slot (B2)..	106
Plate 4 Micrograph of Cerum Ceramic Bracket Base (B2)..	106
Plate 5 Micrograph of Ormco Stainless Steel Bracket Slot (B3)..	107
Plate 6 Micrograph of Ormco Stainless Steel Bracket Base (B3)..	107
Plate 7 Micrograph of Ormco Ceramic Bracket Slot (B4)..	108
Plate 8 Micrograph of Ormco Ceramic Bracket Base (B4)..	108
Plate 9 Micrograph of RMO Stainless Steel Bracket Slot (B5)..	109
Plate 10 Micrograph of RMO Stainless Steel Bracket Base (B5)..	109
Plate 11 Micrograph of RMO Ceramic Bracket Slot (B6)..	110
Plate 12 Micrograph of RMO Ceramic Bracket Base (B6)..	110
Plate 13 Micrograph of A Company Stainless Steel Bracket Slot (B7)..	111
Plate 14 Micrograph of A Company Stainless Steel Bracket Base (B7)..	111
Plate 15 Micrograph of A Company Ceramic Bracket Slot (B8)..	112
Plate 16 Micrograph of A Company Ceramic Bracket Base (B8)..	112
Plate 17 Micrograph of Dentaurum Stainless Steel Bracket Slot (B9)..	113
Plate 18 Micrograph of Dentaurum Stainless Steel Bracket Base (B9)..	113
Plate 19 Micrograph of Cerum Stainless Steel Archwire Sample (W1)..	115
Plate 20 Micrograph of Cerum NiTi Archwire Sample (W2)..	115
Plate 21 Micrograph of Cerum Ortholoy Archwire Sample (W3)..	116
Plate 22 Micrograph of Ormco TMA Archwire Sample (W4)..	116
Plate 23 Micrograph of Ormco Stainless Steel Archwire Sample (W5)..	117
Plate 24 Micrograph of Ormco NiTi Archwire Sample (W6)..	117
Plate 25 Micrograph of RMO Elgiloy Archwire Sample (W7)..	118
Plate 26 Micrograph of RMO Stainless Steel Archwire Sample (W8)..	118
Plate 27 Micrograph of RMO NiTi Archwire Sample (W9)..	119

Plate 28 Micrograph of A Company NiTi Archwire Sample (W10).. 119
Plate 29 Micrograph of Dentaurum Stainless Steel Archwire Sample (W11).. 120
Plate 30 Micrograph of Dentaurum NiTi Archwire Sample (W12).. 120
Plate 31 Photograph of Bracket and Archwire Sample Placement During Testing.. 121
Plate 32 Photograph of Test Stage Utilized for Frictional Coefficient Testing.. 122
Plate 33 Photograph of Electric Motor-Pulley System Utilized for Frictional Coefficient Testing.. 122

Chapter 1

Introduction and Literature Review

Many fixed orthodontic appliance systems use sliding mechanics to produce orthodontic tooth movement. This process produces translation of a ligated tooth along an archwire, through the application of a controlled force. The orthodontist would consider this mechanism of tooth movement when a clinical situation necessitated the consolidation of excess space. The generation of frictional forces between archwire and bracket is inherent in this design, and difficulties associated with appliance generated frictional forces confront the clinician daily.

An applied force tending to produce translation of a tooth must have sufficient magnitude to overcome inherent frictional resistance, and to produce tooth movement. However, application of an excessive force may adversely affect anchorage units, producing unwanted tooth displacement. A reduction in the frictional force between archwire and bracket would result in a concomitant reduction in the force required to move teeth. This would accordingly have the positive effect of reducing strain on anchorage units and diminish the net force to the teeth.

A. Orthodontic Concerns

The clinician may use one of limited methods to manage complications presented by the frictional forces associated with sliding mechanics, each with its own shortcomings. Certain archwire compositions and configurations contribute less friction to a system of sliding mechanics. The choice of bracket material may also favourably affect the genesis of frictional forces. The clinician may also choose alternate methods of ligation or reduce the force of

ligation. Employing a method of tooth movement that does not involve sliding mechanics can circumvent sliding friction. Utilizing segmented archwires to move teeth represents one such technique. With this procedure, spring bends in a discontinuous archwire generate sufficient force to move teeth. Translation then occurs without sliding the bracketed tooth along an archwire, and without associated impeding frictional forces. Similarly, one eliminates the effects of frictional forces through the use of closing loop archwires. All of these methods, whether employed by choice or default, represent a degree of compromise.

A force of friction results from the interaction of two opposed surfaces in relative motion. Any discussion of orthodontic armamentarium, as it pertains to interacting surfaces, must preface any consideration of orthodontic friction. A wide assortment of archwire, bracket, and ligating material currently exist. The clinician may select from four discrete archwire alloys: stainless steel, chrome cobalt stainless steel (heat treatable), nickel titanium, and titanium molybdenum. An assortment of cross sectional configurations also exist, such as round, rectangular, rounded rectangular. Each configuration exists in a variety of dimensions.

Bracket composition and dimension also present choices available to the orthodontist. Brackets exist fabricated from stainless steel in standard or "mini" dimension, or from aluminum oxide ceramic. One may select from two bracket slot dimensions, 0.018 inch or 0.022 inch, and from single or twin wing brackets. Typically, the retracting force exerts its effect on the tie wings of the bracket, however many brackets present an alternate site for force application, such as a gingivally directed hook or arm.

Ligation represents the final piece of related intraoral armamentarium. The orthodontist may choose elastomeric, stainless steel, or Teflon coated stainless steel ligating material. Elastomerics deliver a comparatively uniform initial ligating force, but one may vary this force with the stainless steel materials. Other factors which may influence the production of frictional forces include relative tooth positions, the interbracket distance, and bends in the archwire. Research has examined some facets of the relationship between these numerous variables, but details of many interactions remain unknown.

B. Overview of Friction

An attempt to describe or quantify friction is an endeavour to explain a microscopic event from a macroscopic perspective. Any discussion of friction is necessarily fraught with assumptions based on countless theoretical descriptions of the process. Research has produced some simple assumptions, or 'classical laws' of friction, to allow a fundamental understanding of a complicated process. Simply stated, these laws are: frictional force and applied load are proportional, frictional force remains independent of surface contact area and sliding velocity, a frictional force acts in the opposite direction to applied tangential force, and the frictional force at the instant of initial sliding is greater than that seen during active sliding. Figure 1.1 shows the forces acting on a cuboidal solid in contact with another surface. As the load on the cube exerts a force tending to push it into the surface, the surface exerts the same force, in the opposite direction, to create an equilibrium. This is termed the normal force, measured in Newtons (kilograms x 9.81 m/s^2).

In the absence of an applied force tending to produce sliding, there is no frictional force. As the applied force increases from zero, it will reach a magnitude sufficient to produce

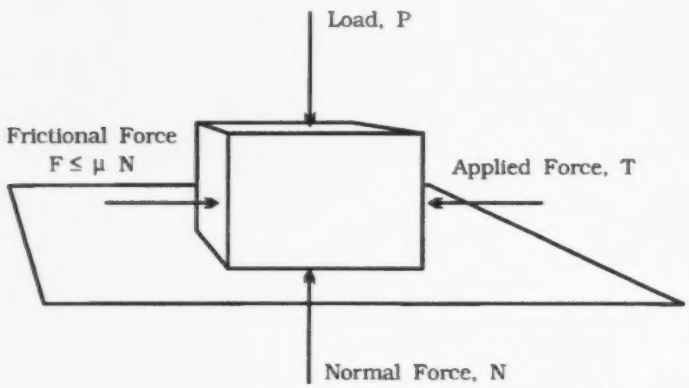

Figure 1.1
Forces Encountered during Sliding

sliding of the cube. When sliding commences, the frictional force equals the applied force. Using the equation shown in Figure 1.1, one may calculate a coefficient of friction, based on the frictional force and the normal load. The Greek letter mu, or μ represents this frictional coefficient, which is a unitless measure. Static friction is the frictional force encountered at the instant sliding begins, and μ is termed the coefficient of static friction. Once sliding has commenced, dynamic frictional force exists, and the corresponding μ is termed the coefficient of dynamic friction.

Many factors enter into a discussion of friction, as each exerts some influence over the frictional force. The most fundamental factor relates to the composition of the surfaces involved. Any material has unique surface characteristics which impact frictional interactions, but a frictional coefficient describes two interacting surfaces; a single surface in isolation may not have a frictional coefficient.

The surface roughness represents another factor. Commonly, one imagines frictional force to escalate with increasing surface roughness. This statement oversimplifies a complex facet of frictional interaction since microscopic characteristics of surface roughness do affect the frictional force.

The presence of surface films can impact the frictional relationship of interacting surfaces. Rarely are materials so devoid of surface films and contaminants that only their constituent atoms interact. Any films or contaminants present on the surfaces of interacting solids have the potential to greatly influence frictional interactions.

Certain aspects of gross surface contact, and the contact area, can influence frictional interactions. Historic assumption generally contends that frictional force is contact area independent, but as the area of contact decreases, one must question the validity of this statement. Effects of interacting edges and small rotations of the materials undoubtedly alter the frictional force.

Elements of the normal force, or the applied load may also influence the friction associated with tangential sliding. Frictional force varies with applied load within a range of loads; with an insignificant load one cannot accurately measure frictional force, and with

immense loads the surfaces become welded. Experimentation must therefore utilize normal forces within a typically encountered range, to ensure valid results.

The presence of a lubricant often profoundly affects frictional force. Many lubricants and modes of lubrication exist, but generally a lubricant acts to displace interacting surfaces to a degree that precipitates a decrease in the frictional force. A more comprehensive explanation of the friction phenomenon, and its many complexities, appears in Appendix A.

Friction, as it exists in orthodontics, results from sliding contact of archwire against bracket during active tooth movement. Another component of friction comes from the contact of archwire and ligating material, but reliable measurement of frictional coefficients between metal and elastomer is difficult. Stainless steel ligation presents the same difficulty with respect to accurate measurement. The bracket-archwire contact likely generates the majority of any frictional resistance encountered during orthodontic tooth movement. This ensues from the manner in which the bracket on an actively moving tooth contacts the archwire. The archwire tends to concentrate all of the force on two small areas of the bracket, as the tooth unavoidably tips during movement (Figure 1.2). This force concentration produces the higher frictional force values.

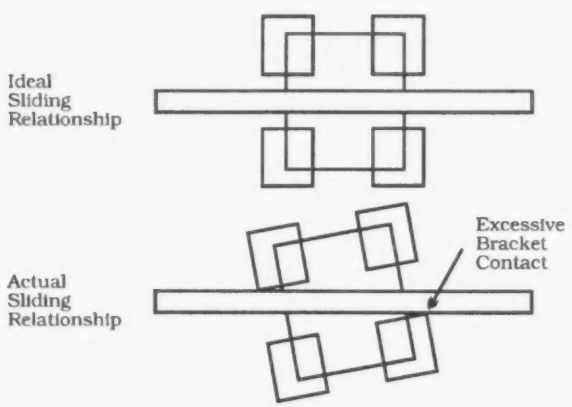

Figure 1.2
Bracket-Archwire Contact during Sliding

Although one perceives orthodontic tooth movement as an apparently continuous process, it likely occurs as a series of infinitely small individual movements. Frictional forces would then exert their influence as a series of static events rather than a single dynamic event. Friction is of two types, static and dynamic. Static friction is that encountered at the instant sliding commences. Dynamic frictional force is that which tends to impede active sliding (Sarkar, 1980, Berger, 1990). Consequently, one must assume that the coefficient of static friction would characterize the most important aspect of this interaction.

C. Review of the Orthodontic Literature

The majority of orthodontic research into the area of bracket-archwire friction utilizes a uniform methodology. Notwithstanding individual experimental variations, this technique involves sliding a ligated archwire sample along a bracket sample, while simultaneously measuring the force required to produce the motion. This method yields a gross force necessary for tangential sliding, but ignores the force that maintains intimate bracket-archwire contact. The effects of ligature-archwire interaction remain unknown, as does the interaction between the archwire and all bracket surfaces it may contact. This type of research does offer some valuable information, as it quantifies the gross force required to produce tangential sliding, and orthodontic tooth movement.

Historic research reveals several variables which influence the generation of archwire-bracket friction. The most commonly cited sources of variation include: archwire alloy type, bracket material, archwire dimension, bracket slot size, bracket width, the presence of lubrication, and the angle between archwire and bracket long axes.

A study by Gardner *et al.* found that friction varied directly with wire size, for stainless steel, nickel titanium and titanium molybdenum wire. These results pertain to a lubricated environment, utilizing a stainless steel Lewis bracket, with bracket and archwire lying along the same long axis. The results suggest an increased friction, when comparing stainless steel

to nickel titanium to titanium molybdenum wire. Stainless steel wire exhibited frictional forces of 55 g (0.54 N) to 75 g (0.74 N), the values for nickel titanium were 80 g (0.78 N) to 100 g (0.98 N), and titanium molybdenum wire produced values of 100 g (0.98 N) to 130 g (1.28 N). A 0.016 x 0.022 inch rectangular wire produced values closer to the lower end of each range, while a 0.017 x 0.025 inch wire resulted in the higher values, for all types of wire tested (Gardner *et al.*, 1986).

Frank and Nikolai found that friction increased with increasing bracket width, and showed, as the main effect, differences of 127 g (1.25 N) for narrow single, 253 g (2.48 N) for medium twin, and 286 g (2.63 N) for wide twin brackets. Frictional resistance increased with the angle formed between bracket and archwire, with main effect differences of 51 g (0.50 N) for 0^0, 114 g (1.12 N) for 3^0, 236 g (2.32 N) for 6^0, and 487 g (4.78 N) for 10^0. Archwire dimension also varied directly with frictional forces, with average values as follows: 95 g (0.93 N) for 0.016 inch round, 156 g (1.53 N) for 0.018 inch round, 229 g (2.25 N) for 0.020 inch round, 294 g (2.88 N) for 0.017 x 0.025 inch rectangular, and 336 g (3.30 N) for 0.019 x 0.025 inch rectangular. Greater ligature force increased friction, but extreme bracket/archwire angulations reduced this effect. When this angle was large, the increased stiffness of an archwire increased friction. Nickel titanium archwire material is rougher than stainless steel so at low angulation a frictional increase resulted. However at higher angulations, friction with nickel titanium decreased because it is about 1/6 the stiffness of stainless steel (Frank and Nikolai, 1980).

Tidy's findings agreed with those of Frank and Nikolai (1980), with respect to angulation, wire stiffness, and wire alloy composition. Contradictory findings included an inverse relation between frictional force and bracket width, since the study demonstrated nearly 400 g (3.92 N) of frictional force with a narrow single bracket, and 100 g (0.98 N) to 150 g (1.47 N) with medium and wide twin brackets. Little relation existed between friction and archwire dimension or bracket slot dimension (Tidy, 1989).

Drescher *et al.* also found that narrow width brackets produced the greatest frictional force, in the range of 4 to 5 N for the narrow, and 2 to 3 N for the medium and wide twin

brackets (Drescher *et al.*, 1989). With medium and wide brackets, archwire alloy composition became the deciding factor. They found that friction increased from stainless steel to nickel titanium to titanium molybdenum wire, with titanium molybdenum producing nearly 5 N of frictional force, while other types produced 2 to 2.5 N of frictional force.

More conflicting data come from a study by Andreason and Quevedo. They found that wire size varied directly with frictional resistance, and bracket width is independent of the force necessary to overcome friction. Frictional force values remained the same for dry sliding, and sliding lubricated with saliva (Andreason and Quevedo, 1970). The angle formed between bracket and archwire emerged as the greatest contributing factor to the generation of frictional forces in this study.

Baker *et al.* found a reduction in friction under conditions of lubrication with Xero-Lube, an artificial saliva substitute, but not with glycerin. They also found that an archwire dimension closely approximating that of the bracket slot decreased the potential for binding forms of friction caused by wire distortion (Baker *et al.*, 1987).

A study by Stannard *et al.* measured frictional forces between archwires and a Teflon surface, in addition to a stainless surface. Under dry conditions, the lowest friction existed between stainless steel and stainless steel, titanium molybdenum and stainless steel, and stainless steel and Teflon. Under wet conditions, friction increased with stainless steel, titanium molybdenum, and nickel titanium on stainless steel. The lowest values resulted from the combination of stainless steel and titanium molybdenum on Teflon. A sliding stainless steel archwire displayed wear tracks after testing, the grain structure of titanium molybdenum became polished, and the fibrous surface of nickel titanium showed neither wear nor polish (Stannard *et al.*, 1986).

Riley *et al.* found that, with the passage of time over a two week test period, immersion of bracket and archwire in distilled water increased friction. They attributed this to the development of corrosion products on the involved surfaces (Riley *et al.*, 1979). They also found that moving from a round to a rectangular archwire, and increasing rectangular

archwire size increased frictional forces. In addition, steel ligatures increased friction when compared to elastomeric ligatures.

The study by Peterson *et al.* also found that frictional resistance increased with rectangular archwires, as compared to round. They found that archwire size varied directly with frictional force, as did the angle between bracket and archwire long axes. Bracket width did not affect the force needed to overcome friction with any wire size or bracket angulation (Peterson *et al.*, 1982).

Pratten *et al.* found that ceramic brackets increased the frictional force associated with drawing an archwire through a bracket, as compared to stainless steel brackets. The frictional resistance with artificial saliva for ceramic brackets was approximately 100 g (0.98 N) with stainless steel wire, and 150 g (1.47 N) with nickel titanium wire, while the values for stainless steel brackets were approximately 75 g (0.74 N) and 100 g (0.98 N) respectively. Dry conditions reduced frictional resistances by approximately 50 g (0.49 N) in all cases (Pratten *et al.*, 1990).

A study by Kapila *et al.* revealed that frictional forces diminished with a decrease in bracket width. When using a 0.022 inch bracket slot, frictional forces ranged from 75 g (0.74 N) to 179 g (1.76 N) for narrow single brackets, 94 g (0.92 N) to 193 g (1.89 N) for medium twin, and 82 g (0.80 N) to 222 g (2.18 N) for wide twin brackets. Increasing wire size, and moving from a round to a rectangular wire, increased frictional forces. Stainless steel wire generally showed the least frictional resistance within any one wire group, while nickel titanium or titanium molybdenum wire demonstrated the greatest (Kapila *et al.*, 1990).

A similar study compared frictional forces inherent in ceramic brackets with those in stainless steel brackets (Angolkar *et al.*, 1990). This study found the same general trends in archwire-bracket interactions, but also found higher frictional forces with the ceramic brackets. When using a medium twin ceramic bracket, frictional resistance ranged from 119 g (1.17 N) to 399 g (3.33 N), as opposed to 94 g (0.92 N) to 193 g 1.89 N) for stainless steel brackets, in the study by Kapila *et al.* (Kapila *et al.*, 1990). Increasing resistance

occurred with larger diameter wires, with rectangular wires, and appeared least for stainless steel and greatest with nickel titanium or titanium molybdenum.

Kusy *et al.* found the lowest coefficients of static and kinetic friction for stainless steel archwires, when compared to the increasing values of chrome-cobalt stainless steel, nickel titanium, and titanium molybdenum wires against stainless steel brackets. The study also found polycrystalline ceramic brackets to increase static friction relative to stainless steel brackets. Increasing the bracket-archwire contact angle increased the frictional resistance, as did stainless steel ligation as compared to elastomeric ligation. The study found that an aqueous environment, designed to simulate the oral environment, had little influence upon the generation of frictional forces (Kusy *et al.*, 1988).

Berger investigated the consequences of using a SPEED self ligating bracket upon frictional forces. This study found a drastic reduction in friction, as compared to brackets requiring external ligation. The mean frictional resistance for a 0.016 inch round wire with stainless steel ligation was 64.92 g (0.64 N), 86.28 g (0.85 N) for elastomeric ligation, and 10.89 g (0.19 N) for self ligation. Interestingly, this study found that using elastomeric ligation resulted in an increase in frictional resistance, as compared to stainless steel ligation (Berger, 1990).

Prososki *et al.* utilized profilometry to test the surface roughness of nickel titanium, titanium molybdenum, stainless steel, and chrome cobalt stainless steel archwires. An Instron material testing machine pushed wire samples through Edgelock self ligating brackets to determine frictional resistance. The archwires, from most to least smooth were stainless steel, chrome cobalt stainless steel, and titanium molybdenum. The nickel titanium wires tested exhibited a range of surface finishes. They could find no relation between surface roughness and frictional resistance, however the chrome cobalt stainless steel and nickel titanium archwires had the lowest frictional values, while titanium molybdenum had the highest (Prososki *et al.*, 1991).

Another study compared the frictional resistance of stainless steel archwires to that of nickel titanium, when drawn through ceramic and stainless steel brackets (Omawa *et al.*,

1992). An increasing weight placed on the bracket created a tipping force which engaged the wire during sliding. The results showed that the force produced by adding the increasing weight was most important in determining the frictional increase seen. No appreciable difference existed between frictional forces for the two archwire types. Ceramic brackets increased the frictional force over metal brackets, as did the use of a narrower bracket, regardless of the material.

Kusy and Whitely analyzed specular reflectance of four archwire alloys to determine optical surface roughness, and to relate this roughness to archwire-bracket friction. Specular reflectance examines the amount that light scatters, when reflected from a surface, which provides a measure of surface roughness. Ranked from least to most surface roughness, the wires tested were stainless steel, chrome cobalt stainless steel, nickel titanium, and titanium molybdenum (Kusy and Whitely, 1990). This study concluded that the rougher the archwire, the more frictional force it would produce.

Some broad conclusions emerge from historic research concerning archwire-bracket frictional interactions. Generally, titanium alloyed archwires offer more frictional resistance than stainless steel archwires. Ceramic brackets generate more friction than stainless steel brackets. Round archwires, and those with smaller cross sectional areas result in decreased frictional forces. The frictional force between archwire and bracket tends to increase as their mutual long axes deviate from parallel. The effects of lubrication remain poorly understood since the addition of a lubricant can increase, decrease, or not affect frictional force, depending on individual experimental results. Finally, increasing archwire surface roughness does not correlate strongly with an increase in frictional force.

One can see that even with the research undertaken in this area, some inconsistencies and unanswered questions persist. A more thorough understanding of bracket- archwire friction requires separate study of all individual frictional processes that occur during tangential sliding of an archwire relative to a bracket. Comprehension of these processes, and the many variables which govern their interrelations, may permit integration into a more clear comprehension of the total orthodontic frictional process.

D. Statement of the Problem

The nature and scope of frictional forces encountered between orthodontic brackets and archwire alloys depends, to a large extent, upon their compositions. Typically utilized orthodontic brackets are composed of aluminum oxide ceramic or stainless steel. Archwire alloys available include stainless steel, chrome cobalt stainless steel (heat treatable), nickel titanium, and titanium molybdenum. Relatively few studies specifically focus on the effect that these materials have on the genesis of frictional forces in fixed orthodontic appliances. Historically, the majority of research examines the force that retards the movement of a ligated bracket along an archwire. Although this approach quantifies the entire force resisting orthodontic tooth movement, it does not reveal the underlying frictional relationship between bracket and archwire.

Analysing the coefficients of static and dynamic friction that exist between various archwire and bracket compositions provided insight into this problem. Determining the role that archwire surface roughness plays in the genesis of frictional forces would also permit a greater understanding of bracket-archwire interactions. Ascertaining the potential impact of archwire morphology in the production of frictional forces may allow the selection of round, rectangular, or specifically sized archwires in specific situations. Examining the effects of lubrication upon frictional forces may yield a closer correlation between *in vitro* experimental results and those conditions found intraorally. Clarification of these associations may furnish a better understanding of the nature and magnitude of forces tending to retard orthodontic tooth movement utilizing sliding mechanics.

E. Purpose of the Study

The objective of the present investigation was to assess and quantify the frictional relationships between various orthodontic archwire and bracket materials. Specifically, the

study measured frictional forces, and from these determined static and dynamic frictional coefficients. The protocol tested the effects of more than one normal force level to determine whether the frictional coefficients are independent of associated normal forces. The experiment established whether differences in bracket compositions resulted in different frictional coefficients. The study also provided the same information for the different archwire alloys. The experiment examined both dry and lubricated sliding between the brackets and archwires, to determine the effect of adding an artificial saliva substitute. The present research also investigated the potential role that archwire surface roughness plays in the determination of frictional coefficients. Microscopic analysis of the involved surfaces also permitted a qualitative comparison of the brackets and archwire materials.

F. Research Questions

1. Does the bracket composition affect the coefficients of static and dynamic friction?

2. Does the archwire alloy affect the coefficients of static and dynamic friction?

3. Do coefficients of friction vary with changes in normal force, or that force which seats the archwire into the bracket?

4. Does the addition of an artificial saliva lubricant affect frictional coefficients?

5. Can one relate changes in frictional forces between the various combinations of brackets and archwires to microscopic differences in archwire surface characteristics?

6. Will the results of frictional testing support the generally held theories of frictional relationships: i.e. is the frictional force proportional to the applied load, and is the frictional force independent of apparent surface contact area?

G. Hypotheses

H^1 H_o:The coefficient of static friction does not differ significantly between stainless steel brackets and stainless steel, chrome cobalt, nickel titanium, and titanium molybdenum archwires.

H_a: The coefficient of static friction differs significantly between stainless steel brackets and stainless steel, chrome cobalt, nickel titanium, and titanium molybdenum archwires.

H^2 H_o: The coefficient of static friction does not differ significantly between ceramic brackets and stainless steel, chrome cobalt, nickel titanium, or titanium molybdenum archwires.

H_a: The coefficient of static friction differs significantly between ceramic brackets and stainless steel, chrome cobalt, nickel titanium, or titanium molybdenum archwires.

H^3 H_o: The coefficient of dynamic friction does not differ significantly between stainless steel brackets and stainless steel, chrome cobalt, nickel titanium, or titanium molybdenum archwires.

H_a: The coefficient of dynamic friction differs significantly between stainless steel brackets and stainless steel, chrome cobalt, nickel titanium, or titanium molybdenum archwires.

H^4 H_o: The coefficient of dynamic friction does not differ significantly between ceramic brackets and stainless steel, chrome cobalt, nickel titanium, or titanium molybdenum archwires.

H_a: The coefficient of dynamic friction differs significantly between ceramic brackets and stainless steel, chrome cobalt, nickel titanium, or titanium molybdenum archwires.

H^5 H_o: The observed coefficients of static and dynamic friction will not differ significantly.

H_a: The observed coefficients of static and dynamic friction will differ significantly.

H^6 H_o: The addition of artificial saliva as a lubricant does not significantly affect the coefficient of friction between stainless steel or ceramic brackets and stainless steel, chrome cobalt, nickel titanium, or titanium molybdenum archwires.

H_a: The addition of artificial saliva as a lubricant does significantly affect the coefficient of friction between stainless steel or ceramic brackets and stainless steel, chrome cobalt, nickel titanium, or titanium molybdenum archwires.

H^7 H_o: Varying the normal force does not significantly affect the coefficient of static or dynamic friction between brackets and stainless steel, chrome cobalt, nickel titanium, or titanium molybdenum archwires.

H_a: Varying the normal force does significantly affect the coefficient of static or dynamic friction between brackets and stainless steel, chrome cobalt, nickel titanium, or titanium molybdenum archwires.

H^8 H_o: The coefficients of friction are not significantly affected by the apparent area of surface contact between sliding surfaces.

H_a: The coefficients of friction are significantly affected by the apparent area of surface contact between sliding surfaces.

H^9 H_o: Microscopic analysis of archwire material will not show significant differences between the surfaces of stainless steel, chrome cobalt, nickel titanium, and titanium molybdenum archwires.

H_a: Microscopic analysis of archwire material will show significant differences between the surfaces of stainless steel, chrome cobalt, nickel titanium, and titanium molybdenum archwires.

H^{10} H_o: Microscopic analysis of bracket material will not show significant differences between the surface characteristics of stainless steel and ceramic brackets.

H_a: Microscopic analysis of bracket material will show significant differences between the surface characteristics of stainless steel and ceramic brackets.

H^{11} H_o: No significant correlation exists between archwire surface roughness and coefficients of friction.

H_a: A significant correlation exists between archwire surface roughness and coefficients of friction.

Chapter 2

Materials and Methods

A. Materials

1. Bracket and Archwire Test Samples

This study used commercially available orthodontic archwires and brackets. The following orthodontic supply companies donated bracket and archwire materials: A Company Orthodontics, Cerum Ortho Organizers, Dentaurum Orthodontics, Ormco Orthodontics, and Rocky Mountain Orthodontics (RMO). Each company has some variation in the materials it manufactures, so some differences exist when comparing the material samples.

The archwires utilized varied in both their alloy composition and dimension. The alloy types included stainless steel (SS), chrome cobalt stainless steel (Cr-Co SS), nickel titanium (NiTi), and titanium molybdenum alloy (TMA). The study utilized maximum dimension archwire, 0.021 x 0.025", wherever possible. However, commercial availability dictated the use of other sizes and dimensions for some alloy types. A full disclosure of the individual archwire types, listed according to the supplying company, appears in Table 2.1.

The study used maxillary right central incisor brackets, of the Roth prescription, with a 0.022" slot. The friction testing employed a sample of stainless steel and aluminum oxide ceramic brackets from each company, an exhaustive list of which appears in Table 2.2.

One may assume that the static or dynamic frictional coefficient for two solid surfaces is independent of their contact area, but the test trials utilized the greatest dimension of the archwire sample to ensure maximum surface to surface contact. Since friction is a function

of surface interaction, the maximum surface contact possible should therefore maximize validity. The bracket slot, in which an archwire would rest, is composed of a base and two walls. Typically, as an applied orthodontic force moves a tooth, the archwire could contact all three of these surfaces at some time during tooth movement. During frictional testing,

Table 2.1
Description of Archwire Materials

	Archwire Characteristics		
Company	Material	Size (inches)	Cross-section
Ormco	SS	0.021 x 0.025	rectangular
	SS	0.018 x 0.25	braided
	NiTi	0.020	round
	NiTi	0.019 x 0.025	rectangular
	TMA	0.021 x 0.025	rectangular
Cerum	SS	0.021 x 0.025	rectangular
	NiTi	0.019 x 0.025	rectangular
	CrCo - SS	0.019 x 0.019	square
Rocky Mountain	SS	0.021 x 0.025	rectangular
	SS	0.020	round
	CrCo - SS	0.021 x 0.025	rectangular
	NiTi	0.021 x 0.025	rectangular
Dentaurum	SS	0.021 x 0.025	rectangular
	NiTi	0.019 x 0.025	rectangular
A Company	NiTi	0.021 x 0.025	rectangular

multiple surface contact against the archwire would create additional sources of frictional resistance, and make determination of a frictional coefficient difficult. The present study involved removal of these bracket walls, allowing the archwire to contact only the bracket base. Consequently, the equation for determination of the frictional coefficient, $F = \mu N$ (from Figure 1.1) is valid, and one may calculate coefficients for the archwire-bracket combinations. The surface finish for all regions of the bracket, in the case of all orthodontic manufacturing companies, is uniform. This point is important since the geometry of some brackets did not allow the testing procedure to occur on an equivalent surface, relative to the other brackets. Depending upon the focus of interest, testing should involve the same area on each bracket type, and the same area occupied by the wire during actual orthodontic treatment. This study did not attempt to ascertain frictional force encountered during *in vivo* orthodontic treatment. Because of the uniformity of bracket finish, testing on nonequivalent areas of different brackets did not influence the testing procedure.

Table 2.2
Description of Bracket Materials

Company	Bracket Material
Ormco	Stainless Steel
	Ceramic
Cerum	Stainless Steel
	Ceramic
RMO	Stainless Steel
	Ceramic
A Company	Stainless Steel
	Ceramic
Dentaurum	Stainless Steel

The bracket has two discrete slot areas: the horizontal archwire slot into which a ligature pulls the archwire, and a vertically oriented space between the bracket wings, which lies at 90^0 to the archwire slot. The procedure tested wire specimens against this vertical interwing space, to ensure single surface archwire-bracket contact. Frictional coefficient testing with an archwire in the horizontal archwire slot would allow contact between the bracket base, and the walls of the archwire slot, introducing unwanted frictional forces. Testing an archwire sample against the vertical interwing space eliminated any contact between the archwire sample and the walls of the bracket slot. This method of testing appeared valid, since the horizontal archwire slot and the vertical interwing space are made of the same metal (or ceramic) and manufacturers' finishing procedures treat all areas of the bracket in the same manner. Ceramic brackets generally do not have a vertical interwing space, so the study made use of the flat surface found on the wing of the bracket, or the larger lateral surface. Ceramic brackets are cast, and the archwire slot does not receive any special treatment relative to other surfaces on the bracket.

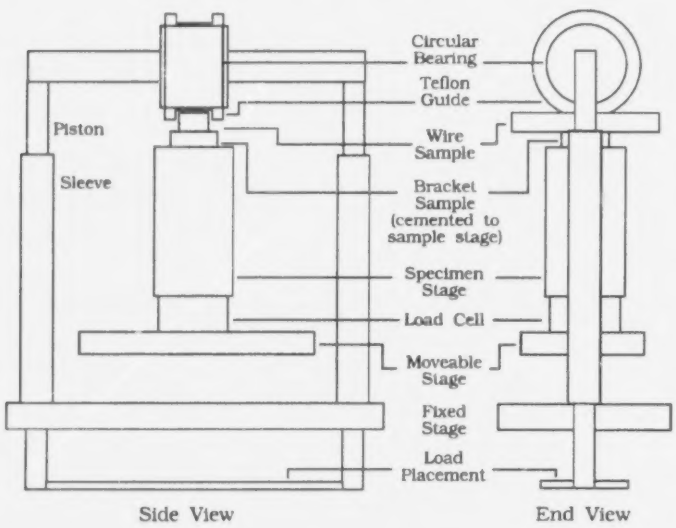

Figure 2.1
Friction Testing Apparatus: Stage Details

2. Testing Apparatus

One may employ many methods to determine frictional coefficients. All methods have, in common, the ability to measure the normal load across the two surfaces, and the tangential force necessary to produce sliding (Bowden and Tabor, 1950). In the current study, the frictional coefficient testing apparatus consisted of three fundamental components, one which applied the static normal force across the archwire sample-bracket interface, a second which generated a tangential force to produce sliding of the archwire sample along the bracket, and a third which measured this motive force (Figure 2.1).

The University of Alberta Mechanical Engineering machine shop custom fabricated all components of the friction testing apparatus. The major components of the apparatus included a test stage, responsible for holding the test samples and maintaining their mutual alignment while simultaneously applying vertical load (Plate 32). A second major component was an electric motor-pulley system to withdraw the archwire sample while measuring frictional resistance associated with this movement (Figure 2.2, Plate 33).

The bracket test sample required mounting on a threaded acrylic dowel prior to installation on the moveable stage of the apparatus. This moveable stage had an integral microscope stage positioner which permitted bracket sample positioning directly beneath the Teflon archwire guide. The archwire guide consisted of a circular bearing with a circumscribed thickness of Teflon. The Teflon coating had a groove, approximately 0.025 inch wide and 0.010 inch deep machined into its surface to aid in the fine positioning of the archwire sample (Plate 31). The mounting assembly for the archwire guide consisted of brass rods in Teflon sleeves to permit free vertical movement of the Teflon archwire guide.

The apparatus used brass weights to supply the normal force. These weights hung below the Teflon archwire guide, while the output from a load cell mounted below the acrylic dowel displayed the load between the archwire and bracket samples to ensure its uniformity. A constant velocity electric motor drew the archwire sample along the bracket. This electric motor system had a second load cell arranged in series with the motor, to measure the force

required to pull the archwire sample across the bracket. The apparatus also permitted testing in both a dry environment, and under conditions created by lubrication with an artificial saliva substitute.

The load cells used in the apparatus were two Omega LCF-5 miniature load cells. The output of the load cells passed through a strain gauge conditioner. This allowed modification of the load cell signals prior to their output to a recording device. A Fluke 8062 A digital multimeter, one for each channel of the strain gauge conditioner, provided information about the forces experienced by the two load cells. This allowed one to simultaneously monitor the output of both load cells, expressed in millivolts, during the experimental trials. Adjusting the gain on each channel of the strain gauge conditioner to approximately 60% of maximum permitted the equipment to display a one gram load as one millivolt. Output from each channel of the strain gauge conditioner passed to a two channel Omega 585 strip chart recorder, set at a chart speed of 10 cm/minute. The trace of one pen represented the sliding force as a graphical plot versus time, and the other represented fluctuations in the normal force. An AC power supply furnished DC current to the electric motor, which pulled

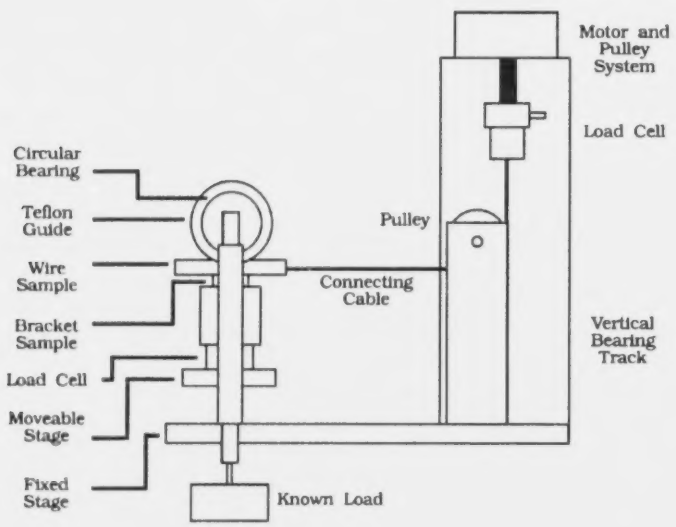

Figure 2.2
Friction Testing Apparatus

the archwire samples. Although the manufacturer rated the motor at 12 volts DC, a power supply setting of 8 volts DC still allowed proper operation of the electric motor, but at the slightly reduced linear speed of 10 cm/minute. This necessary speed reduction enabled the strip chart recorder to produce a more smooth tracing of force fluctuations, as the archwire sample passed across the bracket sample.

3. Materials used for Electron micrographic study

The study employed a Hitachi S - 2500 scanning electron microscope to produce micrographs of the various surfaces involved in the friction testing. An integral still camera exposed an image on 100 ASA Kodak Plus X Pan black and white film for each sample, at each of two magnifications. The micrograph study utilized a sample of each rectangular archwire type and each bracket type. The scanning electron microscope can image both metallic and ceramic bracket samples without gold sputter coating prior to imaging. The microscope created an image of each sample at low and high magnification.

4. Materials used for surface roughness study

The study tested the surface roughness for each type of rectangular archwire utilized in the frictional testing study. The relatively small archwire slot size of all test brackets precluded testing their surface roughness. A Talysurf 4 surface recording instrument provided the means to accomplish nondestructive surface roughness testing of the wire samples. The Talysurf employs a diamond stylus at the end of a cantilever arm, which is drawn across the sample. As the diamond stylus passes over irregularities in the surface, these imperfections cause the cantilever arm to deflect vertically. The apparatus converts these minute deflections into electrical signals, from which it produces an analogue display of the centre line average

of the surface roughness, in micro - inches. The centre line average considers all of the relative 'peaks' and 'valleys' of surface imperfections in describing the surface. Accurate profilometer operation required a flat surface, so this necessitated the use of a 4 x 4 x 1 inch stainless steel plate to mount all archwire samples.

B. Method

1. Method utilized for the friction testing

The actual frictional test performed for each bracket and archwire sample was simplistic, but preparations before trial were complex and demanding. Performing the frictional testing under dry conditions, and also under conditions of lubrication with an artificial saliva substitute, further complicated the procedure.

Prior to the beginning of each trial, the placement of a known brass weight on each of the load cells allowed calibration of the recording equipment. The strain gauge conditioner received balancing to yield a zero reading from each load cell, when unloaded, to ensure consistency of results. The load cell arranged in series with the electric motor measured the force of frictional resistance between the archwire sample and the bracket. The other load cell, in its position beneath the bracket sample, measured the normal force, or that force between the bracket and archwire samples. The graphical output of this frictional resistance versus time, from the strip chart recorder, permitted the calculation of the coefficient of friction, which is the quotient of frictional resistance and normal force. The study repeated the testing for different normal forces, different archwire sample-bracket combinations, and under dry and lubricated conditions.

Bracket wing height on each type of metal bracket did not allow the Teflon wire guide to engage the archwire sample as it rested on the bracket base. A solution to this problem demanded the removal of all metal bracket wings prior to frictional testing. This allowed

intimate contact between the Teflon guide, archwire sample, and bracket base. Without interference from the vertical walls of the bracket, testing only measured frictional forces encountered by the archwire as it passed over the bracket base. A heavy gauge wirecutting plier with carbide blades allowed complete removal of bracket wings. Treatment of any remaining metallic protrusion from the bracket wing with #400 sandpaper ensured that no metal spurs interfered with testing. Some bracket types have integral markings in the bracket base to aid in placement on the tooth. These markings often take the form of a raised ridge, along the entire vertical dimension of the bracket base. This marking precluded testing by the present apparatus, owing to the uncertain surface to surface contact that would result. All companies that donated brackets did provide a metal bracket with a smooth base, conducive to testing with the present apparatus.

Upon satisfactory removal of the bracket wing, visual inspection provided confirmation that the bracket wing removal process had not altered the bracket base surface. This process of inspection appeared adequate, since any introduced surface imperfections dramatically altered the highly reflective surface of the bracket base.

Ormco System 1+ autopolymerizing bracket adhesive allowed adhesive bonding of the test bracket to the acrylic dowel. After a curing period of six minutes, the dowel could be threaded onto the moveable stage of the testing apparatus. A wing nut secured the dowel into position, once the bracket and the Teflon archwire guide were parallel. An ethanol impregnated cotton gauze cleaned any contaminants introduced by handling, and the bonding procedure, from the bracket base prior to testing.

The testing procedure used archwire samples four centimetres long. Alloy types conducive to shaping had small hooks placed at one end to facilitate engagement by the pulley cable. The nickel titanium archwires resisted the placement of permanent deformations, so their testing required the affixing of malleable wire hooks. This necessitated the fabrication of stainless steel hooks from 0.021 x 0.025 inch archwire stock, and their welding to the nickel titanium archwire sample with a Unitek Orthodontic spotwelder. Testing of the welded wire terminated at least 1 cm from the weld joint to avoid involvement

of the heat altered portion of the archwire sample. As with the bracket samples, an ethanol impregnated cotton gauze removed any contaminants from the archwire sample, prior to testing. Once cleaned, the archwire samples air dried on a clean cotton gauze.

Handling of the test samples with latex rubber surgical gloves prevented their contamination after cleaning. The acrylic dowel, with its bonded bracket sample, fit into the moveable stage while permitting some flexibility of orientation. This allowed fine adjustments, to ensure that the bracket sample orientation stayed parallel to the direction of pull for the pulley cable. The microscope stage positioner enabled orientation of the bracket sample directly beneath the Teflon guide, regardless of its position on the acrylic dowel. The Teflon guide, when in the raised position, allowed preliminary positioning of the archwire sample on the bracket sample. Lowering the Teflon guide clarified the exact position of the archwire sample, relative to the bracket sample, and permitted any further fine adjustment with the microscope stage positioner. After relative positioning of the archwire and bracket samples, the appropriate brass weight, hung from the test stage, then provided the static load across the samples.

Once the electric motor lowered the vertical pillow block, enough slack existed in the pulley cable to allow it to engage the archwire sample hook. The completion of this final step readied the apparatus so that an individual trial could proceed. Strip chart recorder activation occurred just prior to the activation of the electric motor. Actuating the motor pulled the pillow block up, and initiated movement of the archwire sample across the bracket sample. This movement terminated after approximately 1.5 cm of the archwire sample passed over the bracket sample. Each archwire-bracket pair received this test at three static loads: 200 grams (1.962 N), 250 grams (2.4525 N) and 300 grams (2.943 N). Each of these tests occurred twice, and the overall procedure occurred six times for each pair. This protocol involved six trials on the same bracket surface, and the use of six brackets for each archwire-bracket sample pair. This generated 36 chart recordings for each archwire-bracket sample pair. Interpretation of the chart recording produced a datum point at the start of movement representing the force of static friction. Once movement began, a second datum point

represented the force of dynamic friction (for diagrammatic explanation, refer to Figure 3.1). This same protocol produced all results. The only modification occurred during the lubricated testing. A method of delivering artificial saliva substitute simulated the condition of oral lubrication, to approximate the *in vivo* frictional behaviour of a bracket sliding along an archwire. A burette filled with Moi-stir Dry Mouth Solution saliva substitute (Kingswood Canada, Inc.) delivered a constant amount of the fluid to the archwire as it rested on the bracket. Sufficient fluid flow created a uniform meniscus surrounding the junction between the archwire and bracket samples for the duration of each trial.

The materials involved in frictional coefficient testing, and their utilization permitted the number of variables in the experiment to total six. However, experimental limitations prevented testing of all variable combinations. These limitations resulted from the fact that not all manufacturers produce the same archwire materials, the experiment did not test an exhaustive selection of all manufacturers' materials, and the extensive time involved to test all combinations of variable alternatives. Tables 2.1 and 2.2 outline alternatives for variables in question. The normal force magnitudes were 1.962 N (200 grams), 2.4525 N (250 grams), and 2.943 N (300 grams). The protocol required testing with and without a lubricant. All variables appear in Table 2.3.

Table 2.3
Description of Frictional Coefficient Experimental Variables

Variable Number	Variable Name	Alternatives per Variable
1.	manufacturer of sample	5
2.	bracket composition	2
3.	archwire composition	4
4.	archwire shape	3
5.	normal force	3
6.	conditions of lubrication	2

The experimental protocol utilized yielded a total of 258 variables. This resulted from the manner in which the protocol dictated variable option combinations for each trial. The total number of trials performed equalled 3660. The testing produced raw force values for each trial. Although all results obtained were forces, the measuring and recording equipment displayed each resultant value as a mass. This did not present a problem, since the coefficient of friction is unitless. Recording both the normal and frictional forces in the same units still means that the frictional coefficient is the quotient of the frictional and the normal forces.

The strip chart recorder produced a graphic representation of the forces involved in each trial. The initial force represented that of static friction and the subsequent force symbolized that of dynamic friction. A mean value for the range of dynamic friction represents the recorded value for dynamic friction, for each trial. The surface roughness testing involved only two variables, the manufacturer of the archwire, and the alloy composition of the archwire sample. Table 2.4 outlines the options for these two variables. The experimental protocol yielded 11 combinations of these variable options. The total number of trials performed equalled 256. Differences between the manufacturers, with respect to the archwires they produce, and a limitation in the sample size available to the experiment, dictated the total number of variables.

To facilitate statistical handling of the data, all values for frictional coefficients, and surface roughness, received an identification code that permitted orderly data entry into SPSS

Table 2.4
Description of Surface Roughness Experimental Variables

Variable Number	Variable Name	Alternatives per Variable
1.	manufacturer of sample	5
2.	wire composition	4

for Windows, a personal computer based statistical analysis program. This program afforded the vehicle for all statistical manipulation of data realized in the experimental trials.

The identification code for surface roughness values permitted blind evaluation of bracket and archwire surfaces. Blinding the frictional coefficient protocol presented a challenge. Since nickel titanium archwires had hooks welded to them, they could not receive effective blinding. The mirror-like surface finish of stainless steel archwires did not facilitate blinding relative to titanium molybdenum archwires, since titanium alloyed archwires generally have a less reflective surface. The protocol could not effectively permit the blinding of bracket types, since the experiment tested only one ceramic and stainless steel bracket for each manufacturer. Blinding the experiment relative to manufacturers proved difficult, since the selection of archwire types varied for each manufacturer. This effectively created a signature to indicate the manufacturer in question. Although the protocol could not provide effective blinding relative to the archwire and bracket types tested, operation of the equipment during testing made appreciation of results difficult until actual analysis of the experimental data. Raw data could not convey much information pertaining to frictional coefficients subsequent to post-experimental data manipulation. Since computer entry dealt with raw data, the comparison of frictional coefficients could not occur until after this manipulation. Consequently, examiner bias did not factor into the experimental results.

2. Method utilized for the surface roughness study

The surface roughness determination protocol used archwire samples three centimetres long. The study used a total of ten specimens of each archwire type. The actual test sampled three areas of each specimen, one area ≈ 3 mm from each end of the specimen and one area in the centre. A water soluble adhesive affixed each to the steel plate, which maintained the specimens in a flat, immobile position. Prior spreading of adhesive on the plate, and subsequent inversion of the plate upon the arranged archwire specimens minimized

the possibility of contaminating a specimen test surface with adhesive. Surface roughness determination occurred after the adhesive had set. In some cases, the surface roughness of certain specimens was below the resolution of the profilometer. To permit inclusion in the study, these readings arbitrarily received the minimum value for resolution of the profilometer, which is 0.01 micro-inch.

3. Method utilized for the microscopy study

The electron microscope facility of the Medicine-Dentistry Electron Microscopy Unit at the University of Alberta created micrographs for all individual bracket types, and one

Table 2.5
Identification Code for SEM Study

SEM Code	Bracket Sample
B1	Cerum SS
B2	Cerum Ceramic
B3	Ormco SS
B4	Ormco Ceramic
B5	RMO SS
B6	RMO Ceramic
B7	A Co SS
B8	A Co Ceramic
B9	Dentaurum SS

SEM Code	Archwire Sample	Size (inches)
W1	Cerum SS	0.021 x 0.025
W2	Cerum NiTi	0.019 x 0.025
W3	Cerum CrCo	0.019 x 0.019
W4	Ormco TMA	0.021 x 0.025
W5	Ormco SS	0.021 x 0.025
W6	Ormco NiTi	0.019 x 0.025
W7	RMO CrCo	0.021 x 0.025
W8	RMO SS	0.021 x 0.025
W9	RMO NiTi	0.021 x 0.025
W10	A Co NiTi	0.021 x 0.025
W11	Dent. SS	0.021 x 0.025
W12	Dent. NiTi	0.019 x 0.025

centimetre specimens of all archwires. Each bracket and wire specimen received a code letter, to permit the inclusion of data relative to the manufacturer of the specimen on the micrograph, as outlined in Table 2.5. Each micrograph provided the observer with a low power view to provide necessary orientation to the specimen, and a high power view to ascertain finer detail.

4. Method error

An experimental protocol that relies on mechanical or electronic testing apparatuses must also determine the relative reliability of the equipment. The present study performed this type of reliability testing to determine equipment performance. This entailed repetitive trials of the frictional coefficient testing described above, at the same normal force, for a single bracket-archwire pairing. This testing involved 21 consecutive trials, conducted with a ceramic bracket and stainless steel archwire, prior to actual data gathering, and again after approximately 1800 individual frictional coefficient trials. The bracket and archwire combination remained the same for each reliability test, but the second 21 consecutive trials utilized different specimens. The reliability testing used the 300 gram (2.943 N) brass weight.

Chapter 3

Results

A. Frictional Coefficient Testing

All statistical designs for frictional coefficient analysis involved two or more means, and analysis, for the purposes of the present investigation, involved some comparison of these means. For designs with only two means, a simple one-way analysis of variance provided the necessary comparison. A design containing four or more means demanded a method capable of multiple paired comparisons. A multivariate ANOVA procedure will show overall differences in any one design, but fails to demonstrate differences between the individual means in that design. The Scheffe procedure will do multiple comparisons , for all possible linear comparisons, not just pairs. However, this procedure requires larger differences for significance when considering pairwise comparisons. All designs examined required only pairwise comparison, and in such circumstances, the Student-Neuman-Keuls (SNK) procedure is appropriate. This procedure examines only pairwise comparisons, by arranging means from smallest to largest. The probability utilized by the SNK, and the one-way procedures is $\alpha = 0.05$. This chapter, and Appendix C contain results of the SNK, and one-way procedures, for all designs tested. The SNK results appear in tabular form as a matrix, comparing the means of all samples in any one design. An asterisk (*) indicates a difference between the two means at the previously mentioned level of significance. For some designs, an exhaustive comparison of means is neither warranted nor informative. The results of any comparisons for these designs appear in text form.

The strip chart recorder produced a graphic representation of the forces involved in each trial. The initial force represented that of static friction and the subsequent force symbolized

that of dynamic friction. A mean value for the range of dynamic friction represents the recorded value for dynamic friction, for each trial. A depiction of the tracing for a typical trial appears in Figure 3.1.

Rigorous statistical analysis demanded that all trial results appear grouped into specific statistical designs. This thesis presents graphical representations of these designs, to allow easier comprehension of the test results. All graphs of the results appear in the form of boxplots. The boxplot format displays the distributions of a dependent variable for each of the cells in the design. The upper and lower boundaries of the boxes are the upper and lower quartiles. The box's vertical dimension is the interquartile distance so a particular box contains the middle 50 percent of values in a group. The solid line within each box identifies the group median. The larger a box, the greater the spread of the observations within that cell of the design in question. The lines emanating from each box are not error bars, but rather refer to spread of the smallest and largest observations within a group that are less than one interquartile range from the ends of the box. Within some cells, for some designs, not all observations fall within one interquartile range. These observations are termed outliers. The size of each graph does not permit the inclusion of outliers. However,

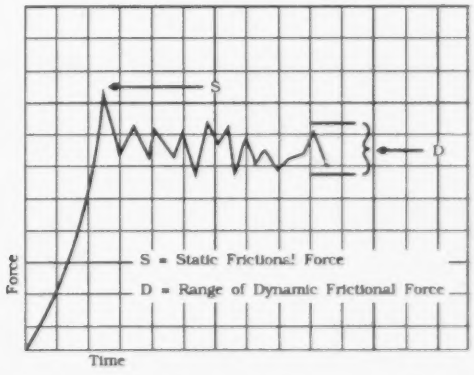

Figure 3.1
Representative Tracing Produced by Recording Equipment

the text of this chapter presents a table of values along with each graph. The table displays complete summary statistics for each design, so one can therefore appreciate the effects of the outliers.

Categorization of the results produces six broad divisions in the data. The first examines static and dynamic friction simultaneously, to determine if any differences exist between the two values. The second deals with the effect of load, or normal force, on the frictional coefficient for various bracket and archwire combinations. The third considers any disparity in frictional coefficient associated with alterations to contact area between archwire and bracket. The experiment achieves this objective by measuring the frictional coefficients of the following different archwire configurations: braided, flat and round. The fourth appraises the effects of artificial saliva lubrication on the frictional coefficient for various bracket and archwire combinations. The fifth division determines whether differences in frictional coefficients exist between the various archwire alloys, when tested against both ceramic and stainless steel brackets. The final division evaluates differences in frictional coefficients between the various companies tested, with respect to the individual company's products.

The raw data afforded 29 individual experimental designs, in an effort to simplify the comprehension of multiple comparisons. This chapter contains a selection of the results for seven experimental designs, pertaining to a selection of the six aforementioned divisions. This selection deals with the effects of normal force, lubrication mode, wire configuration, type of friction and bracket material. A complete disclosure of the remaining 22 experimental design results appears in Appendix C.

Figure 3.2 shows a boxplot for dynamic and static frictional coefficients by increasing normal force by the friction mode, for **ceramic** brackets, flat archwires, and without lubrication. This boxplot does not distinguish between individual archwire types. Table 3.1 shows the data from the boxplot in Figure 3.2 in tabular form. The heading "Number" refers to the number of trials completed for each bracket-archwire combination, for all experimental designs.

A matrix showing SNK results for the design portrayed in Figure 3.2 appears in Table 3.2. This design shows a significant difference between dynamic and static friction at all normal forces (1 = 1.962 N, 2 = 2.4525 N, 3 = 2.943 N loads). No difference exists between the values of dynamic friction at the three normal forces, but one does see a difference between the static frictional values at 1.962 and 2.943 N.

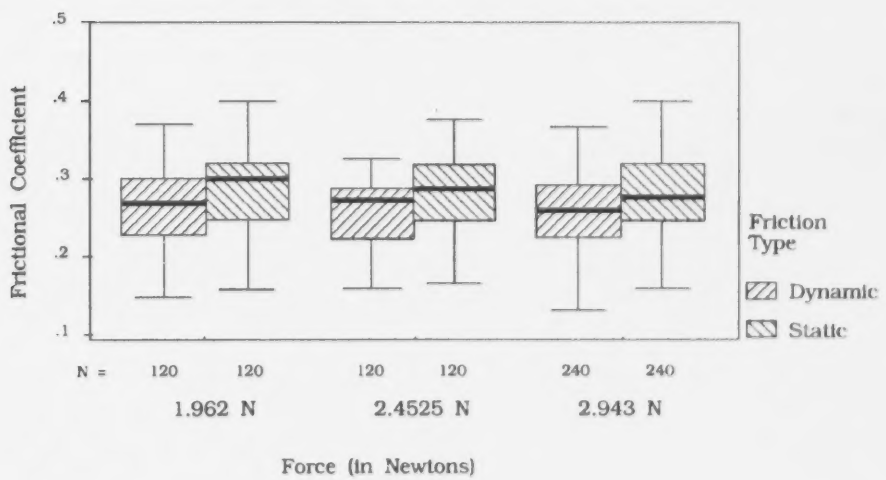

Figure 3.2
Boxplot of Frictional Coefficients by Normal Force by Type of Friction for Ceramic Bracket (flat wire, unlubricated)

Table 3.1
Frequencies - Dynamic and Static Frictional Coefficients for Varying Normal Forces (ceramic bracket, flat wire, unlubricated)

	Load					
	1.962 N		2.4525 N		2.943 N	
	Dy	St	Dy	St	Dy	St
Number	120	120	120	120	240	240
Mean	.267	.293	.260	.283	.259	.280
Median	.270	.300	.272	.288	.260	.277
S.D.	.042	.049	.041	.046	.043	.047

Table 3.2
SNK Multiple Comparison for Varying Normal Forces (ceramic bracket, flat wire, unlubricated)

		Dynamic			Static		
		1	2	3	1	2	3
Dynamic	1				*	*	*
	2				*	*	*
	3				*	*	*
Static	1	*	*	*			*
	2	*	*	*			
	3	*	*	*	*		

Figure 3.3 shows a boxplot for dynamic and static frictional coefficients by increasing normal force by the friction mode, for **stainless steel** brackets, flat archwires, and without lubrication. Again, this boxplot does not distinguish between individual archwire types. Table 3.3 shows the data from the boxplot in Figure 3.3 in tabular form.

A matrix showing SNK results for the design portrayed in Figure 3.3 appears in Table 3.4. This design shows a significant difference between dynamic and static friction at all normal forces (1 = 1.962 N, 2 = 2.4525 N, 3 = 2.943 N) except 1.962 N. The dynamic and static frictional coefficients show no significant difference at each of the three loads.

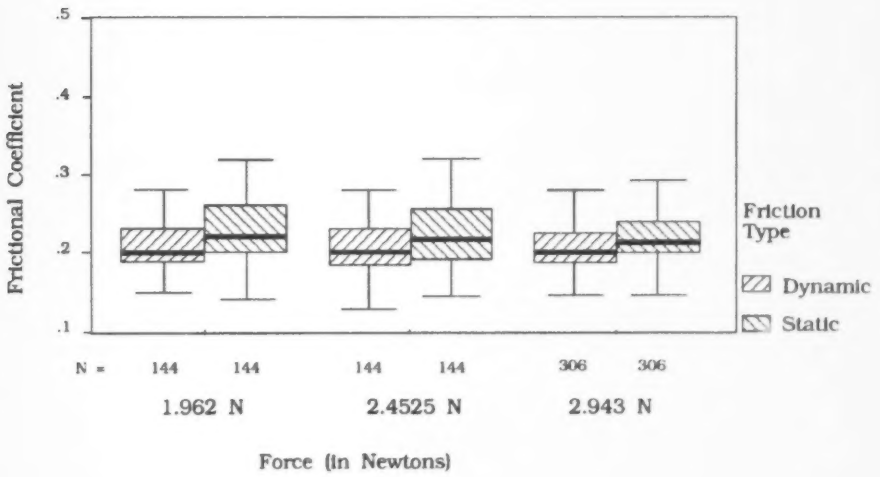

Figure 3.3
Boxplot of Frictional Coefficient by Normal Force by Type of Friction for Steel Bracket (flat wire, unlubricated)

Table 3.3
Frequencies - Dynamic and Static Frictional Coefficients for Varying Normal Forces (steel bracket, flat wire, unlubricated)

	Load					
	1.962 N		2.4525 N		2.943 N	
	Dy.	St.	Dy.	St.	Dy.	St.
Number	144	144	144	144	306	306
Mean	.216	.236	.212	.227	.215	.229
Median	.200	.220	.200	.216	.200	.213
S.D.	.045	.057	.048	.054	.045	.052

Table 3.4
SNK Multiple Comparison for Varying Normal Forces (steel bracket, flat wire, unlubricated)

		Dynamic			Static		
		1	2	3	1	2	3
Dynamic	1				*		*
	2				*	*	*
	3				*		*
Static	1	*	*	*			
	2		*				
	3	*	*	*			

Figure 3.4 shows a boxplot for static frictional coefficients by various archwire types by the lubrication mode, for **ceramic** brackets and flat archwires. This boxplot does not distinguish between individual manufacturers or varying normal forces. Table 3.5 shows the data from the boxplot in Figure 3.4 in tabular form.

A matrix showing SNK results for the design portrayed in Figure 3.4 appears in Table 3.6, where H = heat treatable, N = nickel titanium, S = stainless steel, and T = titanium molybdenum archwires. Lubrication has an insignificant effect on the frictional coefficients for chrome-cobalt stainless steel (heat treatable), nickel titanium, and stainless steel archwires against ceramic bracket material. However one sees a significant difference with lubrication for the titanium molybdenum archwire.

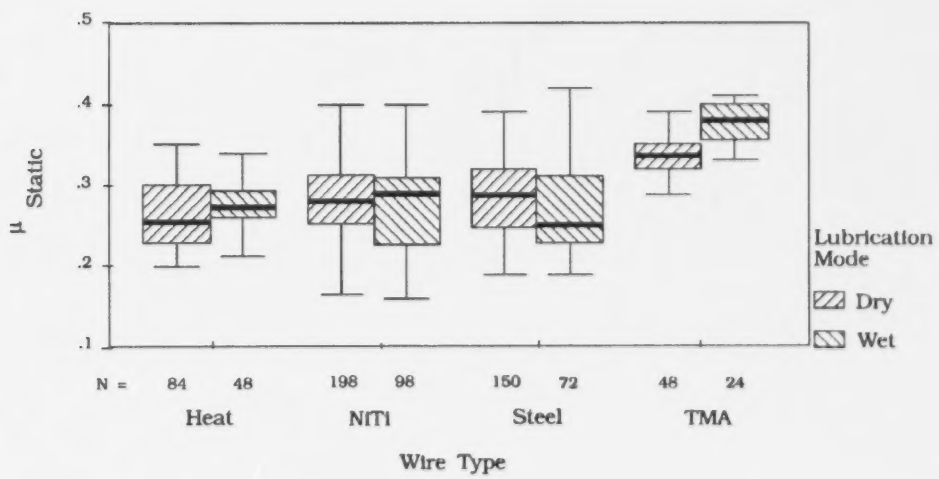

Figure 3.4
Boxplot of Static Frictional Coefficients by Wire Type by Lubrication Mode for Ceramic Bracket (flat wire)

Table 3.5
Frequencies - Static Frictional Coefficients for Various Archwires against Ceramic Bracket, Lubricated and Unlubricated (flat wire)

	Wire Type							
	Heat Treatable		NiTi		Stainless Steel		TMA	
	Dry	Wet	Dry	Wet	Dry	Wet	Dry	Wet
Number	84	48	198	96	150	72	48	24
Mean	.264	.273	.281	.272	.282	.272	.338	.377
Median	.255	.273	.280	.288	.287	.252	.336	.380
S.D.	.039	.033	.048	.049	.045	.055	.026	.024

Table 3.6
SNK Multiple Comparison of Static Frictional Coefficients, Lubricated and Unlubricated, for Various Archwire Types (ceramic bracket, flat wire)

		Unlubricated				Lubricated			
		H	N	S	T	H	N	S	T
Unlubricated	H		*	*	*				*
	N	*			*				*
	S	*			*				*
	T	*	*	*		*	*	*	*
Lubricated	H				*				*
	N				*				*
	S				*				*
	T	*	*	*	*	*	*	*	

Figure 3.5 shows a boxplot for static frictional coefficients by various archwire alloys by the lubrication mode, for **stainless steel** brackets and flat archwires. This boxplot does not distinguish between individual manufacturers or varying normal forces. Table 3.7 shows the data from the boxplot in Figure 3.5 in tabular form.

A matrix showing SNK results for the design portrayed in Figure 3.5 appears in Table 3.8. Against stainless steel bracket material, lubrication does significantly alter the frictional coefficient for heat treatable, nickel titanium and titanium molybdenum archwires. One does not see a significant difference considering the stainless steel archwire.

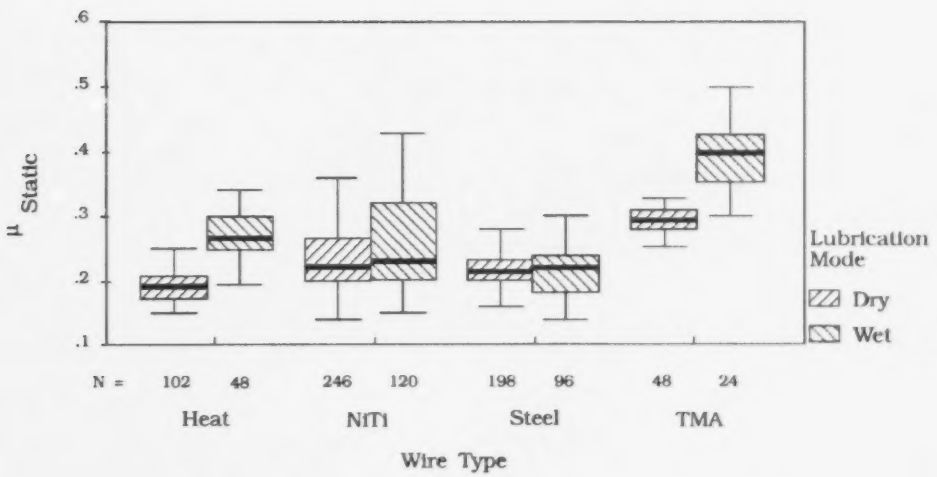

Figure 3.5
Boxplot of Static Frictional Coefficients by Wire Type by Lubrication Mode for Stainless Steel Bracket (flat wire)

Table 3.7
Frequencies - Static Frictional Coefficients for Various Archwires against Stainless Steel Bracket, Lubricated and Unlubricated (flat wire)

	Wire Type							
	Heat Treatable		NiTi		Stainless Steel		TMA	
	Dry	Wet	Dry	Wet	Dry	Wet	Dry	Wet
Number	102	48	246	120	198	96	48	24
Mean	.193	.269	.243	.262	.219	.217	.293	.394
Median	.193	.277	.220	.230	.213	.220	.295	.397
S.D.	.026	.039	.066	.075	.029	.042	.021	.053

Table 3.8
SNK Multiple Comparison of Static Frictional Coefficients, Lubricated and Unlubricated, for Various Archwire Types (steel bracket, flat wire)

		Unlubricated				Lubricated			
		H	N	S	T	H	N	S	T
Unlubricated	H		*	*	*	*	*	*	*
	N	*		*	*	*	*	*	*
	S	*	*		*	*	*		*
	T	*	*	*		*	*	*	*
Lubricated	H	*	*	*	*			*	*
	N	*	*	*	*			*	*
	S	*	*		*	*	*		*
	T	*	*	*	*	*	*	*	

Figure 3.6 shows a boxplot for static frictional coefficients by the various archwire alloys by the archwire configuration, for **ceramic** brackets, without lubrication. This boxplot does not distinguish between individual manufacturers or varying normal forces. Table 3.9 shows the data from the boxplot in Figure 3.6 in tabular form.

A matrix showing SNK results for the design portrayed in Figure 3.6 appears in Table 3.10. The comparisons of interest are between the configurations for the nickel titanium archwire, and the stainless steel archwire. No differences exist, with respect to frictional coefficient, between flat (rectangular) and round nickel titanium archwires against ceramic bracket material. However the frictional coefficient is different between flat and round stainless steel archwires.

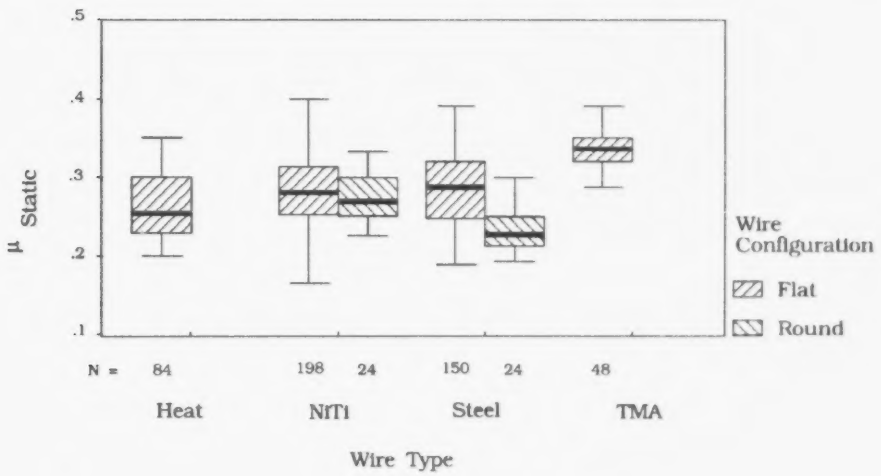

Figure 3.6
Boxplot of Static Frictional Coefficients by Wire Type by Wire Configuration for Ceramic Bracket (unlubricated)

Table 3.9
Frequencies - Static Frictional Coefficients for Various Archwire Types and Configurations against Ceramic bracket (unlubricated)

	Wire Type					
	Heat Treatable	Nickel Titanium		Stainless Steel		TMA
	Flat	Flat	Round	Flat	Round	Flat
Number	84	198	24	150	24	48
Mean	.264	.281	.278	.282	.234	.338
Median	.255	.280	.270	.287	.228	.336
S.D.	.039	.048	.031	.045	.029	.026

Table 3.10
SNK Multiple Comparison for Static Frictional Coefficients, Flat and Round Archwires, for Various Archwire Types (ceramic bracket, unlubricated)

		Flat				Round	
		Heat	NiTi	Steel	TMA	NiTi	Steel
Flat	Heat		*	*	*		*
	NiTi	*			*		*
	Steel	*			*		*
	TMA	*	*	*		*	*
Round	NiTi				*		*
	Steel	*	*	*	*	*	

Figure 3.7 shows a boxplot for static frictional coefficients by the various archwire alloys by the archwire configuration, for **stainless steel** brackets, without lubrication. This boxplot does not distinguish between individual manufacturers or varying normal forces. Table 3.11 shows the data from the boxplot in Figure 3.7 in tabular form.

A matrix showing SNK results for the design portrayed in Figure 3.7 appears in Table 3.12. As in the previous design, no difference exists between frictional coefficients for flat and round NiTi archwires against stainless steel bracket material. Similarly, round and braided stainless steel archwires exhibit no significant differences. Nonetheless, the coefficient of friction for flat stainless steel archwire is significantly different from both braided and round stainless steel archwire.

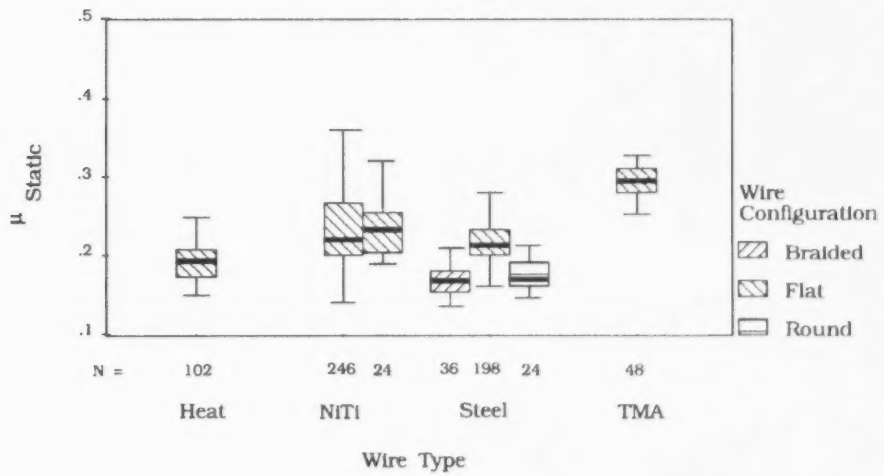

Figure 3.7
Boxplot of Static Frictional Coefficients by Wire Type by Wire Configuration for Steel Bracket (unlubricated)

Table 3.11
Frequencies - Static Frictional Coefficients for Various Archwire Types and Configurations against Steel Bracket (unlubricated)

	Wire Type						
	Heat	NiTi		Stainless Steel			TMA
	Flat	Flat	Round	Braid	Flat	Round	Flat
Number	102	246	24	36	198	24	48
Mean	.193	.243	.240	.170	.219	.176	.293
Median	.193	.220	.233	.167	.213	.170	.295
S.D.	.026	.066	.047	.019	.029	.020	.021

Table 3.12
SNK Multiple Comparisons of Static Frictional Coefficients for Various Archwire Configurations and Types (steel bracket, unlubricated)

		Braid	Flat				Round	
		Steel	Heat	NiTi	Steel	TMA	NiTi	Steel
Braid	Steel		*	*	*	*	*	
Flat	Heat	*		*	*	*	*	
	NiTi	*	*		*	*		*
	Steel	*	*	*		*	*	*
	TMA	*	*	*	*		*	*
Round	NiTi	*	*		*	*		*
	Steel			*	*	*	*	

Figure 3.8 shows a boxplot for static frictional coefficients by the various archwire alloys by bracket type, for flat archwires, without lubrication. Again, this boxplot does not differentiate between individual manufacturers or varying normal forces. Table 3.14 shows the data from the boxplot in Figure 3.8 in tabular form.

Although it is complex, the design illustrated in Figure 3.8 does dictate a matrix, because of the quantity of information it contains. This design compares the static frictional coefficients of all archwire materials against both ceramic and stainless steel bracket material. The matrix appears in Table 3.13, where H = heat treatable archwire, N = nickel titanium, S = stainless steel, and T = titanium molybdenum archwire. The SNK comparison indicates that the frictional coefficients for all archwire types against ceramic bracket material are significantly different from those against stainless steel bracket material. The comparison also indicates a significant difference between the frictional coefficients for all archwire types

Table 3.13
SNK Comparisons of Static Frictional Coefficients for Various Archwire Types against Ceramic and Steel Bracket (flat wire, unlubricated)

		Ceramic				Steel			
		H	N	S	T	H	N	S	T
Ceramic	H		*	*	*	*	*	*	*
	N	*			*	*	*	*	
	S	*			*	*	*	*	
	T	*	*	*		*	*	*	*
Steel	H	*	*	*	*		*	*	*
	N	*	*	*	*	*		*	*
	S	*	*	*	*	*	*		*
	T	*			*	*	*	*	

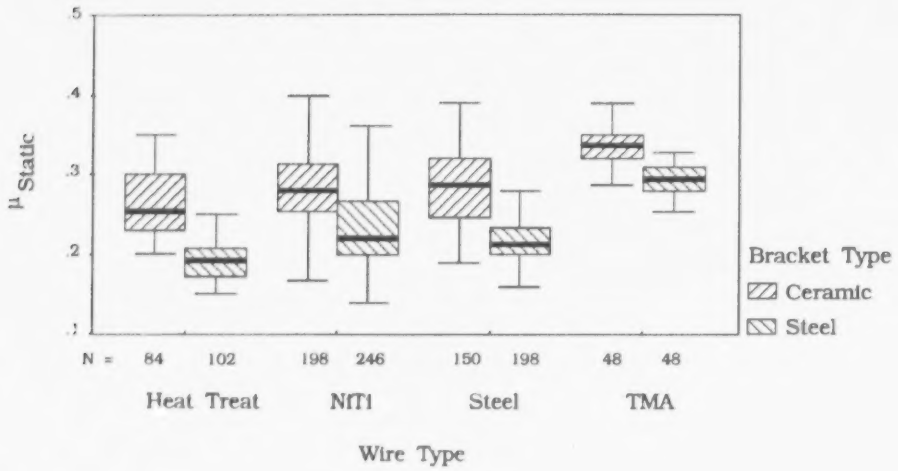

Figure 3.8
Boxplot of Static Frictional Coefficients by Wire Type by Bracket Type (flat wire, unlubricated)

Table 3.14
Frequencies - Static Frictional Coefficients for Various Archwire types against Ceramic and Stainless Steel Bracket (flat wire, unlubricated)

	Wire Type							
	Heat Treatable		NiTi		Steel		TMA	
Bracket	Cer.	Steel	Cer.	Steel	Cer.	Steel	Cer.	Steel
Number	84	102	198	246	150	198	48	48
Mean	.264	.193	.281	.243	.282	.219	.338	.293
Median	.255	.193	.280	.220	.287	.213	.336	.295
S.D.	.039	.026	.048	.066	.045	.029	.026	.021

against ceramic bracket material. Similarly, a significant difference exists between most frictional coefficients for the archwire types against stainless steel bracket material. The only exception is the nickel titanium-stainless steel pairing, for which the comparison indicates no significant difference.

B. Surface Roughness Testing

Profilometer analysis of the various archwire samples produced average surface roughness values for the manufacturer and archwire in question. The testing apparatus displays these surface roughness values in micro-inches (in. x 10^{-6}). A scatter diagram of all archwire surface roughness data, and the frictional coefficients obtained during frictional testing appears in Figure 3.9. Each point on the scatter diagram (▼, ▲, ◆, ■) represents the average surface roughness, in micro-inches, for a particular manufacturer. The scatter diagram represents four types of stainless steel archwire, five types of nickel titanium archwire, two

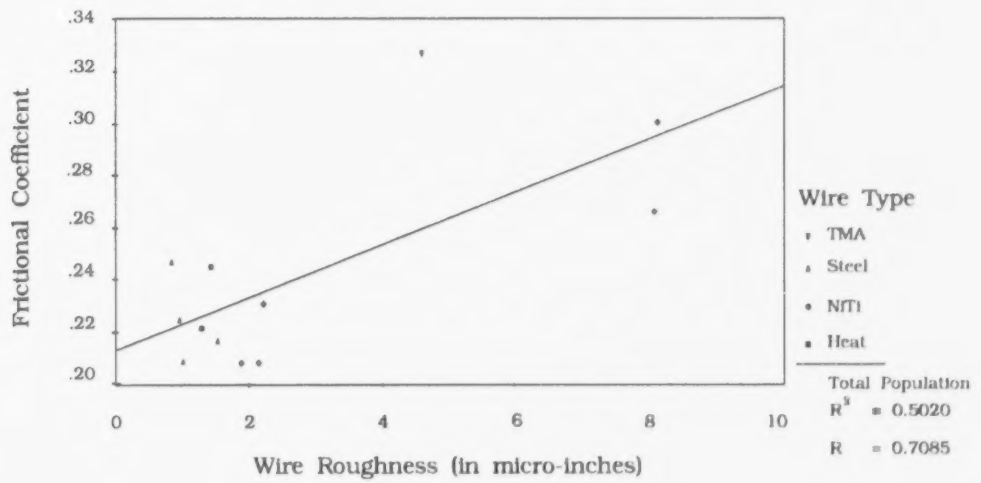

Figure 3.9
Scatter Diagram for Static Frictional Coefficients and Archwire Surface Roughness

types of heat treatable archwire, and one type of titanium molybdenum archwire. A depiction of this data appears in Figure 3.9. Figure 3.10 shows a boxplot of this data, archwire surface roughness by wire type. Table 3.15 shows the data from Figure 3.10 in tabular form. The design in Figure 3.10, pertaining to a comparison of surface roughness for the various archwire types, merits display in matrix form. This matrix, displayed in Table 3.16 indicates significant differences in archwire surface roughness. The comparisons indicate a significant difference in surface roughness between heat treatable archwire, and both nickel titanium and titanium molybdenum archwire. Similarly, the surface roughness for stainless steel archwire is significantly different from that of nickel titanium and titanium molybdenum archwires. However, the surface roughness of heat treatable and stainless steel archwires are not significantly different. Likewise, the surface roughness of nickel titanium and titanium molybdenum archwires are not significantly different.

The Pearson product-moment correlation coefficient for the scatter diagram appearing in Figure 3.9 is $r = + 0.7085$, and the coefficient of determination is $r^2 = 0.502$.

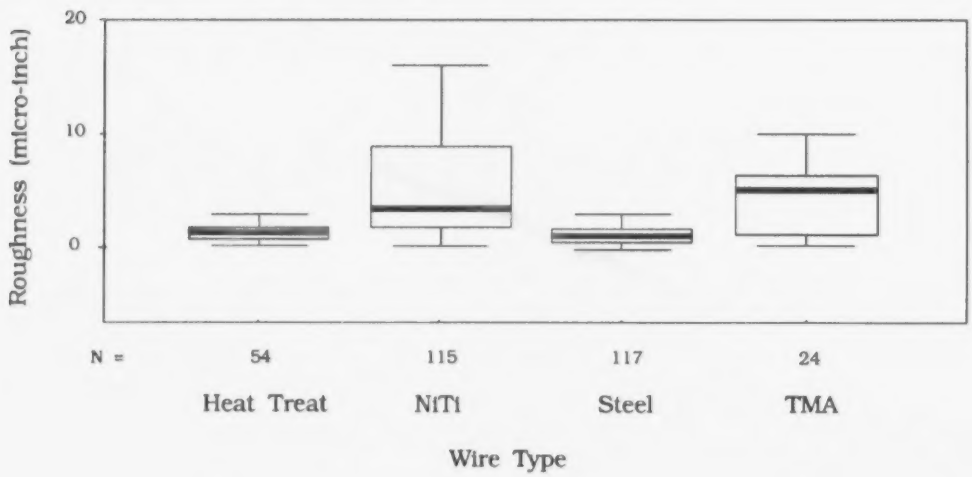

Figure 3.10
Boxplot of Archwire Surface Roughness by Wire Type

Table 3.15
Frequencies - Surface Roughness Values, in Micro-inches, for Various Archwire Types

	Wire Type			
	Heat Treatable	NiTi	Stainless Steel	TMA
Number	54	115	117	24
Median	1.350	3.50	1.0	5.10
Mean	1.363	4.932	1.082	4.592
S.D.	.776	4.221	.780	3.087

Table 3.16
SNK Comparisons of Surface Roughness for Various Archwire Types.

	Heat	NiTi	Steel	TMA
Heat		*		*
NiTi	*		*	
Steel		*		*
TMA	*		*	

C. Scanning Electron Micrographs

All micrographs taken of the archwire and bracket samples appear in Appendix B. A single micrograph represents each archwire sample, while two micrographs illustrate each bracket sample. The first micrograph depicts the base of the archwire slot for the bracket, while the second shows the area utilized for frictional coefficient testing. This allows a visual comparison to determine similarities between the two locations, on each bracket.

Since the evaluation of all micrographs is qualitative, no statistical analysis appears. A discussion individual micrograph characteristics appears in Chapter 4.

D. Method Error

The results of method error testing appear in Table 3.17. The means are represented in grams and Newtons, and standard deviations appear in grams.

Table 3.17
Frequencies for Method Error Test

	Static Friction		Dynamic Friction	
	Initial	During Testing	Initial	During Testing
Number	21	21	21	21
Mean	51.05 g (0.50 N)	48.94 g (0.48 N)	58.01 (0.57 N)	59.72 g (0.59 N)
S.D.	2.73 g	2.77 g	2.79 g	2.84 g

Chapter 4

Discussion

This thesis explored three broad themes in its attempt to disclose the nature of frictional interactions between orthodontic archwires and brackets. The first theme ascertained the nature of these interactions through an examination of frictional coefficients determined for various archwire-bracket pairings, and how certain variables affect these coefficients. The second theme elucidated the effects, if any, of archwire surface roughness on frictional coefficients. The final theme disclosed qualitative differences found in the microscopic surface finishes of various archwire and bracket types.

A. Frictional Coefficients

The experimental protocol scrutinized the effects of several variables on the resulting frictional coefficients, for an assortment of archwire-bracket pairings. These variables included: the normal force, or load across the junction between archwire and bracket; the area of contact between the archwire and bracket, determined by the use of round or rectangular archwires; the type of bracket and archwire material utilized; the difference between static and dynamic friction; the effects of lubrication; and finally, the inclusion of products from a variety of manufacturers, to determine differences between them. While some of these variables represent theoretical considerations, others may demonstrate significance relative to clinical orthodontic treatment.

1. Normal Force

One of the classic laws of friction contends a direct, positive relationship between frictional force and normal force, so the coefficient of friction does not change with alterations to the normal force. One may accept this law as ostensibly valid, within certain ranges of normal force. This relationship does degrade with excessively small or large normal forces, below the 10^{-1} N or above the 10^{3} N order of magnitude (Bowden and Tabor, 1950). The results of the experimental protocol show that, for all designs tested, alterations in the normal force did not change the observed coefficient of friction. This observation was common to ceramic brackets and stainless steel brackets, both lubricated and unlubricated (Figure 3.2, Table 3.1, and Figure 3.3, Table 3.3). The only exception occurred relative to unlubricated static frictional coefficients, with compared results from the smallest and the largest normal forces, against ceramic brackets. However, this difference is small and likely resulted from an inherent difficulty in accurately measuring frictional forces associated with small normal forces. The testing apparatus and measuring equipment tended to respond more smoothly, and create more legible strip chart recordings with the larger normal forces. This presumably resulted from initial equipment settings; at 60% of maximum gain, the strain gauge conditioner greatly amplifies noise in the system, as well as signal strength. Therefore small signals experience this system noise at a higher relative percent, increasing the difficulty in their accurate monitoring and recording.

The applicability of these findings to clinical orthodontic practice remains limited. One may expect that, although the frictional coefficient remains constant with an increasing normal force, the net frictional force will still rise. An increase in ligating force will introduce an increase in the amount of an applied force lost to friction. Conceivably, if the force of ligation reached a great enough level, the applied orthodontic force would not overcome the frictional resistance, and the intended tooth movement would not occur.

2. Area of Contact

Another classic law of friction states that frictional force, hence frictional coefficient, remains independent of contact area. Comparing the frictional coefficients obtained with rectangular and round archwires, of the same composition, allowed the testing of this law. The frictional coefficients for round and rectangular archwires nickel titanium archwires against ceramic or stainless steel bracket material were not significantly different, under conditions of unlubricated sliding (Figure 3.7, Table 3.11). The frictional coefficients for the same archwire configurations in stainless steel are significantly different, against either ceramic or stainless steel brackets, under conditions of unlubricated sliding (Figure 3.6, Table 3.9). Analysis reveals a smaller frictional coefficient for round archwires than for rectangular in these cases. Although not commonly used for this purpose, the frictional coefficient with braided archwire appeared similar to that for round archwire. A single pairing of nickel titanium round and rectangular archwires did show a significant difference with respect to frictional coefficients. Although the present results do not agree with the classic law, they do agree with previously published findings (Andreason and Quevedo, 1970, Frank and Nikolai, 1980, Kapila *et al.* 1990, Angolkar *et al.* 1990).

One must consider that, even with the maximum dimension rectangular archwire tested, the area of contact between an archwire sample and bracket sample was less than 0.9 mm^2. The potential exists for archwire sample rotation to occur during testing, and create possible interactions of 90^0 edges. This effect would greatly increase the ploughing component of friction, and result in the realization of larger frictional force values. In addition, the notion of contact area independence relative to frictional coefficient has a range, as does that of normal force independence (Bowden and Tabor, 1950). One may expect that contact areas below this range **may** result in decreased frictional coefficients.

The observation of decreased frictional coefficients, for the round archwire configuration relative to rectangular, but only with respect to stainless steel archwires defies simple explanation. This may result from the tendency for nickel titanium archwires to exhibit

generally greater frictional coefficients against either bracket surface, eclipsing any small differences between the round and rectangular configurations.

Clinical relevance of these findings relates to the preferential use of a round archwire in cases of tooth movement accomplished with sliding mechanics. The use of a round archwire in this instance should not affect the rate of clinical tooth movement, in strict theoretical terms. However, the application of an orthodontic force, prior to producing actual translation of a tooth, causes some rotation or tipping of the tooth. The amount of excess space, or 'play' between bracket and archwire, dictates the extent of this movement. Consequently, the smaller dimension round archwire permits greater freedom of tooth movement prior to maximal engagement of the bracket against the archwire, and initiation of actual translation. The normal force will increase once this engagement occurs. A rectangular archwire, not tolerating the same freedom of movement, dictates a maximum normal force level sooner after application of an orthodontic force.

These factors lead to the clinical appreciation of an apparent increase in the rate of tooth movement. When examined more closely, this apparent increase, through utilization of smaller dimension round archwire, may correlate with increased tooth rotation and tipping. Reducing the force of ligation will, inadvertently, produce this same effect by creating even more freedom of archwire movement within the bracket slot. This may explain part of the observation that self ligating brackets produce an increased rate of tooth movement. The fact still remains that frictional force is the product of the frictional coefficient and normal force, and the use of round archwires or self ligating brackets alters neither variable in this equation.

3. Archwire and Bracket Type

A frictional coefficient represents a function of surface interaction of two distinct materials. One can appreciate that two pairs of different materials may have different

frictional coefficients. Therefore, the assumption that different archwire-bracket pairings should produce different frictional coefficients, seems logical. The results indeed indicate significant differences between these pairings (Figure 3.8, Table 3.14). Testing with ceramic brackets resulted in uniformly greater frictional coefficients, when compared to stainless steel brackets. Prior experimentation also indicated a similar finding (Kusy *et al.*, 1988, Pratten *et al.*, 1990, Angolkar *et al.* 1990). Significant differences also resulted from the comparison of frictional coefficients for all archwire types tested against ceramic brackets. The archwire types, listed in descending order of frictional coefficients are titanium molybdenum, nickel titanium, stainless steel, and chrome-cobalt stainless steel (heat treatable).

The same comparisons against stainless steel brackets yielded less conclusive results. titanium molybdenum archwire still offered the highest frictional coefficient, and heat treatable the lowest. However, statistical analysis could not demonstrate a significant difference between the frictional coefficients for stainless steel and nickel titanium archwires. These results bear a strong resemblance to previously published data (Kapila *et al.* 1990, Kusy *et al.*, 1988, Pratten *et al.*, 1990, Angolkar *et al.* 1990). The most prevalent findings indicate a lower frictional force, or coefficient, with stainless steel based archwires, and a greater force or coefficient with titanium based archwires. To separate contacting surfaces, one must input energy to overcome adhesive forces. The surface free energy of the surfaces in question determine the amount of this energy input, and as surface free energy increases so does the energy input required to overcome adhesive forces (Johnson *et al.*, 1971). One may conjecture that the surface free energy of the titanium archwires is higher than stainless steel archwires.

The effects of using a particular archwire and bracket combination represent an area of great clinical significance, since the clinician may choose from many pairings. The present research suggests an approximate average 25% increase in frictional resistance, with any archwire type, when using ceramic instead of stainless steel brackets. It follows from this finding that, with a ceramic bracket, the applied orthodontic force must be 20% greater to produce the same effect as with a stainless steel bracket. An applied force of 150 grams (1.47

N) for a stainless steel bracket must increase to 188 grams (1.84 N), to overcome friction and produce the same net force. The prime consideration with any force application in a system of sliding mechanics relates to producing movement in the target tooth, while monitoring the response of the anchor unit. In a maximum anchorage situation, excessive force application may cause unwanted mesial movement of the anchor teeth. The target tooth and the anchor unit experience the same applied orthodontic force, but the response may differ. The metal bracket on a molar band and on a premolar tooth, by virtue of a smaller coefficient of friction against the archwire, may permit mesial movement of the anchor unit prior to distal translation of the target tooth. This 'loss of anchorage' tends to occur with excessive force application, whether unintentional or dictated by the use particular materials.

Some situations may indicate mesial movement of the anchor unit, and therefore necessitate anchorage loss. Application of the present results suggests utilization of ceramic brackets, and the associated increased orthodontic force levels, in these cases. The higher force levels required to overcome increased frictional resistance will presumably strain the anchorage and cause some mesial movement.

Similar findings, but to a smaller degree, apply to individual archwire types. The titanium molybdenum archwire demonstrated an approximate 25% increase in frictional coefficient, with respect to both bracket types, relative to the other three archwire types. This increase would likely impact clinical treatment in the same fashion described above for ceramic and stainless steel brackets. Differences smaller than 10% exist between stainless steel, chrome-cobalt stainless steel, and nickel titanium archwires. These differences are likely below the level of detectable clinical significance. Consequently, the clinician may expect the greatest frictional force with ceramic brackets and titanium molybdenum archwire, and the least with stainless steel archwire alloys and stainless steel brackets.

4. Dynamic versus Static Friction

One may consider clinical orthodontic tooth movement as a large number of individual movement events. A microscopic translation of the tooth determines each event. Orthodontic tooth movement is not a continuous, linear process but rather a series of "starts" and "stops". Therefore, it seems logical to examine static frictional coefficients in addition to dynamic frictional coefficients. A classic law of friction states that dynamic frictional force, and the associated coefficient is smaller than that for static friction. The experimental results indicate that the dynamic frictional coefficient is smaller than the static frictional coefficient in almost all designs (Figure 3.2, Table 3.1, and Figure 3.3, Table 3.3). The only exception occurred with lubricated sliding against stainless steel brackets, where statistical analysis failed to show a significant difference. Earlier research exhibits this same tendency toward a smaller dynamic frictional coefficient (Kusy *et al.*, 1988). A force producing tangential sliding breaks the adhesive junctions that form during static loading. This event requires an input of work proportional to the static frictional force. Once sliding commences, the formation of new adhesive junctions becomes less extensive. One can recognize a concomitant reduction in the force level required to continue tangential sliding.

5. Lubrication

The orthodontic literature contains several accounts of the effects of *in vitro* lubrication on archwire-bracket friction. Three findings emerged from previous research. The first suggests that lubrication decreases the frictional force encountered during sliding (Baker *et al.* 1987, Pratten *et al.*, 1990). The second result proposes that addition of a lubricant increases the frictional force (Riley *et al.*, 1979, Stannard *et al.*, 1986). The final finding indicates no net effect for the addition of a lubricant (Andreason and Quevedo, 1970, Kusy *et al.*, 1988).

The results of the present research support two of these possibilities. The addition of a lubricant did not affect frictional coefficients for the archwires when tested against ceramic brackets (Figure 3.4, Table 3.5). Titanium molybdenum archwire presented an exception since the addition of a lubricant increased the frictional coefficient. The same testing against stainless steel brackets found that the addition of a lubricant increased the frictional coefficients over the unlubricated state (Figure 3.5, Table 3.7). Stainless steel archwire presented the exception in this instance, since the frictional coefficient remained unaffected by lubrication.

A lubricant acts to produce some separation of two opposed surfaces in relative motion, and as a consequence, reduces friction, wear, and heat production. The quality of lubrication depends upon several factors. Some of these factors include: the load placed across the surfaces, the speed of sliding, the temperature, the nature of the surfaces and lubricant in question, and their interaction with each other. Under certain circumstances, lubrication is ineffective and may serve to increase friction. Under light loads, sliding surfaces do not display the classical laws of frictional interaction, and the addition of a lubricant may increase measured friction (Bowden and Tabor, 1950). In this case, the friction results from interaction of the lubricant film itself, since separation of the surfaces is complete. One generally makes this observation at loads less than 9.81×10^{-2} N (10 grams).

Depending on the nature of the lubricant, nonreactive metals generally receive less lubrication than reactive metals. With a lubricant such as a fatty acid, a reaction occurs between the metal surface and the fatty acid to produce a metallic soap, which actually contributes the lubrication. Such lubricants demonstrate greater efficacy with metals such as copper and zinc, and more poorly lubricate metals such as silver and stainless steel (Bowden and Tabor, 1950).

Lubricants which interact poorly with the surfaces in question, and with each other display decreased lubrication. An effective lubricant must interact strongly with the surface and its molecules must possess a strong adhesive force. Substances with highly polar molecules may exhibit poorer lubrication when compared to nonpolar substances (Bowden

and Tabor, 1950). An example of this is the superior lubricating qualities of long chain hydrocarbons and fatty acids.

In vitro archwire-bracket friction testing most often uses some form of artificial saliva substitute as a lubricant. These saliva substitutes are water based mixtures of electrolytes, cellulose compounds and possibly glycerine. The polar nature of these materials may contribute to the unpredictability their use creates in this type of experimentation. One may also expect such highly polar compounds to interact more poorly with surfaces possessing a high surface free energy. This may explain some of the results that show frictional coefficient increases with titanium based archwires.

Since artificial saliva material differs greatly from that experienced *in vivo*, any extension of the present results to a clinical setting is tenuous at best. The theoretical significance of these findings relates to any possible ability of the orthodontic materials in question to respond to lubrication. Since the results indicate some *in vitro* response to lubrication, it follows that *in vivo* lubrication may also produce a response.

6. Manufacturer Differences

The orthodontic clinician may show interest in which combination of bracket and archwire will offer the lowest frictional resistance. Therefore the clinician may also wish to know which manufacturers offer materials conducive to reducing the frictional force. Appendix C contains detailed comparisons of the archwires and brackets of five manufacturers. Any discussion of these results would simply focus on the rote listing of widely varying frictional coefficients. Many differences in frictional coefficients exist between archwire-bracket pairings for the various manufacturers, however the aforementioned results mirror the general trends in these differences.

These results definitely indicate the tendency for some frictional force differences, depending upon the manufacturer in question. This is true when comparing both different

and equivalent archwire-bracket pairings. Such information presents further choices to the clinician, with the intent of modifying frictional forces and applied orthodontic forces to meet the needs of specific situations. One may find a complete disclosure of the results concerning manufacturers' differences in Appendix C.

B. Archwire Surface Roughness relative to Frictional Coefficient

The standard deviations for archwire surface roughness means indicated a high degree of variation on surface finish (Figure 3.10, Table 3.15). Since the samples tested originated from different archwire lots, but occasionally from the same strand of archwire, one may expect surface finish to vary with location, even on an individual piece of archwire material. Previous research demonstrates this variation in surface finish, especially with reference to titanium archwires, but the present results suggest a greater degree of variation than seen historically (Kusy *et al.*, 1988, Prososki *et al.*, 1991).

Appendix A presents an overview of frictional theory, and from this one can appreciate the number of factors, including surface roughness, which influence frictional interactions. Certainly a rough surface will offer greater frictional resistance than a smooth surface, with all other conditions kept constant. However surface roughness represents a small determinant in a larger scheme. One may speculate about the role of surface roughness in frictional coefficient determination, and ultimately, frictional force determination. The results of the present research indicate a correlation coefficient for surface roughness and frictional coefficient of $r = +0.7085$, and the value of $r^2 = 0.502$. The value of r suggests a moderately strong relationship between surface roughness and frictional coefficient. One must realize that this relationship only explains about 50% of the variance of the frictional coefficient based on the variance of surface roughness. Notwithstanding this reasonably inaccurate prediction of one variable based upon knowledge of the other, it appears likely that archwire surface roughness does have a significant role to play in the frictional behaviour of

the material. Surface roughness relates to total frictional resistance as part of the deformation component of friction. One can recognize a concomitant increase in the ploughing and deformation component of friction between two surfaces in relative motion as their surface uniformity decreases.

Research conducted by Prososki *et al.* attempted to demonstrate a relationship between archwire surface roughness and frictional coefficients (Prososki *et al.*, 1991). Their results suggested r values ranging from - 0.48 to + 0.53, for a selection of stainless steel, nickel titanium, chrome-cobalt stainless steel, and titanium molybdenum archwires. Their conclusions indicated insufficient strength of correlation to dictate a significant relationship. This also represents a much poorer correlation than demonstrated by the present research. Their archwire surface roughness analysis also failed to demonstrate the same variation between the archwire types as the present research discloses. The range determined by Prososki *et al.*, for all types of archwire surface roughness, spanned 0.02 to 0.2 μm. One may expect a small r^2 value in a correlation where one correlate displays little variation.

These findings, pertaining to archwire surface roughness and frictional coefficient correlation, likely do not contain strong clinical significance. Actual frictional coefficient determination does support the trend indicating higher frictional coefficients with rougher titanium molybdenum archwire, and lower coefficients with smoother stainless steel archwire. In the absence of definitive experimental results, the clinician may wish to employ an archwire with a more uniform surface to reduce frictional force.

C. Archwire and Bracket Surface Roughness

An examination of micrographs for the various archwires leads to the creation of three distinct groups. The stainless steel based archwires show uniform linear surface striations and a homogeneity of appearance that differentiates them from the other samples. The titanium based archwires display a more random surface finish without linear striations. The surface

appears textured, with many surface inclusions. The titanium molybdenum archwire merits distinction into a separate group, owing to the degree of this texturing, mottling, and random surface finish.

A comparison of micrographs for ceramic and stainless steel brackets displays a definite distinction between the two materials. The ceramic material appears plate-like and crystalline, while the stainless steel material demonstrates surface homogeneity and uniformity. A single sample of mono-crystalline ceramic bracket material represents the only exception to this observation. This bracket shows a similar, or possibly superior degree of surface uniformity, and the lack of surface inclusions. When one compares the high magnification views of the bracket base and that area of the bracket utilized for frictional coefficient testing, one can discern only slight differences. One may expect this result, since surface finishing procedures for all brackets are uniform, and do not treat certain areas of the bracket differently. This finding can only increase the validity of tests conducted on areas of the bracket other than those intended to contact an archwire.

D. Method Error

The 21 trials performed to test the method reliability, both prior to and during actual testing, show only slight variation in means and standard deviations for their respective forces (Table 3.17). This indicated that the actual testing protocol demonstrated a consistency necessary to attain reliable data.

E. Clinical Implications

A question that remains unanswered pertains to the amount of an applied orthodontic force which one loses to the effects of friction. One must know the frictional coefficient for the materials under scrutiny and the normal force involved to answer this question. Simply

measuring the force required to drag a ligated bracket along an archwire does not provide this information. Rather, it provides a measure of the total force resisting the bracket movement. This total force has several parts, such as the friction of the archwire against the bracket base, the internal surfaces of the bracket wings, and the ligating material. One must isolate and measure each prior to estimating the losses to friction.

The present research did not examine archwire-ligating material friction. This subject is a complex one since the force of ligation varies with time, the method of ligation used, and the technique of the operator. Frictional coefficient determination for elastomeric ligation materials also poses problems, due to the nature of currently utilized ligating materials. The elastomeric ligatures commonly utilized in orthodontics demonstrate some viscous properties, in addition to their elastic properties. Likely one could consider that this material is viscoelastic in nature. Viscoelastic materials often present some difficulty to the direct experimental determination of frictional coefficients (Halling, 1976). This results from their flow properties and hysteresis (damping and rebound). Presumably orthodontic ligatures, which exhibit some viscoelastic properties, would possess the same inherent difficulties in frictional coefficient determination.

One may only estimate the amount of an applied orthodontic force lost to frictional interactions. This estimation requires a frictional coefficient for the archwire-bracket pairing, and a normal force acting across the contact area. The calculation appearing in Appendix D describes a hypothetical normal force acting between the archwire and the internal surfaces of the bracket wings. The calculation proceeds to explain the derivation of a hypothetical resultant frictional force, representing that portion of the applied force lost to frictional interaction. This resultant force, for some archwire-bracket comparisons, appears in Table 4.1. These forces represent a part of the actual force lost to frictional interaction, but estimation of the total force defies simple calculation. One can appreciate that this calculation predicts the loss of approximately 40% of a 1.47 N (150 grams) applied force to frictional interactions, considering a stainless steel archwire against a stainless steel bracket. Interestingly, the predicted loss with the use of nickel titanium and titanium molybdenum

alloy archwires is less than that associated with stainless steel archwires. This seems contradictory, since the frictional coefficients pertaining to the titanium based archwires are generally greater than those for steel archwires. However, the more resilient titanium archwires produce a smaller normal force against the internal surface of the bracket wings, after the application of an orthodontic force. The determining factor in this calculation becomes this normal force, and not the frictional coefficient. Certainly this is only a partial explanation, since the anecdotal clinical evidence still suggests a slower rate of tooth movement when utilizing titanium archwires, as compared to steel archwires.

F. Limitations

The major limitation in the present study related to maintaining standardization of the testing equipment throughout the multiple trials. Since frictional testing occurred between the archwire sample and the vertical bracket slot, rather than the horizontal archwire slot, one may question testing validity. A limitation in the number of bracket samples necessitated multiple trials with each bracket. Two trials of 200 grams (1.962 N), 250 grams (2.4525 N), and 300 grams (2.943 N) occurred on one bracket before it was discarded. The two trials at each static load employed a single archwire sample, but different sides of the same

Table 4.1
Force Losses due to Friction for Various Bracket-Archwire Combinations

	Steel Bracket	Ceramic Bracket
Steel Archwire	58.8 g (0.577 N)	75.7 g (0.743 N)
TMA Archwire	27.6 g (0.271 N)	31.8 g (0.374 N)
NiTi Archwire	11.0 g (0.108 N)	12.7 g (0.125 N)

sample were used for each trial. Each bracket sample had six separate trial conducted on its surface. The use of artificial saliva substitute creates a potential validity problem, if one generalizes the results to a clinical situation. Although the study attempted to minimize and account for frictional forces introduced into results by the apparatus, these aberrant frictional forces remained problematic and presented a limitation. Each piece of the electronic measuring, conditioning, and display equipment had its own sensitivity rating and error associated with its use; this also represented a limitation which impacted the results of the study. A final limitation in the frictional coefficient testing related to testing randomness. Ideally, each individual trial should involve a new bracket and a new archwire sample, tested blindly. These samples should also originate from different manufacturer lots. This testing regimen would result in completely random values, permitting ideal statistical analysis. However, the limited supply of testing samples did not permit a completely random experimental design.

G. Discussion of Hypotheses

Based on the results of statistical analysis, one must accept the null for Hypotheses 1, 3, and 7. No difference exists between nickel titanium and stainless steel archwires, with respect to static and dynamic frictional coefficients against stainless steel brackets, resulting in null acceptance for Hypotheses 1 and 3. Statistical analysis showed no differences in frictional coefficients with varying normal forces, demanding null acceptance for Hypothesis 7. One must accept the alternate for Hypotheses 2, 4, 5, 6, 8, 9, 10, and 11. The results indicate significant differences between static and dynamic frictional coefficients for all archwire types against ceramic brackets, resulting in alternate acceptance for Hypotheses 2 and 4. All static frictional coefficients were greater than the associated dynamic frictional coefficients, indicating alternate acceptance for Hypothesis 5. Lubrication affected frictional coefficients in a variable fashion, with some instances of increasing coefficients, and some instances of no

alteration when compared to an unlubricated case, forcing the acceptance of the alternate for Hypothesis 6. Since frictional coefficients changed with an alteration in wire configuration, one must accept the alternate for Hypothesis 8. Although Hypotheses 9 and 10 demand qualitative judgements for determinations, differences exist which are significant enough to require alternate acceptance. Since the correlation analysis shows a significant relationship between archwire surface roughness and frictional coefficients, one must accept the alternate for Hypothesis 11.

Some of the Hypotheses involved multiple simultaneous comparisons, especially concerning archwire characteristics. Many of these multiple comparisons demonstrated uniform results, with the exception of a single comparison. A single observation may force the acceptance of either a null or alternate hypothesis. Owing to the number of such multiple comparison designs, it becomes impractical to state all single comparisons as individual Hypotheses. One must exercise caution in reaching conclusions based solely upon null and alternate Hypotheses. An overall design containing multiple comparisons merits close scrutiny to separate the significant from the insignificant.

Chapter 5

Conclusions

The experimental protocol for this thesis consisted of three broad designs. The first determined frictional coefficients for various orthodontic archwire-bracket pairings and investigated the effects of altering several variables. The second design attempted to relate the archwire surface roughness to the frictional coefficient. The third design involved a qualitative comparison of scanning electron micrographs for all archwire and bracket samples.

The first design produced results which indicated significant differences between frictional coefficients for various bracket types, archwire types and types of friction. The results showed minimal differences in frictional coefficients for varying normal forces. Classic laws of friction and previous orthodontic research lend substance to these findings. The results also exhibited significant differences in frictional coefficient determination based on the archwire configuration, and the mode of lubrication. These findings run contrary to classic laws of friction, but receive some substantiation from previous orthodontic research.

The second design showed a moderate relationship between archwire surface roughness and frictional coefficients. This finding suggests that increasing surface roughness results in a concomitant increase in frictional coefficient.

The final design demonstrates qualitative differences between the surface finishes observed on various orthodontic archwires and brackets. Qualitative analysis suggests that standardized manufacturing processes do create orthodontic brackets and archwires with only minimal individual differences. The same analysis also implies that a bracket or archwire alloy may demonstrate microscopic distinctions, based on surface characteristics.

A. Suggestions for Further Study

Although many previous studies have focused on archwire-bracket friction, one sees similarities in the underlying methodology, and consequently the results. Exploring the problem from different perspectives may provide previously unknown information, and consequently a increased understanding of the orthodontic frictional phenomenon.

1. Other Sources of Friction

This thesis has suggested that three discrete elements comprise the total force of archwire-bracket friction. The first of these is the friction encountered between archwire and ligature. Friction between the archwire and the bracket's archwire slot represents the second. The third consists of friction encountered between the archwire and inner bracket wing surfaces. Previous research has disclosed an estimation of the total frictional force. The present research, through elucidation of archwire-bracket frictional coefficients, has estimated the frictional force between the archwire and inner bracket wing surfaces. Further experimentation could lead to realization of the frictional force experienced between the archwire and ligature, and between archwire and the bracket's archwire slot. This would involve measurement of the force exerted against the archwire, seating it into the bracket's archwire slot, and a determination of frictional coefficients between archwire materials and ligature materials.

2. Ion Implantation

One possible method for reducing friction in the orthodontic setting involves the use of a specialized metal surface treatment procedure. Engineering research has recognized the process, known as ion implantation, for over a decade, but its application to the field of

orthodontics is just beginning. Ion implantation improves the surface properties of metals, resulting in increased wear resistance and decreased friction. One may typically see ion implantation done with nitrogen ions (N^+), but may also see the use of metal ions, such as aluminum and copper. A device called an ion implanter accomplishes the procedure of implantation, onto a clean metal surface, under high vacuum (5×10^{-7} torr, fluence of 10^{17} ions/cm^2, current density of 4-6 μA/cm^2). The procedure produces alloyed surface layers not attainable through conventional processes. These surface layers significantly modify the surface chemistry of the metal, resulting in improved friction and wear characteristics. However, research has not yet provided a complete understanding of the effects of ion implantation on the chemical and physical behaviour of the alloyed metal (Shepard and Suh, 1982).

Experimentation with ion implanted iron and titanium show a significant reduction in friction, attributable to the formation of a hard surface layer. This layer minimized the ploughing and deformation components of friction, but does not alter stress distribution in the surface. The experimental values for frictional coefficients for iron are 0.13 unimplanted and 0.065 implanted, and for titanium 0.47 unimplanted and 0.1 implanted. Under reduced loads and with suitable lubrication, ion implantation results in superior friction and surface wear reduction, owing to the surface finish (Shepard and Suh, 1982).

Nonetheless, ion implantation does have some shortcomings. The main weakness stems from the thinness of the ion implanted layer, and possibility that it would not withstand a excessive loading or cycling. The thickness of the alloyed surface generated with an implanter energy of 100 keV is only 0.1 μm. Energy production in the MeV range increase the depth of the alloyed layer, but also the cost of implantation. Experimentation with 60 keV, 100-500 μA/cm^2 at increased temperature produces an alloyed layer several hundred Å thick, with an increased nitrogen concentration (atomic percent of 25-30% nitrogen, 70-75% base metal). Implantation at increased temperature and with increased ion dose produces an increased depth of alloy (Wei *et al.*, 1990).

Simply increasing the quality of surface finishes for brackets and archwires would likely not affect frictional interactions to an appreciable degree. Handling in a clinical setting may introduce surface imperfections which would act to negate any manufacturer introduced surface improvements. It seems the only plausible method for predictably and uniformly reducing the impact of frictional interactions would involve alteration to the metallic structure of the surfaces in question. Since ion implantation creates a new, and otherwise unattainable surface alloy, it may become a viable approach to reducing inherent frictional interactions between archwire and bracket.

It seems probable that efforts to engineer future archwire alloys would include the process of ion implantation. Frictional testing of such archwires would prove interesting, and may determine if one could realize the same friction and wear reducing advantages of the ion implantation process, as applied to orthodontics.

Bibliography

Andreason, G.F., Quevedo, F.R.: **Friction forces in the .022x.028 edgewise bracket *in vitro***. J Biomech, 1970:3(2) 151-160.

Angolkar, P.V., Kapila, S., Duncanson, M.G., Nanda, R.S., **Evaluation of friction between ceramic brackets and orthodontic wires of four alloys**. Am J Orthod Dentofac Orthop, 1990:98(6) 499-506.

Baker, K.L., Nieberg, L.G., Weimer, A.D., Hanna, M.A., **Frictional changes in force values caused by saliva substitution**. Am J Orthod Dentofac Orthop, 1987:91(4) 316-320.

Berger, J.L., **The influence of the SPEED bracket's self ligating design on force levels in tooth movement: A comparative study**. Am J Orthod Dentofac Orthop, 1990:97(3) 219-228.

Berry, G.A., Barber, J.R., **The division of frictional heat A guide to the nature of sliding contact**. Transactions of the ASME Journal of Tribology, 1984:106 405-415.

Bowden, F.P., Leben, L., **The nature of sliding and the analysis of friction**. Proceedings of the Royal Society of London, 1939:A169, 371-391.

Bowden, F.P., Tabor, D., **The area of contact between stationary and between moving surfaces**. Proceedings of the Royal Society of London, 1939:A169, 391-413.

Bowden, F.P., Tabor, D., **The friction and lubrication of solids**. Oxford University Press, 1950.

Buckley, D.H., **The metal to metal interface and its effect on adhesion and friction**. Journal of Colloid and Interface Science, 1977:58(1) 36-52.

Campbell, W.E., Thurber, E.A., Hill, M., **Studies in boundary lubrication II Influence of adsorbed moisture films on coefficients of static friction between lubricated surfaces**. Transactions of the ASME, 1948:70 401-408.

Chang, W.R., Etsion, I., Bogy, D.B., **Static coefficient model for metallic rough surfaces**. Transactions of the ASME Journal of Tribology, 1988:110 57-63.

Chang, W.R., Etsion, I., Bogy, D.B., **Adhesion model for metallic rough surfaces**. Transactions of the ASME Journal of Tribology, 1988:110 50-56.

Czichos, D., **Tribology: A Systems Approach**. Elsevier Scientific Publishing Company, 1978.

Cooks, M., **Surface oxide films in intermetallic contacts**. Nature, 1952:170 203-204.

Derjaguin, B.V., Muller, V.M., Toporov, Y.P., **Effect of contact deformation on the adhesion of particles**. Journal of Colloid and Interface Science, 1971:53(2) 314-326.

Dowson, D., **History of Tribology**. Longman Group, 1979.

Drescher, D., Bourauel, C., Schumacher, H.A., **Frictional forces between bracket and archwire**. Am J Orthod Dentofac Orthop, 1989:96(5) 397-404.

Frank, C.A., Nikolai, R.J., **A comparative study of frictional resistances between orthodontic bracket and archwire**. Am J Orthod, 1980:78(6) 593-609.

Gane, N., Pfaelzer, P.F., Tabor. D., **Adhesion between clean surfaces at light loads**. Proceedings of the Royal Society of London, 1974:A340, 495-517.

Gardner, L.D., Allai, W.W., Modre B.K., **A comparison of frictional forces during simulated canine retraction on a continuous edgewise archwire**. Am J Orthod, 1986:90(3) 199-203.

Greenwood, J.A., Tripp, J.H., **The contact of two nominally flat rough surfaces**. Proceedings of the Institution of Mechanical Engineers, 1971:185, 625-633.

Greenwood, J.A., Williamson, J.P.B., **Contact of nominally flat surfaces**. Proceedings of the Royal Society of London, 1966:A295, 300-319.

Halling, J., **Introduction to Tribology**. Wykeham Publications Ltd., 1976.

Hirst, W., Lancaster, J.K., **The influence of oxide and lubricant films on the friction and surface damage of metals**. Proceedings of the Royal Society of London, 1954:A223, 324-338.

Hisakado, T., **Effect of surface roughness on contact between solid surfaces**. Wear, 1974:28, 217-234.

Hisakado, T., **The influence of surface roughness on friction and wear in boundary lubrication**. Journal of Mechanical Engineering Science, 1971:20(5), 247-254.

Hondros, E., **Tribology**. Mills and Boon Ltd., 1971

Johnson, K.L., Kendall, K., Roberts, A.D., **Surface energy and the contact of elastic solids**. Proceedings of the Royal Society of London, 1971:A324, 301-313.

Kapila, S., Angolkar, P.V., Duncanson, M.G., Nanda, R.S., **Evaluation of friction between edgewise stainless steel brackets and orthodontic brackets of four alloys**. Am J Orthod Dentofac Orthop, 1990:98(2) 117-126.

Kato, S., Marui, E., Kobayashi, A., Senda, S., **The influence of lubricants on static friction under boundary lubrication**. Transactions of the ASME Journal of Tribology, 1985:107 188-194.

Khazanie, R., **Elementary Statistics in a World of Applications**. Scott, Foresman and Company, 1979.

Komvopoulos, K., Saka, N., Suh, N.P., **The mechanism of friction in boundary lubrication**. Transactions of the ASME Journal of Tribology, 1985:107 452-462.

Komvopoulos, K., Saka, N., Suh, N.P., **The significance of oxide layers in boundary lubrication**. Transactions of the ASME Journal of Tribology, 1986:108 502-513.

Komvopoulos, K., Saka, N., Suh, N.P., **Plowing friction in dry and lubricated metal sliding**. Transactions of the ASME Journal of Tribology, 1986:108 301-312.

Kragelsky, I.V. (editor), **Friction Wear Lubrication Tribology Handbook**. Pergamon Press, 1978.

Kusy, R.P., Whitely, J.Q., **Coefficients of friction for archwires in stainless steel and polycrystalline alumina bracket slots. I. The dry state**. Am J Orthod Dentofac Orthop, 1990:98(4) 300-312.

Kusy, R.P., Whitely, J.Q., Mayhew M.J., Buckthal, J.E., **Surface roughness of orthodontic archwires**. Angle Orthodontist, 1988:58(1) 33-45.

Moore, D.F., **Principles and Applications of Tribology**. Pergamon Press, 1975.

Miller, I., Freund, J.E., **Probability and Statistics for Engineers. Third Edition**. Prentice-Hall, 1985.

Omawa, H.M., Moore, R.N., Bagby, M.D., **Frictional properties of metal and ceramic brackets**. J Clin Orthod, 1992:14(7), 425-432.

Peterson, L., Spencer, R., Andreason, G., **A comparison of friction resistance for Nitinol and stainless steel wire in edgewise brackets**. Quintessence International, 1982:13(5) 563-571.

Pratten, D.H., Popli, K., Germaine, N., Gunsolly, J.C., **Frictional resistance of ceramic and stainless steel orthodontic brackets**. Am J Orthod Dentofac Orthop, 1990:98(5) 398-403.

Proffit, W.R., **Contemporary Orthodontics**, The C. V. Mosby Company, 1986.

Prososki, R.R., Bagby, M.D., Erickson, L.C., **Static frictional force and surface roughness of nickel-titanium Archwires**. Am J Orthod Dentofac Orthop, 1991:100(4) 341-348.

Riley, J.L., Carrett, S.G., Moon, P.C., **Frictional forces of ligated plastic and metal edgewise brackets**. J Dent Res, 1979:58, A21

Sarkar, A.P., **Friction and Wear**. Academic Press, 1980.

Shepard, S.R., Suh, N.P., **The effects of Ion Implantation on Friction and Wear of Metals**. Transactions of the ASME Journal of Lubrication Technology, 1982:104(1) 29-38.

Stanley, H.M., Etsion, I., Bogy, D.B., **Adhesion of contacting surfaces in the presence of boundary lubrication**. Transactions of the ASME Journal of Tribology, 1990:112(1) 98-104.

Stannard, J.G., Gua, J.M., Hanna, M.A., **Comparative friction of orthodontic wires under dry and wet conditions**. Am J Orthod, 1986:89(6) 485-491.

Tabor, D., **Friction - The present state of our understanding**. Transactions of the ASME Journal of Lubrication Technology, 1981:103 169-79.

Tabor, D., **Part III Boundary and extreme pressure lubrication Mechanism of boundary lubrication**. Proceedings of the Royal Society of London, 1952:A212, 498-505.

Tabor, D., **Introduction to the discussion The mechanism of friction**. Proceedings of the Royal Society of London, 1952:A212, 498-505.

Tidy, D.C., **Frictional forces in fixed appliances**. Am J Orthod Dentofac Orthop, 1989:96(3) 249-254.

Whitehead, J.R., **Surface deformation and friction of metals at light loads**. Proceedings of the Royal Society of London, 1950:A201, 109-124.

Wei, R., Wilber, P.J., Sampath, W.S., Williamson, D.L., Qu, Y., Wang, L., **Tribological studies of Ion-Implanted Steel Constituents using an Oscillating Pin-on-Disc Wear Tester**. Transactions of the ASME Journal of Tribology, 1990:112(1) 27-36.

Appendix A

Overview of Tribology

A. Historical Aspects of Frictional Theory

All types of motion that one may consider have, as a common trait, some resistance to that motion. This resistance is the friction that results from the physical interactions of solids, liquids or gases in relative motion. The study of friction, wear, and lubrication gets its name from the word 'tribology', based upon the Greek word *tribos* which means rubbing. Although a thorough understanding of tribology has only recently evolved, it has influenced the affairs of man since the use of frictional heat to ignite fires in his prehistory. One may also consider that surface interactions have governed the functioning of every apparatus built. Although historical information is incomplete and lacking during some periods, a chronology of tribology shows initially attempts to overcome the effects of friction, and then an attempt to explain friction. The history of tribology tends to parallel the development of civilizations and their technological advancements.

During early civilizations, such as those of Mesopotamia and Egypt prior to 1000 B.C., the discovery of various bearing materials and substances to act as lubricants give testimony to the desire to reduce friction. In the period from 900 B.C. to 400 A.D., advancing Greek and Roman civilization devised increasingly complicated machinery, and demanded more efficient transportation. Both necessitated the evolution of better ways to reduce friction, such as the development of better bearing materials, rolling-element bearings, and axle systems. During the Middle Ages, approximately 400 A.D. to 1450 A.D., the need for advances in the field of tribology was small, and the existing materials, bearings, and

lubricants sufficed. It was not until the Renaissance, around 1450 A.D. to 1600 A.D., and Leonardo da Vinci, that tribology began to bear the hallmark of a distinct science. His work was the first recorded quantitative study of friction, although Aristotle had recognised the force of friction 2000 years prior to da Vinci's experiments. Leonardo outlined the friction reducing effects of lubrication, and the difference between rolling and sliding friction. He realized and stated the first two historic laws of friction, namely that the force of friction varies directly with the load and is independent of the apparent area of contact. He also realized that surface roughness influenced friction, but concluded, for smooth surfaces in relative motion, the force of friction is equal to one quarter the force approximating the surfaces (Dowson, 1979).

The period prior to 1750 A.D. and the Industrial Revolution, saw the beginnings of scientific study of friction. Perhaps the most well known and influential figure in this period was Amontons, after whom the historic laws of friction are named. The results of his experiments led to three broad conclusions, the first two being restatements of da Vinci's two laws of friction, and the third indicating that the force of friction equalled approximately one third of the load. Amontons believed that the interactions of asperities on opposing surfaces provided the resistance to movement and the force of friction. Desagulier's study during the same period led to the supposition that cohesion between opposed surfaces may contribute to sliding friction. The Industrial Revolution, from approximately 1750 A.D. to 1850 A.D., saw the rapid introduction of new technology and machines that demanded an increased understanding of friction. Perhaps most influential in this period was Coulombe. Experimentation led him to the conclusion that friction resulted from the interaction of microscopic surface roughness elements, and that cohesion did play a part in frictional forces. After the Industrial Revolution, more formal study of tribology occurred, with primary emphasis on lubrication. Important figures in the late Nineteenth and early Twentieth centuries were Reynolds, for his theory of fluid-film lubrication, and the description of boundary lubrication by Hardy and Doubleday (Dowson, 1979).

Into the Twentieth century, scientific understanding of friction and lubrication continued to grow. Areas of primary interest included surface topography, contact mechanics, and surface interactions. Researchers synthesized a great deal of prior thought and fact with the results of modern experimentation and have formulated theories to explain many aspects of tribology. Current ideologies enable the understanding of the nature of surfaces, their interactions, and provide insight into the nature of frictional interactions.

B. Surface Characteristics of Solids

To facilitate an understanding of surface interactions and the roles they play in the generation of friction, one must appreciate important aspects of the surfaces in question. Several general characteristics of surfaces exist. These characteristics relate to the theoretical geometry of surfaces, which lays a foundation for the comprehension of actual surfaces. Measurement of surface characteristics likewise involves examination of degrees of roughness. One must also consider the contaminant layers present on nearly all surfaces and their function in surface characteristic determination. Overall, surfaces are not simply extensions of a solid, and do not have the same bulk properties of the solid (Buckley, 1977).

Although a metallic surface may appear smooth, even mirror-like, the microscopic reality is that any surface displays a striking, random roughness. This quality of a surface is the most important determinant of its frictional behaviour, even more significant than any potential lubrication (Moore, 1975). In this context, one may consider surface texture the cause and friction the result, for the sliding interaction of solids. The roughness of a surface exists in three quantifiable degrees, macro-roughness, micro-roughness, and molecular roughness (Figure A.1). An individual microscopic projection from a surface is termed an asperity, and is a representation of micro-roughness. Macro-roughness is a term which describes asperities collectively. The term molecular roughness delineates the irregularities associated with an asperity, or some other aspect of micro-roughness. To characterize a surface, one must consider five attributes of macro-roughness, which in turn, describe average

asperities projecting from the surface. These attributes are size, spacing, shape, and relative height of asperities, and the micro-roughness at asperity peaks (Moore, 1975).

Several methods exist to measure surface roughness, but the majority are macroscopic and mechanical. The three most commonly used methods are profilometry, cross sectional analysis, and cartography. Profilometry is a nondestructive test where the testing apparatus passes a stylus across the surface in question. The surface of the stylus tip, usually diamond or some similar material, is sufficiently small to allow its passage between and over individual asperities. The apparatus magnifies the vertical deflection of the stylus to represent surface roughness as a profile. However this examination only represents a portion of the surface equal in width to the stylus tip. Cross sectional analysis involves taking an impression of a surface, and flowing another material into the impression. Machining this combination of the two materials will yield cross sections of the surface for analysis. Cartography involves plotting the information obtained from cross sectional analysis to produce a contour map, which is a three dimensional representation of the surface (Moore, 1975).

The profile of a machined metal surface is random. As a consequence, one may apply

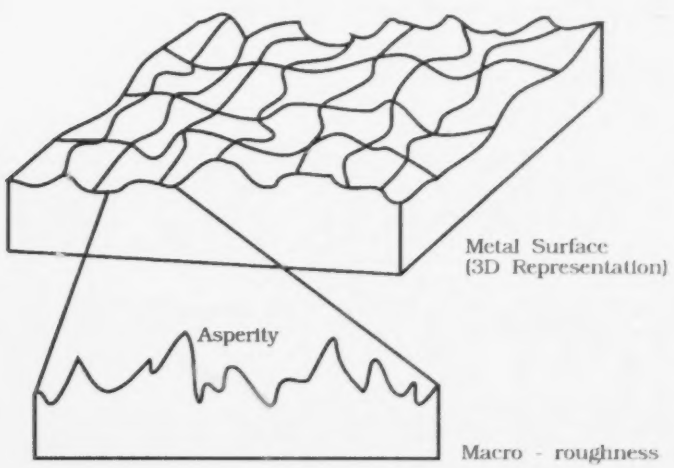

Figure A.1
Surface Topography
(modified from Czichos, 1978)

the statistical property of mean, or centre line average to a profile. This centre line average is the arithmetic mean of both positive and negative vertical deviations in a surface, relative to a reference mean line. The profile of a surface, and the centre line average provide some information about a surface. However, to theoretically characterize a surface topography is a complicated matter, due to its random geometry. Three possibilities exist in an attempt to simplify the explanation of the surface characteristics. One may consider all asperities to be one of three shapes, cuboidal, pyramidal, or hemispherical, and the surface composed of the three in a random fashion with a uniform asperity height. The second possibility is for a unique, prototype asperity with a random height distribution. The third is a constant height distribution with a random asperity configuration. Although a machined metal surface is random in nature, surface theory demands the assumption of profile constancy between all locations and in all directions, and that asperity attributes are similar. To further complicate the consideration of actual metal surfaces, one must recognise that such a surface has many components (Figure A.2).

One may only consider a metal surface to be a uniform lattice of atoms under the most exacting conditions. Typical metal surfaces exhibit an inner and outer surface layer (Figure A.2). The outer surface layer is composed of a 5 nm contaminant layer, a 0.5 nm adsorbed

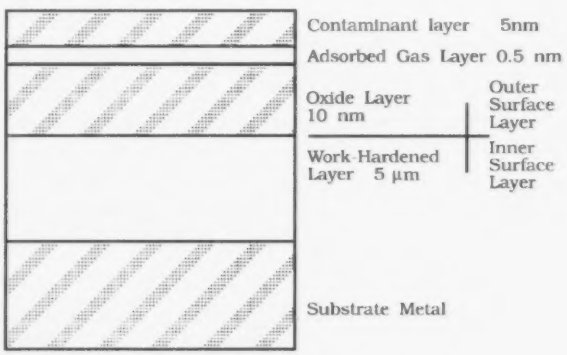

Figure A.2
Theoretical Metal Surface
(modified from Czichos, 1978)

gas layer, and a 10 nm oxide layer. The bulk material and a 5 μm work-hardened layer constitute the inner surface layer. The values for individual layer dimensions depend upon the method of surface preparation, the environmental conditions, and the nature of the material in question (Moore, 1975). A clean metal surface, under the normal indoor atmospheric conditions of temperature and humidity, may produce a surface oxide layer to a depth of 100 Å in just a few minutes. Most 'regular' surfaces will behave differently from 'ideal' surfaces.

C. Surface Interactions and Contact Mechanics

Macroscopically, one may suppose that the interaction of opposed surfaces is a simple process. However at the microscopic level, where interaction determines frictional behaviour, one requires a more thorough understanding of surface contact. Several factors govern this contact, and determine its form. Extensive deformation of opposed surfaces occurs, with the formation of specific surface to surface interactions. Atomic and electric forces dictate these interactions, and theories of surface contact attempt to simplify their comprehension. Only with an understanding of contact mechanics can one begin to understand the nature of frictional interactions.

Two terms help describe the nature of solid surface contact. The nominal, or apparent contact area refers to overt zone of overlap between the two surfaces. The real, or actual contact area describes the sum of all microscopic asperity contacts (Moore, 1975). This real contact area is extremely small when compared to the apparent contact area (Figure A.3). The real contact area is also independent of the apparent contact area (Tabor, 1952). Several general variables govern this interaction of two opposing solid surfaces. The first of these includes the macro, micro, and molecular surface roughness of the two solids. The second relates to the mechanical properties of the surfaces such as their hardness and modulus of elasticity. The third factor is the mode of deformation of the surfaces, and the fourth is the normal, or contact force across the surfaces. The final factors relate to the motion itself, first

the form taken by the motion, such as rolling or sliding, and second the velocity of the motion (Moore, 1975). In the interaction and deformation that occurs between two contacting surfaces, transmission of mechanical work occurs across the surfaces. Loading two completely elastic surfaces creates potential energy that becomes transformed into kinetic energy when the contact is released (Moore, 1975).

Interaction between two opposing surfaces in relative motion produces, in the surfaces, elastic deformation, plastic deformation, or a combination of the two processes (Kragelsky, 1981). However the majority of surfaces show plastic deformation even at light loads (Greenwood and Williamson, 1966). Nonetheless, the bulk material, in the area of these junctions shows elastic deformation (Tabor, 1952). This surface interaction produces adhesions or pressure welds between opposed asperities, leading to the creation of small metallic junctions. When two absolutely clean metal surfaces are in contact, the strength of the adhesive junctions formed is the same as the cohesive strength of the bulk metal. With

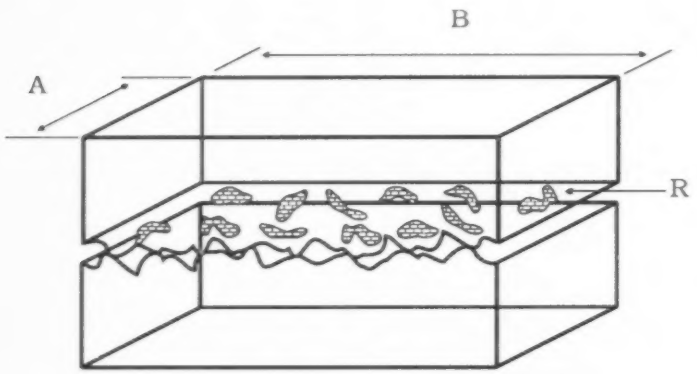

Figure A.3
Apparent and Real Area of Contact
(modified from Czichos, 1978)

two normal surfaces, adhesion is relatively slight, due to adsorbed gas and other films which prevent the formation of metallic bonds. Two other factors of importance are: the flatness of the surface, which controls the amount of the surface brought into the range of the short range electrostatic forces; and the ductility of the metal, as it affects the behaviour of the adhesive junction under a tangential load (Gane *et al.*, 1974).

In general surface theory, one may consider a rough surface as an array of identical asperities differing only in their heights above a reference plane. The mode of deformation, shape of asperities, and location of asperities are unimportant if one considers a normal height distribution of asperities. Meeting these conditions results in real contact area varying directly with the load applied across the surfaces, and experimental results validate this observation (Tabor, 1952; Greenwood *et al.*, 1971). This statement is valid whether deformation of asperities is elastic, plastic, or a combination of the two processes (Moore, 1975). However the average size of any individual microcontact is independent of the load (Czichos, 1978). Also the number of micro-contacts, and the total area of real contact between the surfaces is independent of the load (Greenwood and Williamson, 1966). This implies that as the load across the surfaces is increased, the appearance of new micro-contacts exactly matches the increase in size of individual microcontacts (Moore, 1975). The real area of contact increases due to elastic or plastic deformation, and also increases with decreasing surface roughness (Hisakado, 1974). This leads to the concept of elastic hardness, where the load predicts the area of contact. The plasticity index is a ratio of the real to the elastic hardness, and can determine whether the contact is elastic or plastic. A high plasticity index indicates elastic contact and a low index signifies plastic contact, as for metal surfaces. For most surfaces, load does not affect the deformation mode. Contact is affected by material properties such as elastic modulus and hardness, and topographical properties like the surface density of asperities, their mean radius, and the standard deviation of the centre line average (Greenwood and Williamson, 1966).

As previously stated, the normal loading of contacting surfaces produces both plastic and elastic deformation. With surface contamination, metallic surface interaction is weak, but it

becomes strong enough to cause plastic deformation with clean metal surfaces (Chang *et al.*, 1988). The resulting close union of asperities consequently produces bonding of the surfaces to create adhesive junctions. The junction of two individual asperities is termed a micro-contact. In metal and polymer interactions, two types of interactions are primarily responsible for this type of bonding are van der Waals forces are relatively long range bonding forces, acting from a few nanometres down to about one nanometre, resulting from charge distribution fluctuations in the two surfaces. Below one nanometre in metallic surfaces, metallic bonding forces supersede other forces. Covalent and ionic forces may also act, depending upon the materials in question. Metallic bonding forces are the result of surface electron interactions between the two surfaces. However, metal bonding depends on the degree of atomic lattice mismatch between the two opposed surfaces. As the amount of mismatch increases, the interfacial energy increases. The interfacial energy decreases as the two lattices come into correspondence, and falls to zero when the lattices are in register. The interfacial bonds formed between two dissimilar metals are stronger than the cohesive bonds in the weaker of the two metals (Buckley, 1977). Other factors which affect the adhesion of opposing surfaces include the nature of the solids' deformation which influences the actual contact area, and the existence of surface contaminants and films which affect adhesive forces (Czichos, 1975). Asperities separated by greater than 20 Å are subject to van der Waal's forces, but if the distance is a single atomic diameter, then metallic bonding occurs, with a tenfold increase in strength. However separation by more than 1 Å causes breakage of the metallic bond. When one considers that an adsorbed gas film is 5 Å thick, van del Waal's forces will govern the interaction, resulting in decreased intersurface adhesion (Tabor, 1981).

There are two basic models for the adhesion of materials, through asperity contacts, for approximated surfaces. These are the DMT and JRK models, named after the investigators responsible for the derivations (Derjaguin *et al.*, 1975 and Johnson *et al.*, 1971). The models assume a theoretical interaction between a spherical and a planar surface. The first theory that attempted to explain the mature of this contact was that of Hertz. This theory predicts

the distribution of pressure over the contact area between a planar and a spherical surface, such that

$$P = \frac{3N}{2\pi a^2}\left(1-\frac{p^2}{a^2}\right)^{\frac{1}{2}} \qquad (1)$$

where P = pressure, N = normal force, a = radius of the contact circle, p = distance from the centre of the contact circle to the point considered (Derjaguin *et al.*, 1975). The JRK model is based upon the assumption that surface attractive intermolecular forces result in elastic deformation of the sphere component, resulting in increased contact area beyond that given in the Hertz theory of two convex bodies in contact,

$$a = \sqrt[3]{\frac{3}{4}\pi\left(k_1+k_2\right)\frac{R_1R_2}{R_1+R_2}P_o} \qquad (2)$$

where a = radius of the circular contact area, P_o = load, R_n = respective radii, and k_n = respective elastic constants of the materials. The attractive forces in this model are in the area of the contact only, and are zero outside the contact. The JRK model represents the situation found with materials that deform elastically, and possess low surface energy, such as rubber or gelatine. To separate surfaces in contact, work must be done to overcome adhesive forces. This work creates a new surface, and is referred to as the surface free energy (Johnson *et al.*, 1971).

The DMT model assumes that, despite the ability of van der Waal's forces to increase the contact area, the tangential force required to overcome this molecular force does not increase concomitantly. Although, attractive forces exist outside the contact area (Derjaguin *et al.*, 1975). One may apply the DMT model to hard materials, like metals, which have higher surface energy. One must consider some basic assumptions when regarding surface interactions. A rough surface is isotropic , or of an average uniform composition, when considering asperities. The apex of asperities are spherical. All asperities have the same radius but the heights vary randomly. Asperities are relatively far apart, such that no interaction

occurs between asperities. No bulk deformation occurs in surface interactions, rather the asperities only experience deformation (Chang *et al.*, 1988).

The consideration of frictional interactions begins with the application of a force tending to slide one surface relative to another, but prior to the initiation of motion between the opposing surfaces. Deformation of surface contacts occurs prior to the initiation of movement, and may involves four possible forms. Minuscule movements, or microslips may occur in adhesive junctions. The degree of microslip depends upon the bond strength in the junction, and is a function of the materials involved and the type of bonding. Beyond the consideration of microslips, plastic deformations of contacts occurs prior to overt sliding (Czichos, 1978). As plastic deformation occurs, the adhesive junctions tend to increase in size, which produces a concomitant increase in the real contact area through a phenomenon called junctional growth (Figure A.4). This plastic deformation of micro-contacts can produce an increase in contact area of three to four times, depending on the metal surface cleanliness (Moore, 1975). A reduction in the strength of interfacial bonds reduces the amount of junctional growth. However the theoretical models cannot completely account for all junctional growth (Tabor, 1981). The oxide and contaminant layers found on

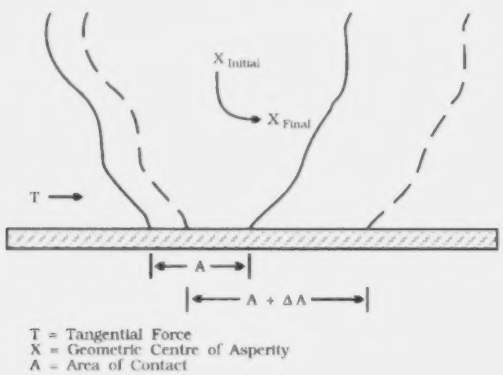

Figure A.4
Junctional Growth Phenomenon
(modified from Moore, 1975)

otherwise 'clean' metal surfaces result in the separation of opposed surfaces, to such a degree that only long range van der Waal's forces may act in the formation of adhesive junctions. Prior to initial movement, the applied force will cause shearing of these layers, a more intimate approximation of the metal surfaces, the initiation of short range metallic bonding forces, and an increase in total adhesion. Microdisplacements also occur, demonstrating that elastic and plastic processes precede actual sliding (Czichos, 1975). Decreased adhesion may also result from decreased malleability in opposed asperities, which results in fracture with sliding (Moore, 1975). General conclusions also exist to predict asperity behaviour in the true contact area. If one considers the number of asperity contacts as a constant, the true contact area increase due to elevated load is proportional to two thirds the power of the load. If the average size of asperity contacts is constant, the true contact area is directly proportional to the load. This is true for conical or spherical asperities, and with plastic deformation of the contact area. These theoretical generalizations meet with some obstacles when considering real surfaces. Contaminating metal oxide layers alter the plastic properties of the underlying metal. The small area represented by a single asperity may contain no dislocations, or breaks in its atomic continuity, and be harder than the surrounding material. The manner in which contacting asperities yield is a function of both the normal and the tangential forces (Tabor, 1981).

With fundamental elements of surface interactions understood, one may then consider the events and processes that the govern frictional interaction of surfaces in relative tangential motion.

D. Frictional Interactions

Beginning over four hundred years ago, researchers have made many attempts to uncover the relationships that dictate frictional interactions. Surprisingly, the earliest attempts to explain these associations still hold some validity today. Several terms and equations have evolved to explain the primary events in the production of friction between metals. In the

most general nomenclature, friction results from the effects of adhesion and deformation. The notion of adhesion refers to the metallic interactions of opposed surfaces and the welds, or junctions formed between their interacting asperities. The deforming aspect of friction indicates the processes of plastic flow and shearing of asperity junctions, and ploughing of one surface through another. A commonly held notion is that frictional surfaces are rough and frictionless surfaces are smooth. While this statement may have some validity, the correlation is generally false. Three basic elements govern the friction of unlubricated surfaces. The first is the area of true contacts between the sliding surfaces. The second is relates to the strength of the adhesion in the true contact areas. The third involves the mechanism of distortion for the material in proximity to the true contact areas (Tabor, 1981). However, during tangential sliding, the real area of contact fluctuates rapidly (Bowden and Tabor, 1939). The presence of oxide and contaminant films also plays a dominant role in the frictional interaction of solids. Tangential sliding produces and dissipates heat, which also influences the characteristics of the sliding and of friction.

Once an applied tangential force is sufficient to cause sliding, several assumed relationships exist to describe the observations related to frictional interactions. These relationships are historical in nature, and advances in research methods have established some question as to their validity. The first states that the maximum frictional force is proportional to the applied load. The second indicates that a frictional force is independent of the apparent area of contact between two solid surfaces. The third asserts that the coefficient of static friction is greater than that of dynamic friction. The fourth indicates that the force of friction remains independent of the velocity of sliding. The final law relationship states that a frictional force acts in the opposite direction to the direction of sliding. The following equation describes the frictional relationship between two sliding solids:

$$F = \mu \times N \qquad (3)$$

where F indicates the force required to produce tangential sliding (Newtons, $kg \cdot m/s^2$), μ represents the coefficient of friction (unitless), and N signifies the applied load or normal

force (Newtons - mass, kg x gravity, 9.81 m/s^2), as shown in Figure A.5.

The first assumed relationship is valid for circumstances other than those encountered at high pressure. The second relationship requires some qualification. It holds validity for materials that possess a definite yield point, such as metals, but is not valid for elastic or viscoelastic surfaces. The same is true for the third relationship. Sliding speed does influence frictional forces in all materials, but to a smaller degree in metals (Moore, 1975). Friction occurs as an interaction of asperities. The matching of opposed metal surface lattices in asperities therefore governs their interaction. The notion of welds forming between opposed asperities and creating microcontacts is fundamental to the understanding of the adhesion component of friction. One may consider the interaction of two opposing asperities as the most elementary occurrence in sliding interaction. The elementary processes of deformation and adhesion exert their effects on the frictional force at the level of interacting asperities (Czichos, 1978). The total frictional force is the sum of the frictional force produced by deformation and that produced by adhesion. Expressed as an equation, one may

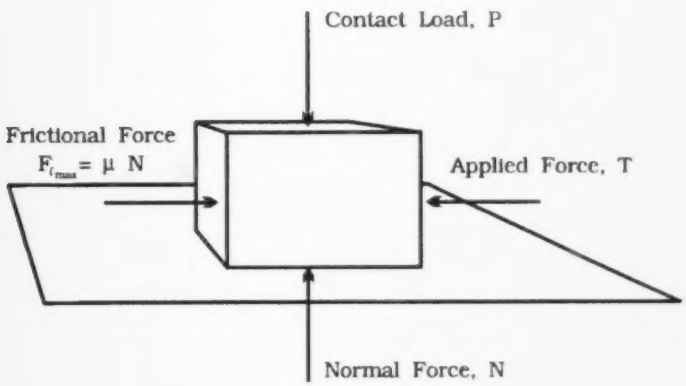

Figure A.5
Forces Encountered during
Tangential Sliding

indicate the following:

$$F_{Total} = F_{Adhesion} + F_{Deformation} \quad (4)$$

where F represents the frictional force. Dividing by the normal force produces:

$$\mu_{Total} = \mu_{Adhesion} + \mu_{Deformation} \quad (5)$$

where μ represents the coefficient of friction (Moore, 1975). The classic model of friction arising from interfacial bonding assumes that plastic flow occurs at the apices of asperity contacts. One may represent the true area of contact as

$$A_t = \frac{N}{H} \quad (6)$$

where A_t denotes the true contact area, N symbolizes the normal force, and H indicates the surface hardness. Due to interfacial bonding alone, one may represent the force required to shear the junction, or the frictional force of adhesion as

$$F_{Adhesion} = A_t \times s \quad (7)$$

where s represents interfacial shear strength. Substituting into (8) produces

$$F_{Adhesion} = \frac{N}{H} \times s \quad (8)$$

and considering (3) with (8)

$$\mu = \frac{s}{H} \quad (9)$$

For most metals, the value of $s \approx 0.2$ H, so $\mu \approx 0.2$. However this model neglects the effects of surface forces in obtaining the true contact area, and the effects of the contact load in prestressing asperities. Only asperities that do not reach their elastic limit under the contact

load can support a tangential load. As the tangential load increases, asperities not yet at their elastic limit approach a yield point. All asperity contacts fail at the point of sliding and the force at this point represents that of static friction (Chang *et al.*, 1988). The deformation component of friction accounts for the remainder of the frictional force (Moore, 1975). The static coefficient increases as the plasticity of the surfaces decreases, as with hard and smooth surfaces. One also sees an increase as the surface free energy increases, as with clean surfaces. The surface with low plasticity is smoother with more uniform asperity heights and larger asperity radii, more asperity contacts may form and the adhesion force is greater. Increasing surface energy also increases adhesion force. With a consequently lower adhesion force, rougher and softer surfaces can support smaller tangential forces (Chang *et al.*, 1988). In intermetallic interactions, a mismatch between opposed atomic lattices results in a decreasing tangential force required to produce sliding (Buckley, 1977).

Even prior to any tangential movement, the effects of adhesion can influence aspects of surface interaction, with respect to the applied load, or normal force . The normal force is a combination of the contact load and the adhesion force, associated as follows:

$$N = P - F_s \qquad (10)$$

where P indicates the contact load and F_s indicated the adhesive force. By manipulating equations (3) and (10), one understands:

$$\mu = \frac{F}{P - F_s} \qquad (11)$$

As F_s approaches P the value of μ approaches infinity. This indicates that the contact load must be significantly greater than the adhesive force for accurate experimental results (Stanley *et al.*, 1990).

Several processes comprise the deformation aspect of frictional interaction. Plastic deformation of interacting asperities on metal surfaces produces two distinct outcomes. The metal of the asperity undergoes work hardening adjacent to the micro-contact, often increasing its yield point to beyond that of the softer metal. An applied tangential force

produces the deformation that generates junctional growth. However the effects of junctional growth are generally so much greater than those of work hardening that one may disregard the influence of the latter (Moore, 1975). The interaction and subsequent separation of a micro-contact involves three theoretical events: ploughing which is composed of elastic and plastic deformation of the asperities, adhesion bonding, and junctional shearing with elastic rebound. Ploughing refers to passage of the asperities from one surface through those of the other, most easily understood if one considers a hard surface sliding across a soft one (Czichos, 1978). The nature of ploughing is the creation of grooves in the opposing surface, such that one may ascribe a portion of total frictional force to grooving. In addition, the grooving process creates a surplus of material ahead of an individual asperity producing a groove, and a portion of total friction relates to this accumulation and its deformation (Moore, 1975). So that sliding may occur, a force which produces sliding must be sufficient to shear the adhesion bonding that exists between the opposed surfaces (Czichos, 1978). Ploughing by hard asperities and wear debris plays a predominant role in sliding friction. The coefficient of friction depends upon the surface roughness, the size of wear debris, and the environmental conditions. Overall, frictional coefficients are the sum of asperity deformation, ploughing of wear particles trapped between sliding surfaces, and adhesion. In unlubricated sliding, the ploughing component may be more important than that of adhesion. Under specific conditions lubrication, ploughing is the most important, with adhesion and lubricant film shearing playing smaller roles. Ploughing becomes so important since its action creates ridges and wear debris. Lubrication acts to reduce the depth and width of ploughing grooves. The presence of oxide films on metal surfaces may result in essentially elastic deformation of the surfaces during sliding, that results in reduced frictional forces. The reduction of plastic deformation and ploughing reduces friction (Komvopoulos *et al.*, 1986). In the case of opposing hard and soft surfaces, the coefficient of friction, and the wear rate of the softer surface increase with the roughness of the hard surface. This is due to wear particle formation through ploughing into the softer surface. The coefficient of friction, and wear of the softer surface decrease as yield increases prior to the onset of plastic

flow of asperities (Hisakado, 1978). Ploughing may account for the greater part of a frictional force if the adhesive force of friction is small. As asperities plough the opposing surface, work hardening of both surfaces occurs, and they may or may not form adhesive junctions. During sliding, the true area of contact remains indeterminate (Tabor, 1981).

Friction will depend, to a certain degree, upon the experimental conditions under which one measures it (Bowden and Tabor, 1950). At slow tangential sliding speeds, the strength of metallic junctions is often greater than that experienced at increased speeds. One sees that static friction is generally greater than dynamic friction. One consequence of this observation is that the process of tangential sliding is not a continuous one; surfaces "stick" until a sufficient tangential force produces a break in the processes of surface interaction. At this point a "slip" occurs, the surfaces slide past one another, they reestablish a "stick" relationship, and the process repeats. One observes this behaviour regardless of surface finish (Bowden and Leben, 1939). The "stick" results from the momentary increase in static friction between the surfaces, and the "slip" is a consequence of the decreased dynamic friction experienced during the slip episode (Bowden and Tabor, 1950).

Unless a surface receives specialized preparation and handling, one invariably sees contaminants associated with the surface. These contaminants commonly take the form of adsorbed gases and moisture, and oxidation products. Placing a load across two surfaces does not generally break down their surface oxide films; this occurs as a consequence of tangential sliding. The formation of oxide films usually acts to decrease the associated coefficient of friction. The coefficient of friction for stainless steel on stainless steel, oxidized at room temperature for $\approx$ 10 weeks is $\mu = 0.20$, and for clean stainless steel surfaces $\mu \approx 0.60$ (Hirst and Lancaster, 1954). An increase in the applied load causes a breakdown of the oxide film, with a concomitant increase in the friction between the surfaces. Through the disruption of oxide films, tangential sliding may increase the frictional force by increasing the amount of clean metal surface available to participate in metallic contact (Cooks, 1952). However the exact manner in which oxide films act to influence frictional relationships remains a mystery. This is largely due to the fact that current interfacial bonding models do not completely

explain oxide layer bonding (Tabor, 1981). The presence and nature of other surface contaminants such as gases, or contaminants from handling, plays a paramount role in the frictional behaviour between seen between common, or ordinary surfaces (Tabor, 1952). Handling contaminants in a layer as little as one molecule thick will affect frictional behaviour, and partial removal has little effect since such contaminants have the ability to migrate over a metal surface.

In any tribological system, such as the sliding of opposed metal surfaces, there is an input of work, an output of work, and a concomitant storage, transfer and loss of energy. The input of work must equal the sum of the output of work and the radiant loss of energy, storage of energy, and transfer of energy to another part of the system. Transmission of power, or the rate at which work occurs, occurs through the system, from input to output. However the system does not transmit all of the input power. Frictional loss accounts for this power that the system does not transmit. The dissipation of energy through frictional loss occurs through several mechanisms. Energy may be stored in the system, through distortions in the atomic lattice of surfaces. Energy may be dissipated through the emission of vibrations or acoustic waves, light, and electrons. Most importantly, energy dissipated through the generation of heat. At the atomic level, asperity interactions lead to distortions of the atomic lattice of the material, and vibration that become evident as heat. Since the ultimate site of heat production is the micro-contact, local increases in temperature occur. These temperature fluctuations result when sufficient tangential force produces a "slip". The rise in temperature occurs quickly, followed by an equally rapid fall, with the entire event taking less than $1/1000^{th}$ of a second (Bowden and Leben, 1939). The remainder of the system conducts this heat so that heat generation also occurs as an increase in temperature of the entire system (Czichos, 1978). Frictional heat in sliding surfaces produces an increase in temperature except in cases of slow speeds or light loads. This temperature increase has an effect on the mechanical and metallurgical properties of the surface, and also on the oxide film. The local increases in temperature at micro-contacts are termed flashes. In addition to their fleeting duration, they are small in area, and are constantly changing location with

the areas of real contact. Generally an oxide layer increases the resistance of surfaces, producing increased temperature changes (Berry *et al.*, 1984).

Frictional behaviour of surface results from a complex interrelation of conditions, events and affiliations, some momentary and others ongoing. Under ideal conditions, some appreciation of these processes exists, but for 'real life' surfaces, their explanation and understanding remains a complexity. Current thinking can explain some aspects of adhesion between metal surfaces, but poorly interprets the adhesion between surfaces and oxide films. The deforming effects of sliding remain beyond comprehension (Tabor, 1981). Despite many theories and strides in experimentation, frictional behaviour eludes a complete understanding.

E. Lubrication

One may influence and alter frictional processes by incorporating the process of lubrication. Lubrication functions to disassociate surfaces sliding past one another, through the use of a film of material which shears easily and does no damage to the surfaces in question (Moore, 1975). The lubricant also acts to prevent the growth of metallic welds (Cooks, 1952). Based on the potential thickness of the lubricant film, its distribution on the sliding surfaces, and the nature of the surfaces, one may distinguish three main categories of lubrication. Hydrodynamic lubrication occurs when the lubricant film thickness is greater than the combined surface roughness dimensions of the sliding surfaces. The shear resistance, or viscosity of the lubricant film provides the resistance to motion in this type of lubrication. A high lubricant viscosity, high tangential speed or small normal force characterize this mode of lubrication. When elastic deformation of the interacting surfaces influences hydrodynamic lubrication, the lubrication mode becomes known as elastohydromdynamic lubrication. Important in a consideration of elastohydrodynamic lubrication are the effects of high pressure on the lubricant viscosity, and the behaviour of the elastic surfaces. Mixed lubrication results when conditions do not allow complete hydrodynamic separation of the

surfaces. Some asperity interaction occurs, with the lubricant filling surrounding voids between the two surfaces. The lubricant film may exist as a layer just a few molecules thick, bonded to the surface by strong molecular forces, with no bulk fluid properties. However, more complex situations exist where surface interaction may completely remove this molecular layer and allow extensive surface contact. This represents the condition of boundary lubrication. This mode of lubrication governs the interaction of metal surfaces (Moore, 1978). Bulk viscosity of the lubricant plays little part in determining the frictional behaviour of the surfaces under this mode of lubrication (Bowden and Tabor, 1950).

One must consider that in almost all surface to surface interactions, a substance such as water or a surface contaminant exists in the interface, and will act as a lubricant. If such a lubricant forms a uniform layer over both interacting surfaces, rather than existing as a free flowing liquid, the situation is termed sub-boundary lubrication. However the presence of liquids in the interface of solid surfaces may increase adhesive forces. This phenomenon is attributed to fluid pressure within the liquid bridges that join the solids. These liquid bridges have negative mean curvatures, consequently the fluid pressure pulls liquid from surrounding areas into discrete bridges. A classic observation finds greatly increased adhesion in high relative humidity, which forms many liquid bridges at the contact zones. This situation would likely occur where the liquid has a low affinity for the surface. With a strong interaction between liquid and solid, an equilibrium would favour the formation of a uniform layer of liquid, however the actual situation likely exists between the two extremes. The model presented shows that even though the surface free energy of lubricant may be less than that of a solid, one may see an increase in adhesion force relative to the unlubricated state, with out the formation of liquid bridges. There exists a critical lubrication thickness above which adhesion force increases rapidly, and smoother surfaces reach this point with thinner lubricant films. Rough surfaces are less sensitive to increasing lubricant film thickness, and therefore have less adhesion force relative to the unlubricated condition (Stanley *et al.*, 1990).

A model of boundary lubrication suggests that the friction between boundary lubricated surfaces is the sum of the force required to shear the lubricant layer and the force resulting

from plastic deformation of contacting asperities. The force required to shear metallic junctions also factors into the equation that comprises the total friction (Tabor, 1952). Difficulties encountered when applying this model to actual situations include uncertainty related to the ratio of asperity and lubricant supported contacts, and differences between actual and theoretically calculated frictional coefficients. Komvopoulos *et al.* performed a study which showed that the principal mechanism of friction in boundary lubricated sliding is ploughing (Komvopoulos *et al.*, 1985). They contend that lubricant shear and asperity adhesion contribute to a smaller degree. The coefficient of friction depends upon the particle size and shape of trapped wear debris. However for a surface with diminished mean asperity height, and smaller wear debris particles, adhesion and lubricant shear may play a prominent role in the genesis of friction. Kato *et al.* present a model of surface contact in boundary lubricated surfaces. At an asperity contact which becomes larger than the lubricant thickness layer, the area of metallic contact carries the normal force, as shown in area A, Figure A.6. Where asperities do not contact, the lubricant layer carries the normal load, as shown in area C. Where the metallic contact area is smaller that the lubricant thickness, both the lubricant and the metallic contact sustain the normal load, as shown in area B.

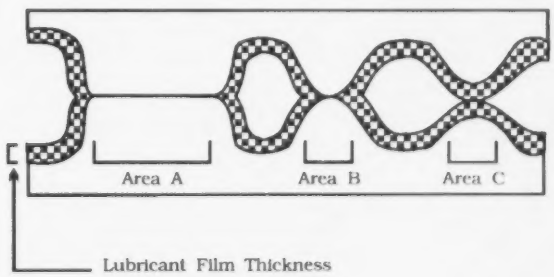

Figure A.6
Contact under Boundary Lubrication
(modified from Kato et al., 1985)

Where the lubricant thickness supports the normal load, the pressure on the lubricant equals the yield pressure of the metallic contact (Kato *et al.*, 1985).

Another investigation by Komvopoulos *et al.* attempted to determine whether the presence of oxide films on metal surfaces minimized plastic deformation of these surfaces during sliding, reducing friction and wear. The study finds that under conditions of lubrication with mineral oil, oxidized metal surfaces had lower frictional coefficients than non-oxidized surfaces. Actual frictional coefficients found included 0.45 for unoxidized aluminum and 0.1 for an oxidized surface, with similar results of 0.18 and 0.12 for unoxidized and oxidized copper (Komvopoulos *et al.*, 1986). Light loads combined with the oxide thickness tend to reduce frictional coefficients, conceivably by reducing the effects of ploughing. The oxide surface in such cases appears to deform elastically, rather than plastically. This study suggests that an oxide film of any thickness may reduce the effects of friction, depending on the normal load. This is in contrast to previous thought, which assumed a frictional reduction with oxide layer thickness beyond a critical value. When sliding does not rupture the oxide film, oxide-oxide contacts deform elastically, with the result of frictional reductions. Under conditions of boundary lubrication, the oxidized metal surface may exhibit reduced friction. This follows since, without plastic deformation of the surface, lubricant shear primarily contributes to the frictional force. Oxide-oxide contacts deform elastically if thick and compact, but if thick and porous, rupture occurs easily and plastic deformation of the surface occurs with its attendant increase in frictional force. Disruption of the surface oxide layer results in increased wear and a higher frictional force (Komvopoulos *et al.*, 1986). However the protective action of the oxide breaks down under heavy loads, resulting in increased friction. The slowly formed, thin oxide layer acquired at room temperature, can reduce friction more than a thick layer produced by a rapid oxidation process, which predisposes to a higher frictional coefficient (Whitehead, 1950). However, the prevalent finding is that the presence of an oxide film supplements the effects of lubrication (Hirst and Lancaster, 1954).

Ideally under boundary lubrication metallic interactions should contribute minimally to friction, but should only be responsible for wear processes (Tabor, 1952). However surface damage will likely occur under conditions of boundary lubrication. Since extensive surface to surface contact is possible, ploughing and wear debris formation occurs. A good boundary lubricant should therefore shear easily, while reducing metallic interactions. Fatty acids tend to act as the best substances for boundary lubrication. However reaction between the fatty acid and metal surface produces a metal soap, which is the actual substance of boundary lubrication (Bowden and Tabor, 1950). The conditions of lubrication also affect the coefficients of friction, which tend to vary with the applied loads. However one can normally relate the breakdown of boundary lubrication to deformation of the bulk material rather than to alterations in the applied load (Hirst and Lancaster, 1954).

A lubricant may not always act to facilitate tangential sliding through a reduction in frictional processes. Campbell *et al.* found that contamination by a film of adsorbed water at the solid-lubricant interface increased the static coefficient value. Steel surfaces, lubricated with paraffin, experienced a static frictional coefficient of 0.35 under dry conditions, and a coefficient of 0.6 when wet. Their general finding was a 40-70% increase in the static frictional coefficient in 75% relative humidity, as compared to dry conditions (Campbell *et al.*, 1948). A possible explanation relates to a weaker bond between the lubricant and an adsorbed water surface, allowing asperity proximity to increase. Boundary lubrication at light loads may also result in a frictional increase, possibly due to adhesion between surface films of the lubricant (Whitehead, 1950).

A variety of events and processes govern the result of surface interactions that one ultimately interprets as friction. Characteristics of individual surfaces, and associated contaminant films influence their mutual interaction, and the nature of their contact mechanics. The actual mechanisms responsible for friction have many possible influences, including the effects of associated lubrication. All interactions that collectively produce friction have many individual complexities. One can appreciate the intricacies of the phenomenon known as friction.

Appendix B

Plates of Bracket and Archwire Samples

A. Plates of Bracket Samples

The following is a complete photographic representation of all bracket samples utilized by this study. The plates illustrate a total of nine bracket samples. Two photographs depict each bracket, with the first revealing the surface which would be in contact with an archwire. The second photograph depicts the area of the bracket against which the archwire sample rested during testing. Each photograph portrays two different views. The lower half of each frame is a low magnification portrayal of a large section of the bracket, to permit one's orientation to the surface of the bracket in question. A smaller area in this frame delineated by white rectangular box represents the view that one sees in the upper half of the frame, at a corresponding increase in magnification. The letter-number combination in brackets, after the plate's caption, refers to the SEM identification code utilized to catalogue each sample bracket.

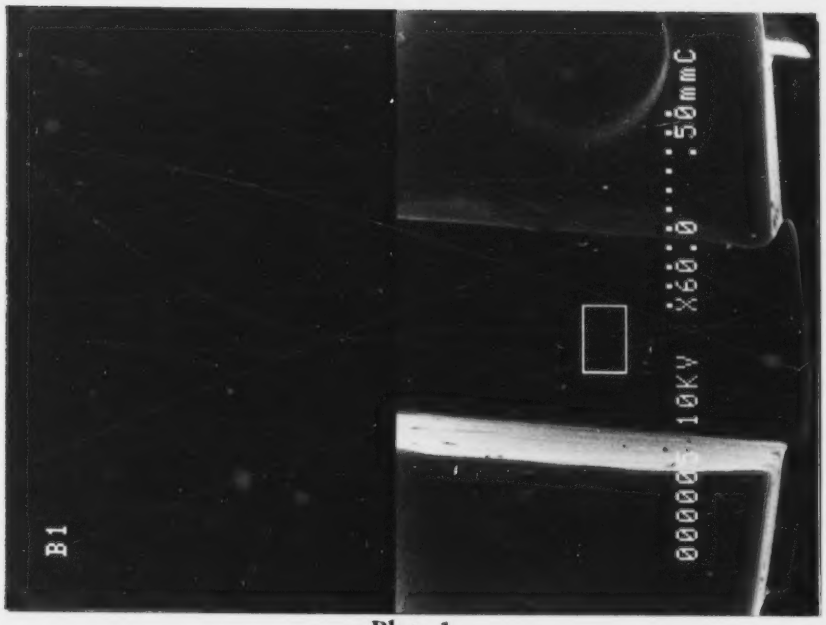

Plate 1
Micrograph of Cerum Stainless Steel Bracket Slot (B1)

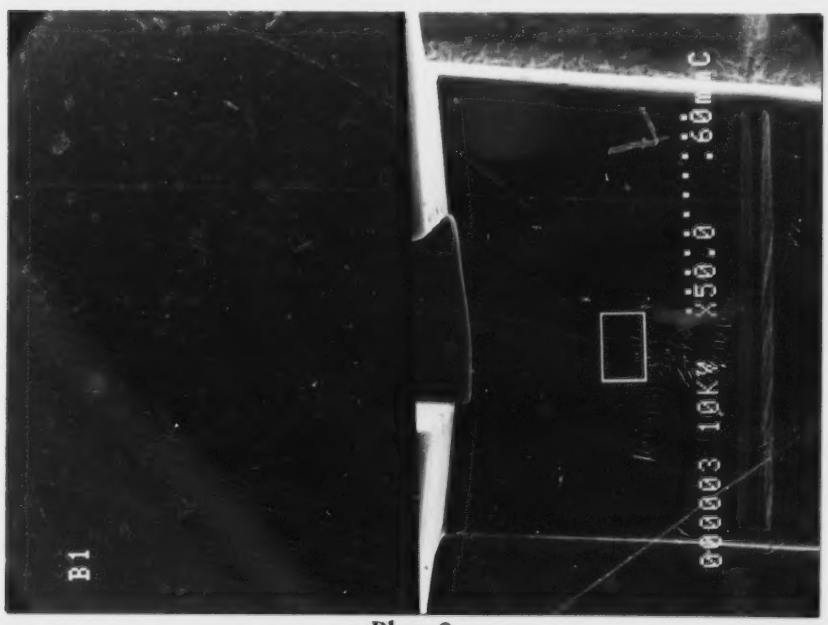

Plate 2
Micrograph of Cerum Stainless Steel Bracket Base (B1)

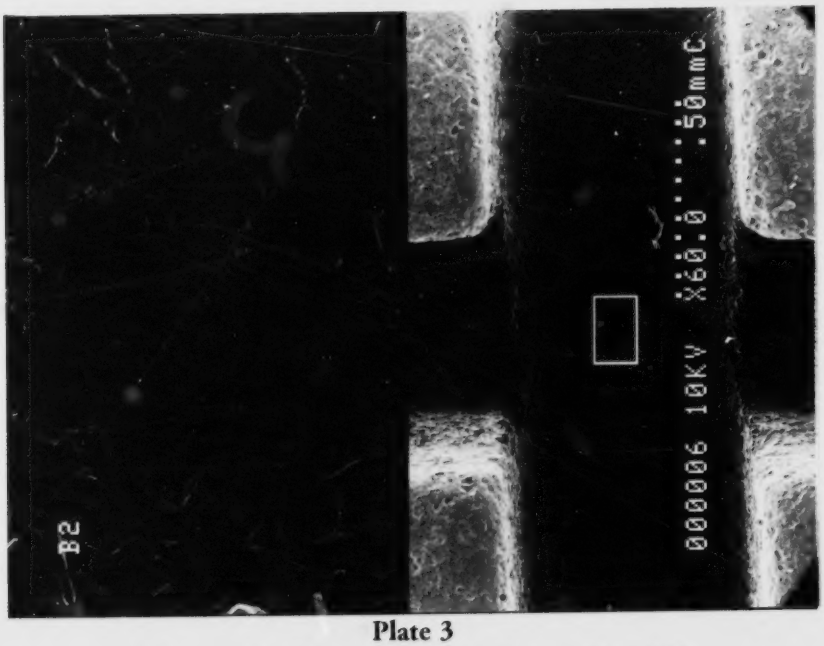

Plate 3
Micrograph of Cerum Ceramic Bracket Slot (B2)

Plate 4
Micrograph of Cerum Ceramic Bracket Base (B2)

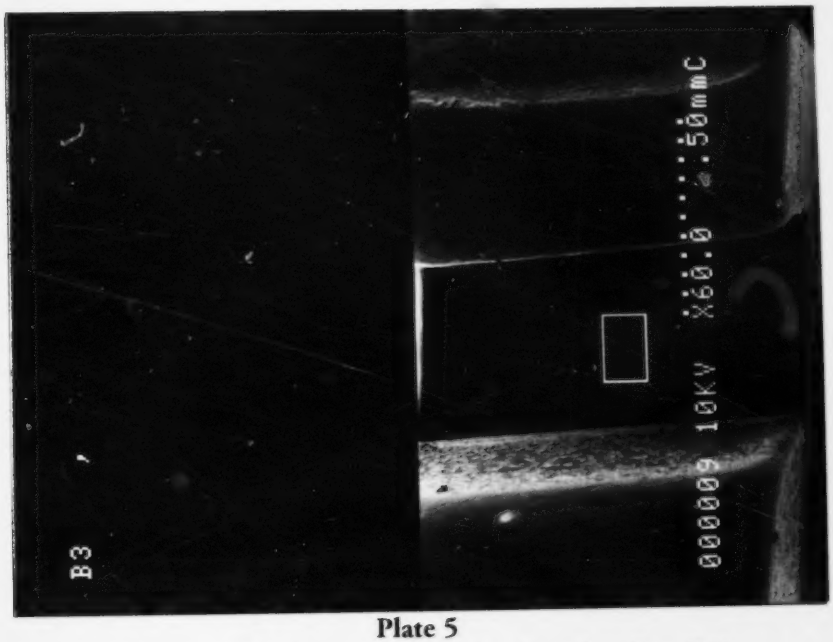

Plate 5
Micrograph of Ormco Stainless Steel Bracket Slot (B3)

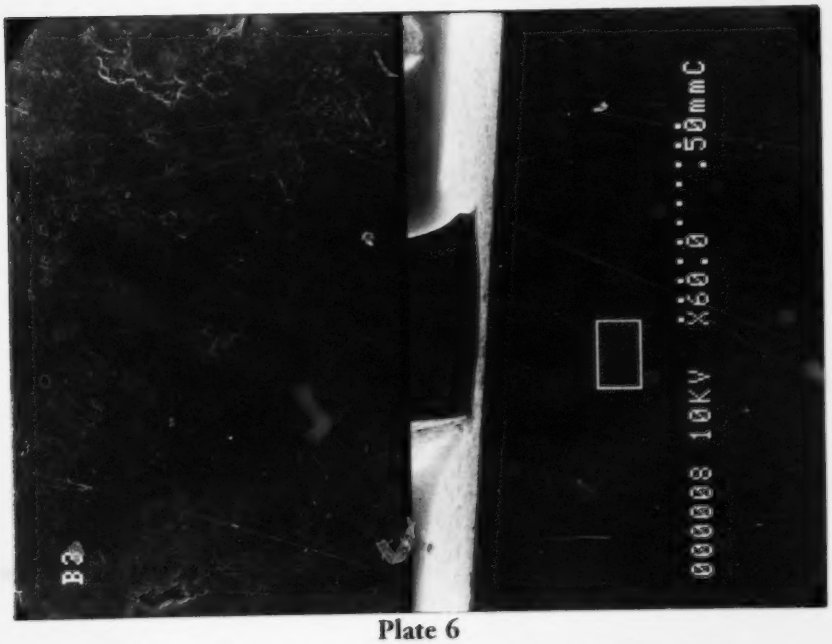

Plate 6
Micrograph of Ormco Stainless Steel Bracket Base (B3)

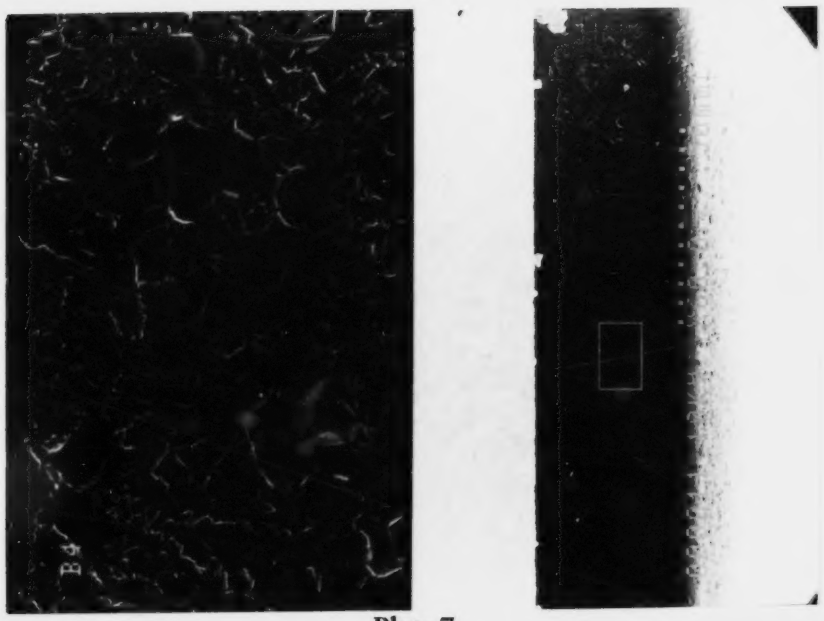

Plate 7
Micrograph of Ormco Ceramic Bracket Slot (B4)

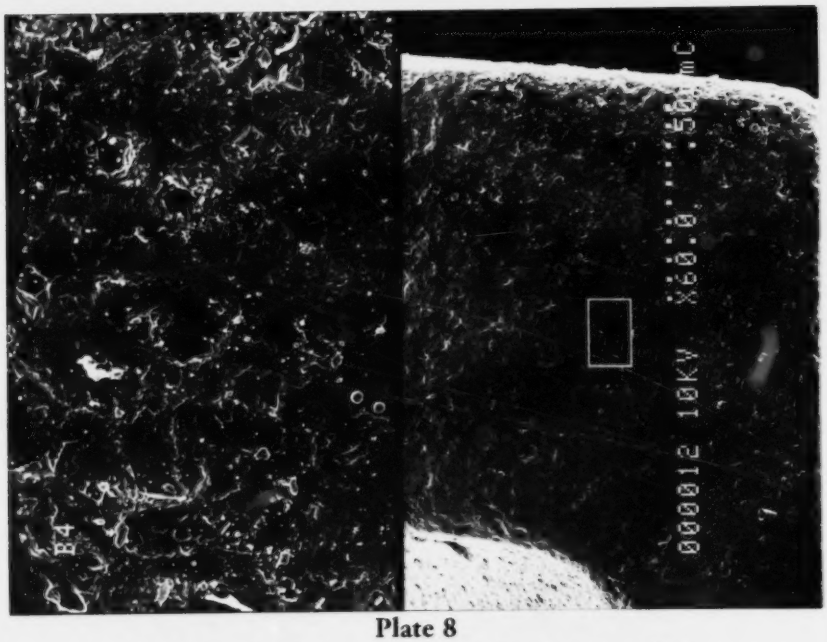

Plate 8
Micrograph of Ormco Ceramic Bracket Base (B4)

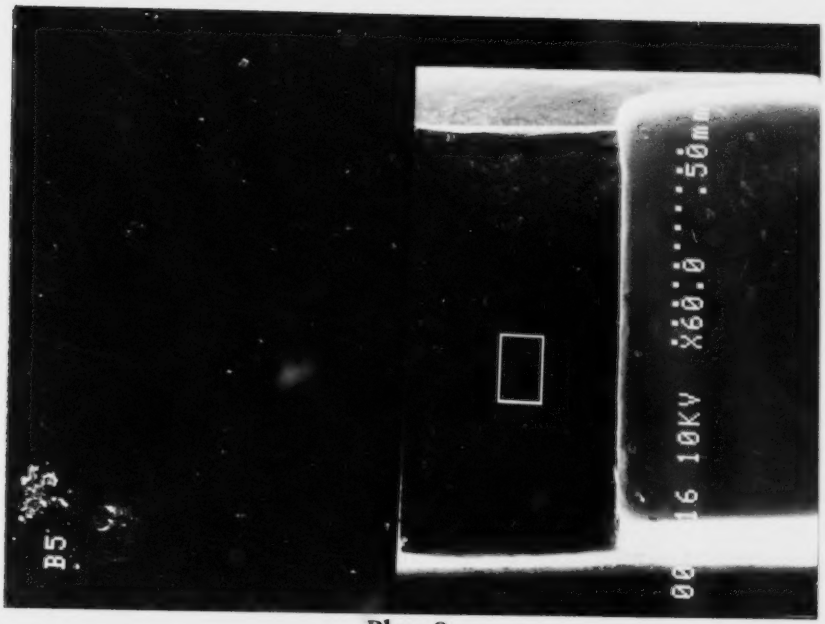

Plate 9
Micrograph of RMO Stainless Steel Bracket Slot (B5)

Plate 10
Micrograph of RMO Stainless Steel Bracket Base (B5)

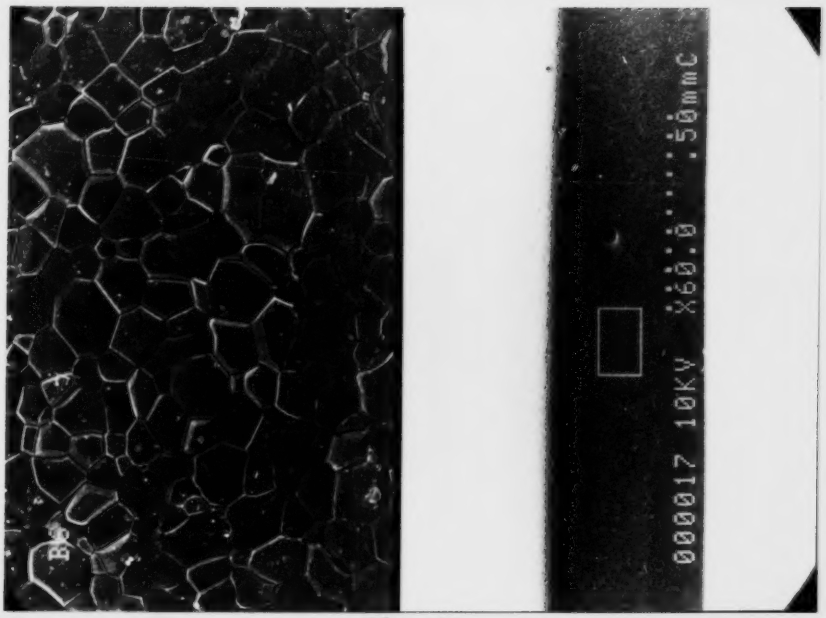

Plate 11
Micrograph of RMO Ceramic Bracket Slot (B6)

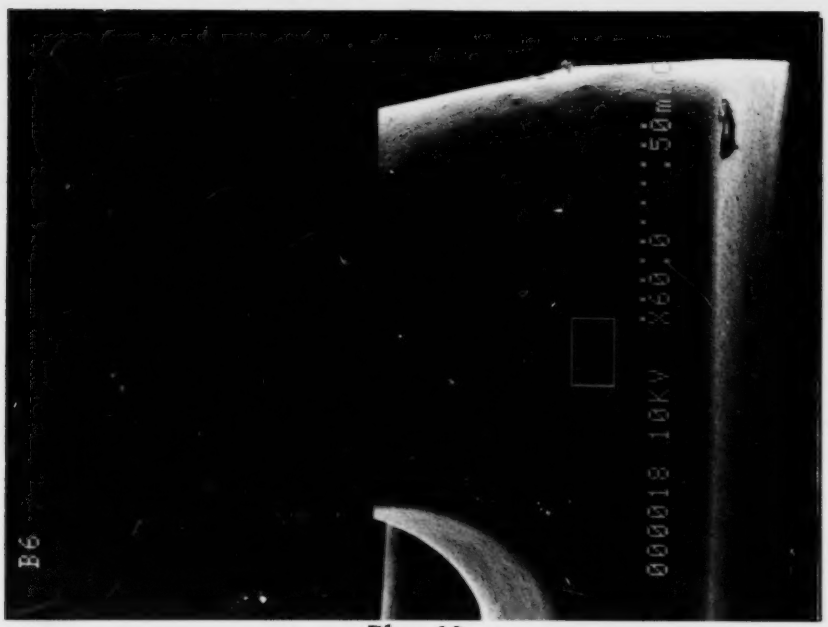

Plate 12
Micrograph of RMO Ceramic Bracket Base (B6)

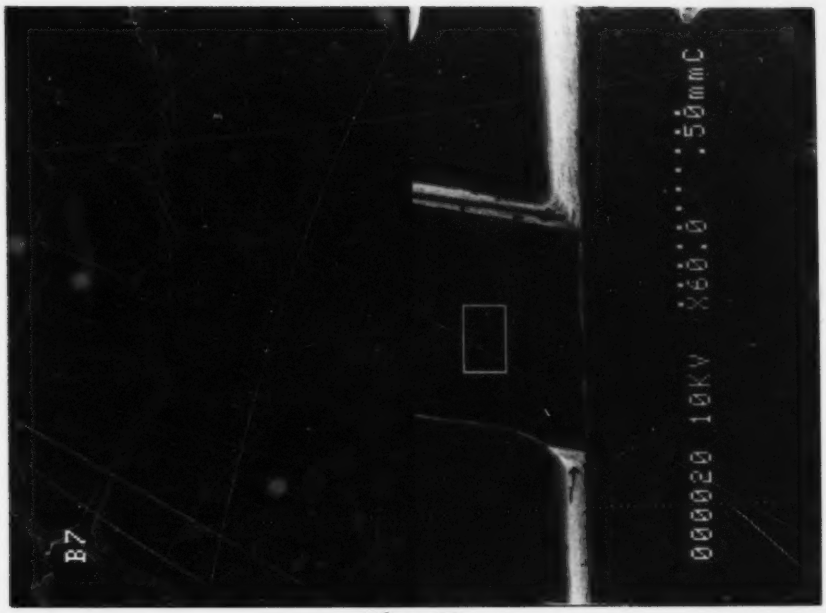

Plate 13
Micrograph of A Co. Stainless Steel Bracket Slot (B7)

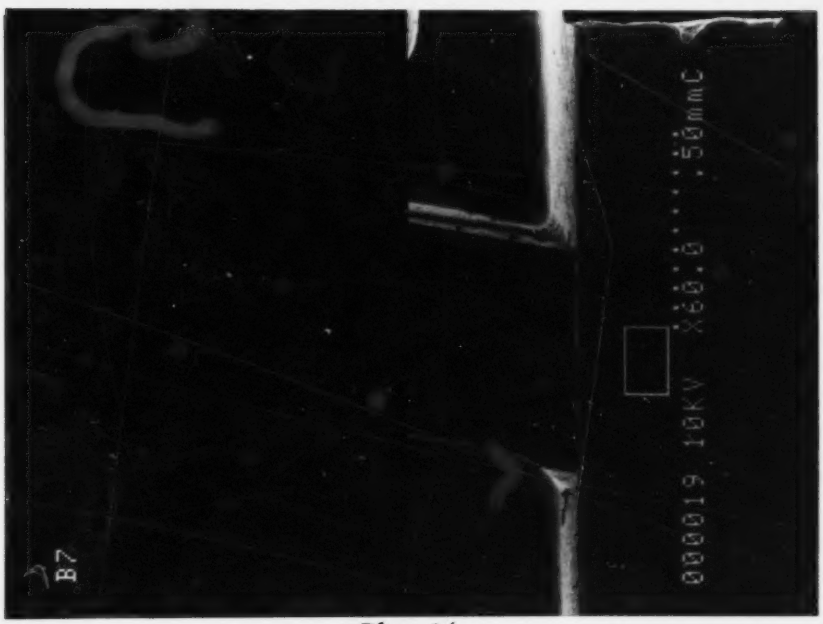

Plate 14
Micrograph of A Co. Stainless Steel Bracket Base (B7)

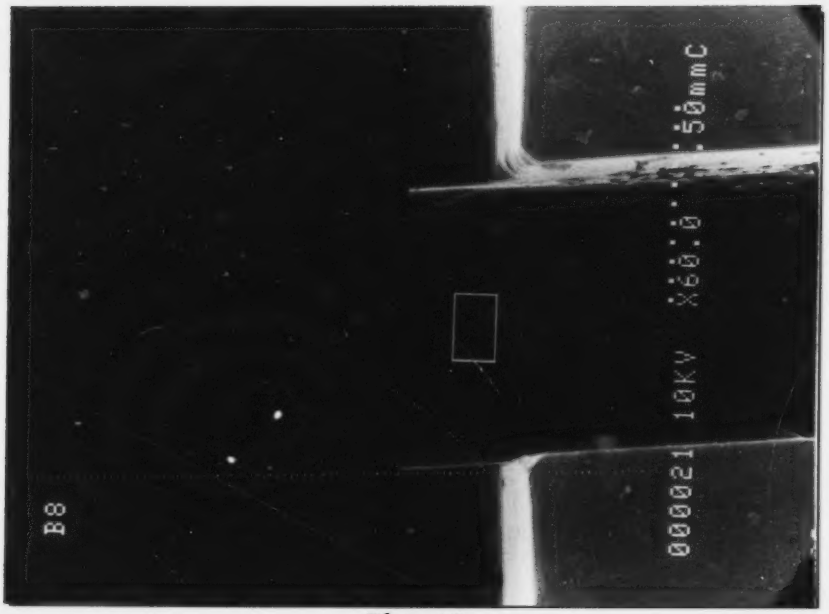

Plate 15
Micrograph of A Co. Ceramic Bracket Slot (B8)

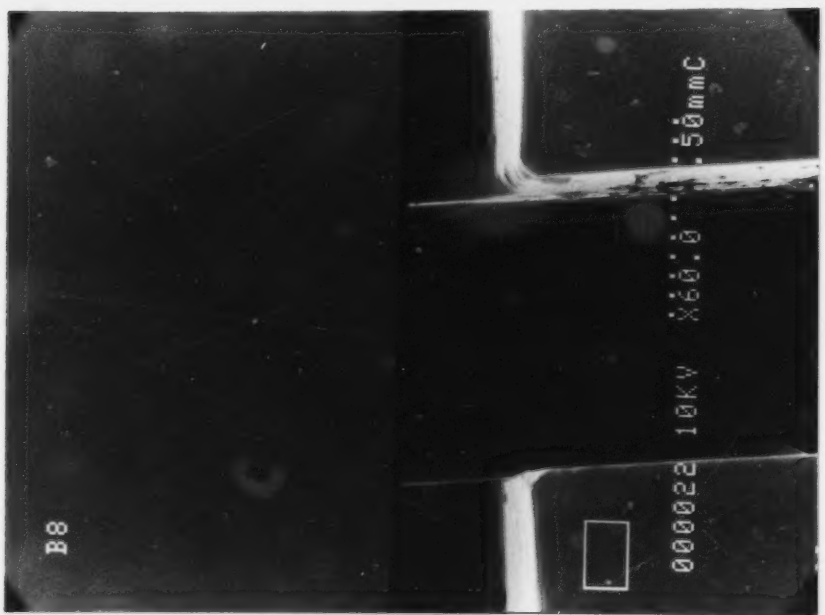

Plate 16
Micrograph of A Co. Ceramic Bracket Base (B8)

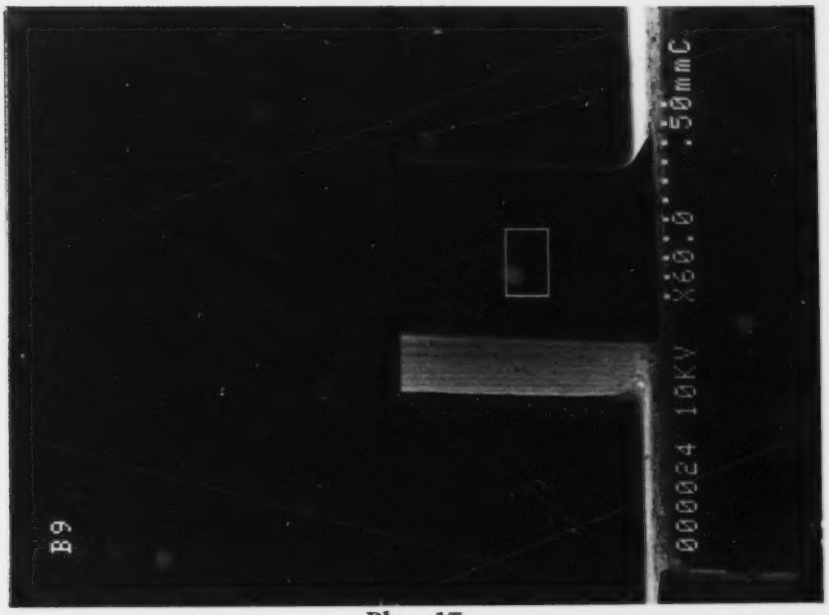

Plate 17
Micrograph of Dentaurum Stainless Steel Bracket Slot (B9)

Plate 18
Micrograph of Dentaurum Stainless Steel Bracket Base (B9)

B. Plates of Archwire Samples

The following is a complete photographic representation of all archwire samples utilized by this study. The plates illustrate a total of twelve archwire samples. A single photograph depicts each sample, with each photograph portraying two different views. The lower half of each frame is a low magnification portrayal of a large section of the archwire, to permit one's orientation to the surface in question. A smaller area in this frame delineated by white rectangular box represents the view that one sees in the upper half of the frame, at a corresponding increase in magnification. The letter-number combination in brackets, after the plate's caption, refers to the SEM identification code utilized to catalogue each sample archwire.

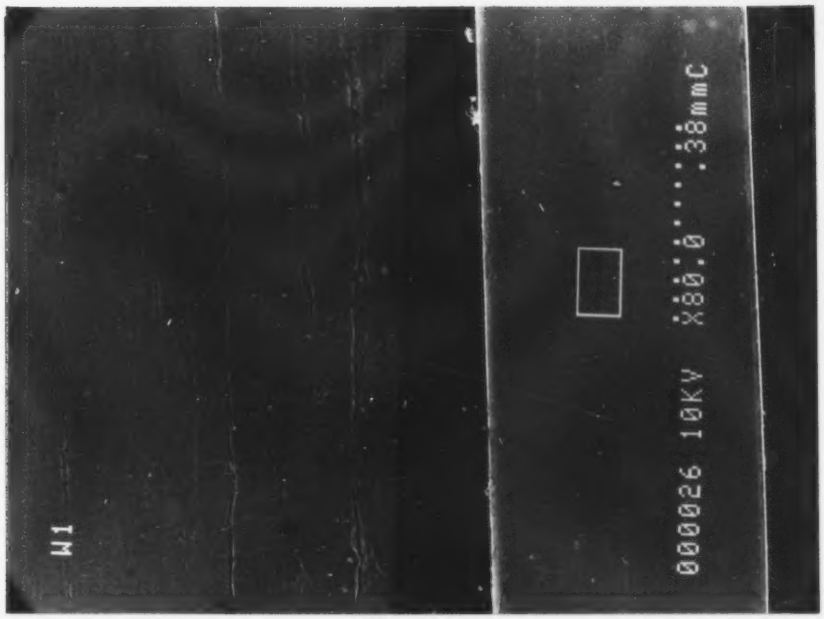

Plate 19
Micrograph of Cerum Stainless Steel Archwire Sample (W1)

Plate 20
Micrograph of Cerum Nickel Titanium Archwire Sample (W2)

Plate 21
Micrograph of Cerum Ortholoy Archwire Sample (W3)

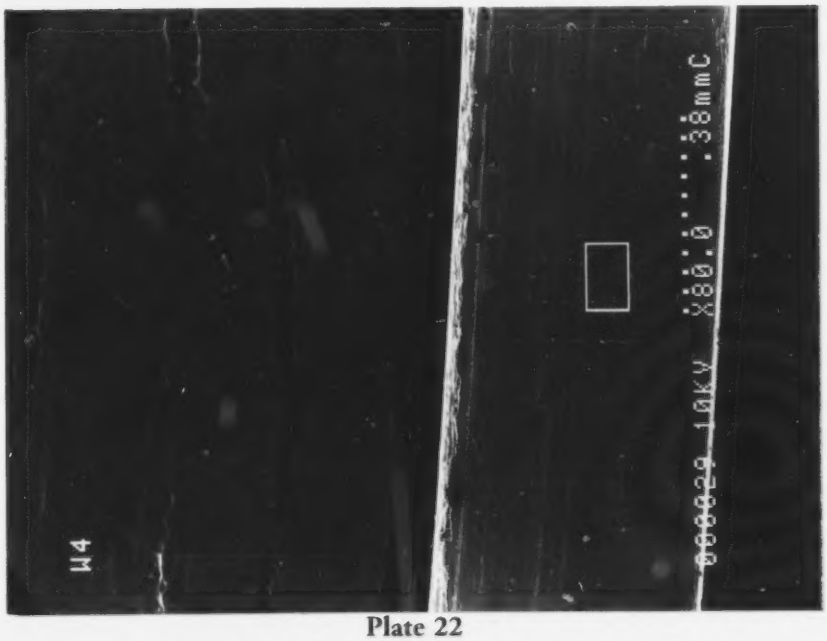

Plate 22
Micrograph of Ormco TMA Archwire Sample (W4)

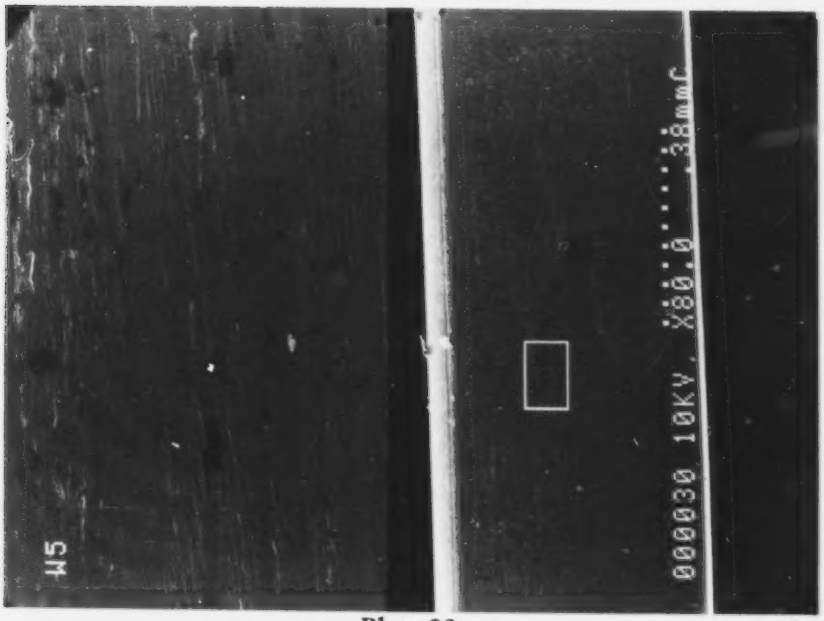

Plate 23
Micrograph of Ormco Stainless Steel Archwire Sample (W5)

Plate 24
Micrograph of Ormco Nickel Titanium Archwire Sample (W6)

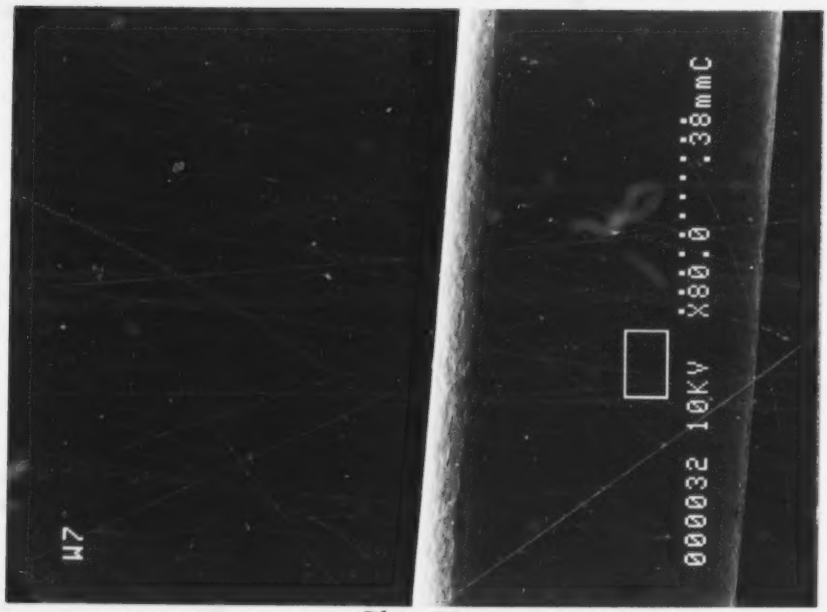

Plate 25
Micrograph of RMO Elgiloy Archwire Sample (W7)

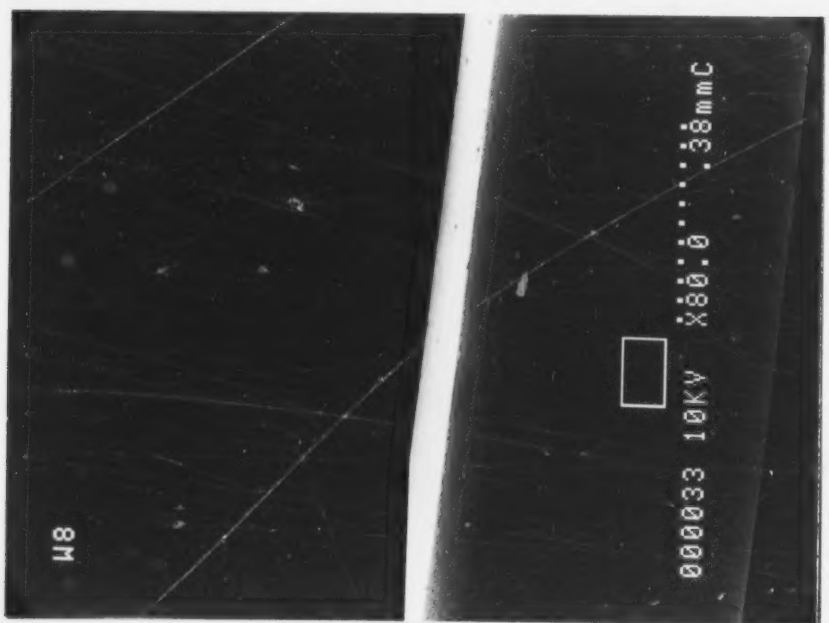

Plate 26
Micrograph of RMO Stainless Steel Archwire Sample (W8)

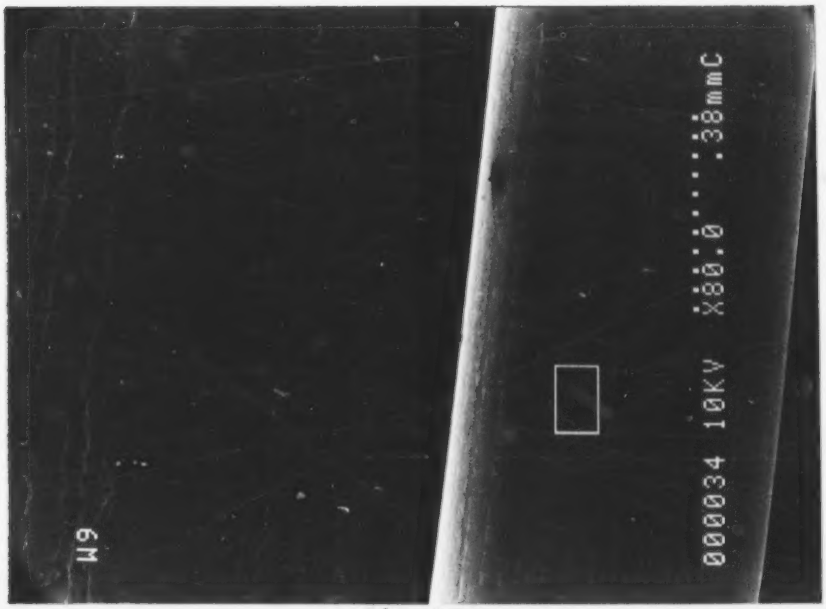

Plate 27
Micrograph of RMO Nickel Titanium Archwire Sample (W9)

Plate 28
Micrograph of A Company Nickel Titanium Archwire Sample (W10)

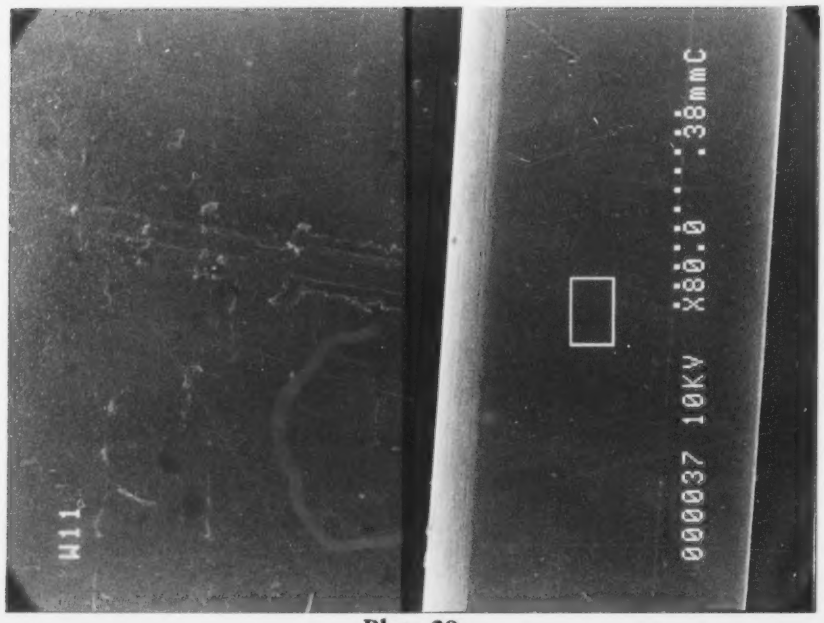

Plate 29
Micrograph of Dentaurum Stainless Steel Archwire Sample (W11)

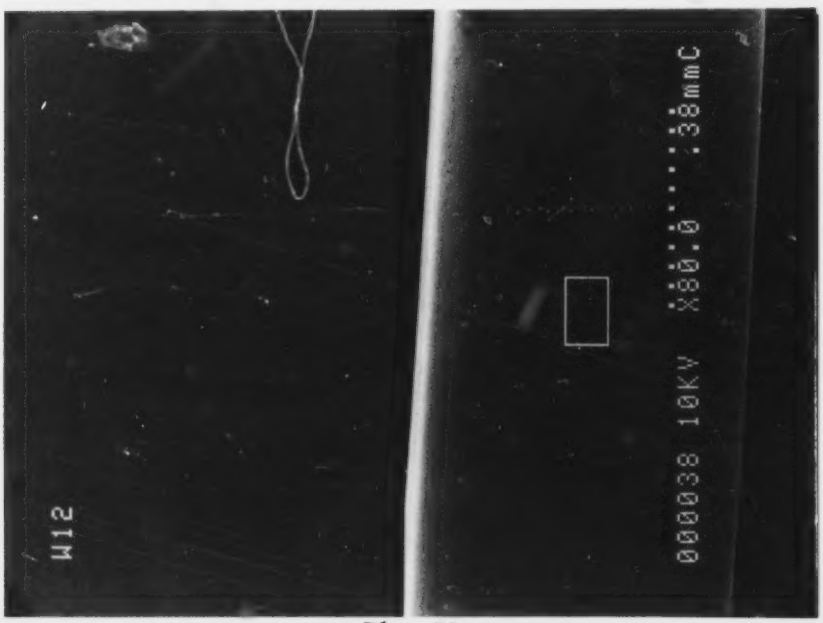

Plate 30
Micrograph of Dentaurum Nickel Titanium Archwire Sample (W12)

C. Plates of Testing Apparatus

The following is a photographic representation of the frictional coefficient testing apparatus. Plate 31 shows a high magnification view of the way the apparatus held an archwire sample against a bracket sample. Plate 32 shows the test stage and Plate 33 shows the electric motor-pulley system.

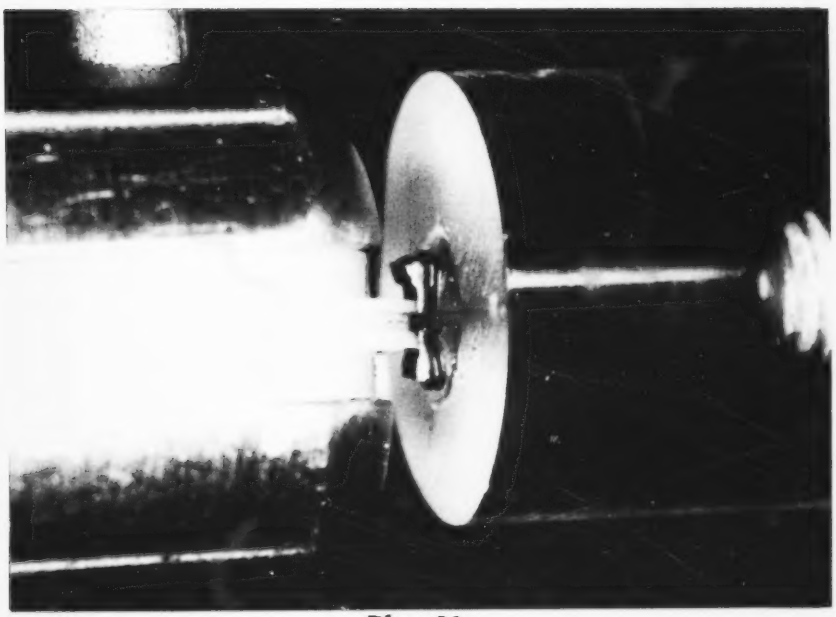

Plate 31
Photograph of Bracket and Archwire Sample Placement During Testing

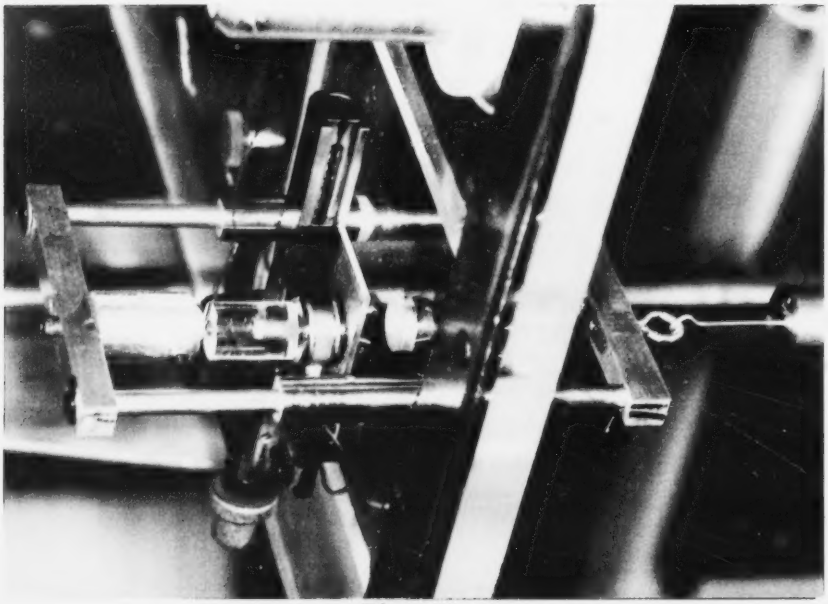

Plate 32
Photograph of Test Stage Utilized for Frictional Coefficient Testing

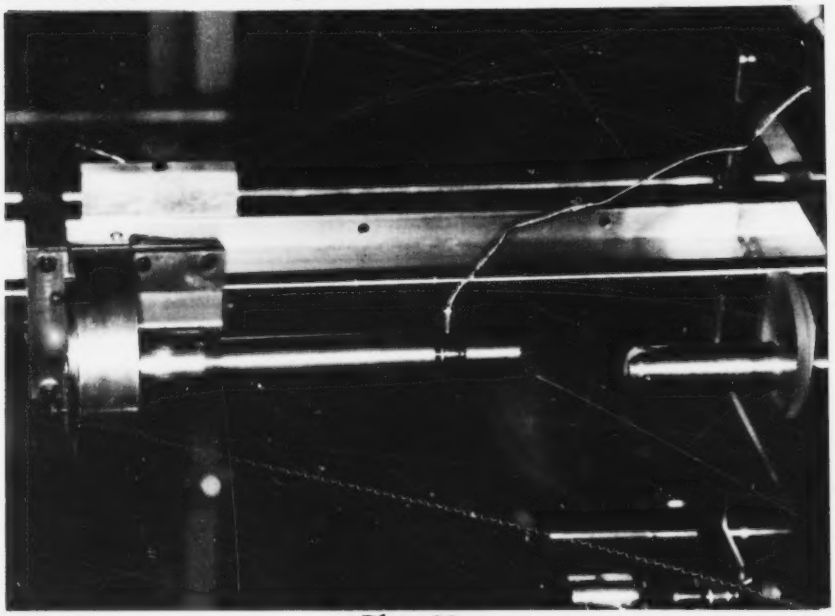

Plate 33
Photograph of Electric Motor-Pulley System Utilized for Frictional Coefficient Testing

Appendix C

Statistical Analysis

A. Results of Statistical Analysis

The following completes the statistical analysis of the remaining experimental data not covered in the Chapter 3. Statistical handling of the data demanded reducing the analyses to 29 individual statistical designs. Chapter 3 considered seven of these designs, and this Appendix appraises the balance, or the remaining 22 designs. Each design appears in the form of a boxplot, displayed in Figure C.1 to C.22. A tabular representation of the data in that design follows each boxplot. The statistical analysis pertaining to each design follows the table. The analysis for each design consists of a one-way analysis of variance, where the number of means in the design equals two. Designs with four or more samples, and associated means require a Student-Neuman-Keuls multiple comparison to determine statistical significance. As in Chapter 3, if the design merits complete disclosure of all pairwise comparisons, a matrix comparing all means follows the tabular data for that design. Again, an asterisk (*) indicates significantly different means. One-way ANOVA tables accompany designs with only two means. Designs that do not warrant complete disclosure have their results explained in text form.

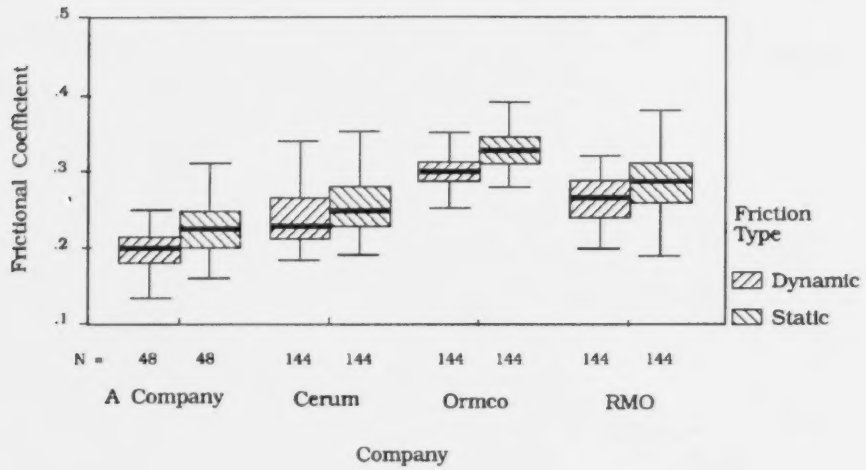

Figure C.1
Boxplot of Frictional Coefficient by Company by Type of Friction for Ceramic Bracket (flat wire, unlubricated)

Table C.1
Frequencies - Dynamic and Static Frictional Coefficients for Varying Companies (ceramic bracket, flat archwire, unlubricated)

	Company							
	A Co.		Cerum		Ormco		RMO	
	Dy	St	Dy	St	Dy	St	Dy	St
No.	48	48	144	144	144	144	144	144
Mean	.199	.225	.239	.255	.302	.328	.264	.288
Median	.200	.227	.230	.250	.300	.327	.267	.288
S.D.	.028	.034	.033	.032	.022	.026	.027	.038

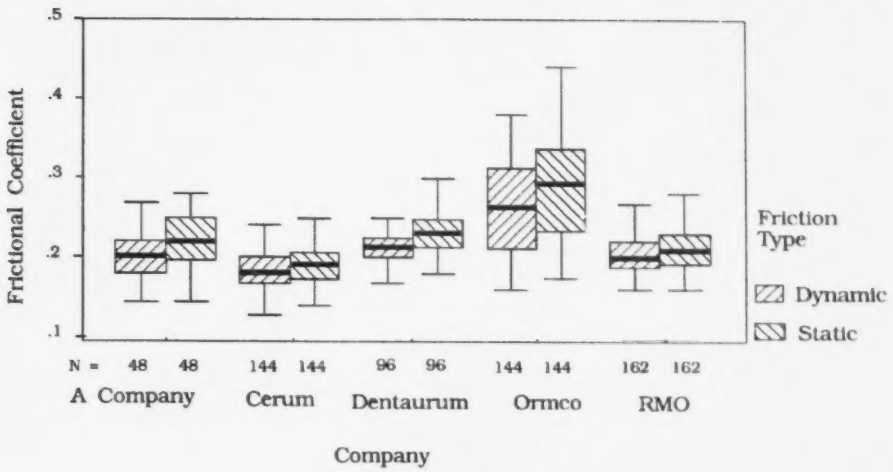

Figure C.2
Boxplot of Frictional Coefficients by Company by Type of Friction for Steel bracket (flat wire, unlubricated)

Table C.2
Frequencies - Dynamic and Static Frictional Coefficients for various Companies (Steel bracket, flat wire, unlubricated)

	Company									
	A Co.		Cerum		Dent.		Ormco		RMO	
	Dy	St	Dy	St	Dy	St	Dy	St	Dy	St
No.	48	48	144	144	96	96	144	144	162	162
Mean	.200	.220	.180	.191	.213	.231	.267	.291	.203	.213
Median	.200	.220	.181	.191	.213	.232	.264	.293	.200	.210
S.D.	.029	.034	.021	.026	.018	.026	.057	.064	.020	.026

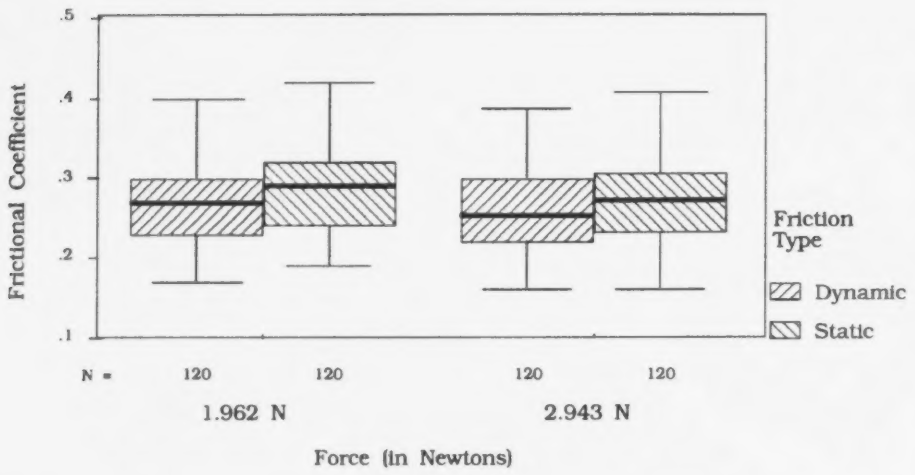

Figure C.3
Boxplot of Frictional Coefficient by Load by Type of Friction for Ceramic Bracket (flat wire, lubricated)

Table C.3
Frequencies - Dynamic and Static Frictional Coefficients under Varying Normal Forces (ceramic bracket, flat archwire, lubricated)

	Load			
	1.962 N		2.943 N	
	Dynamic	Static	Dynamic	Static
Number	120	120	120	120
Mean	.269	.289	.259	.277
Median	.270	.290	.253	.273
S.D.	.051	.055	.054	.056

Table C.4
SNK Multiple Comparisons of Frictional Coefficients for Varying Normal Force (ceramic bracket, flat wire, unlubricated)

		Dynamic		Static	
		1	3	1	3
Dynamic	1			*	
	3			*	*
Static	1	*	*		
	3		*		

Table C.5
SNK Multiple Comparisons of Frictional Coefficients for Varying Normal Force (steel bracket, flat wire, unlubricated)

		Dynamic		Static	
		1	3	1	3
Dynamic	1				
	3			*	
Static	1		*		
	3				

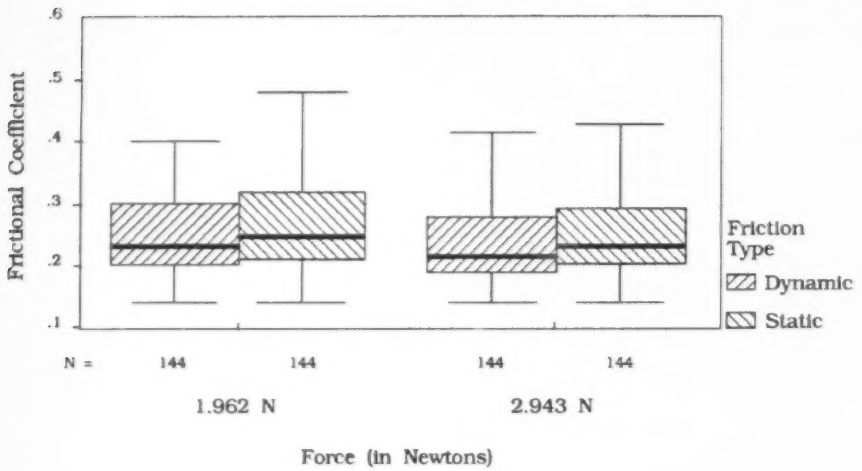

Figure C.4
Boxplot of Frictional Coefficient by Company by Type of Friction for Steel Bracket (flat wire, lubricated)

Table C.6
Frequencies - Dynamic and Static Frictional Coefficients under Varying Normal Forces (steel bracket, flat archwire, lubricated)

	Load			
	1.962 N		2.943 N	
	Dynamic	Static	Dynamic	Static
Number	144	144	144	144
Mean	.251	.264	.241	.254
Median	.230	.245	.213	.230
S.D.	.068	.074	.073	.074

A SNK multiple comparison of means in the design appearing in Figure C.1 shows a significant difference between static and dynamic frictional coefficients in all cases. Further, the comparison shows a significant difference when comparing the means associated with any one company to those of another. The SNK procedure for the design in Figure D.2 indicated a significant difference between static and dynamic frictional coefficients in all cases except for A Company.

The SNK analysis, explained by the matrix appearing in Table C.4 involves the design appearing in Figure C.3. It indicates no significant differences between the dynamic frictional coefficients at 1.962 N or at 2.943 N, and the static frictional coefficients at 1.962 N or at 2.943 N. The comparison indicates significant differences between the coefficient of static friction and the coefficient of dynamic friction, at each of the two normal forces.

The SNK analysis, defined by the matrix appearing in Table C.5 involves the design shown in Figure C.4. It indicates no significant differences between the dynamic frictional coefficients at 1.962 N or at 2.943 N, and the static frictional coefficients at 1.962 N or at 2.943 N. However, the comparison fails to show a significant difference between the static and dynamic frictional coefficients at either of the two normal forces.

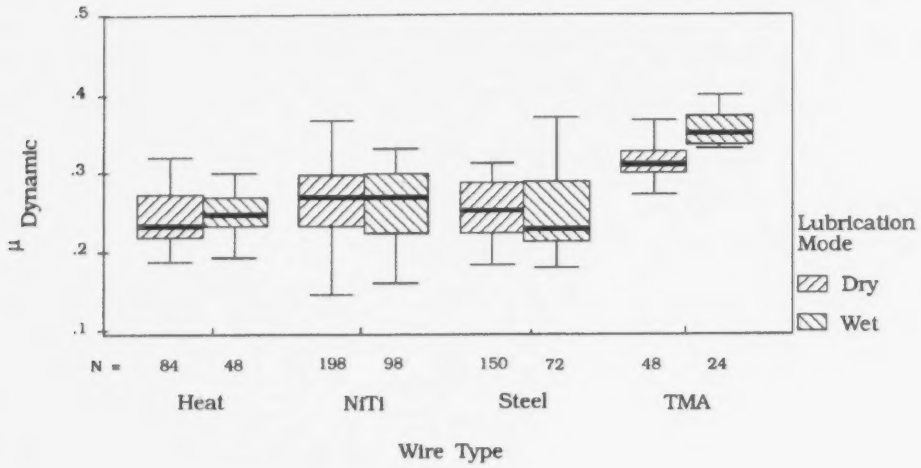

Figure C.5
Boxplot of Dynamic Frictional Coefficient by Wire Type by Lubrication for Ceramic Bracket (flat wire)

Table C.7
Frequencies - Dynamic Frictional Coefficients for Various Archwire Types, both Lubricated and Unlubricated (ceramic bracket, flat wire)

	Wire Type							
	Heat Treatable		NiTi		Steel		TMA	
	Dry	Wet	Dry	Wet	Dry	Wet	Dry	Wet
Number	84	48	198	96	150	72	48	24
Mean	.244	.250	.262	.259	.254	.249	.312	.358
Median	.233	.247	.270	.270	.243	.230	.310	.350
S.D.	.034	.024	.045	.046	.035	.050	.021	.022

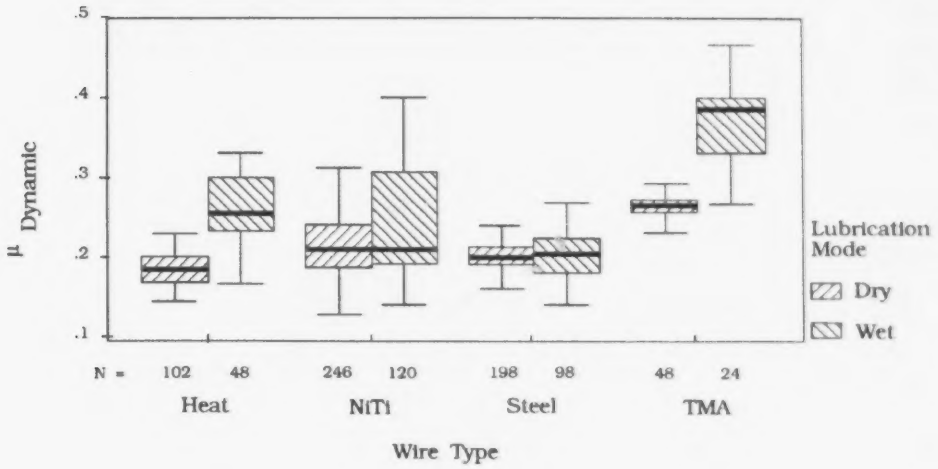

Figure C.6
Boxplot of Dynamic Frictional Coefficient by Wire Type by Lubrication for Steel Bracket (flat wire)

Table C.8
Frequencies - Dynamic Frictional Coefficients for Various Archwire Types, both Lubricated and Unlubricated (steel bracket flat wire)

	Wire Type							
	Heat Treatable		NiTi		Steel		TMA	
	Dry	Wet	Dry	Wet	Dry	Wet	Dry	Wet
Number	102	48	246	120	198	96	48	24
Mean	.183	.259	.226	.249	.203	.204	.266	.374
Median	.184	.255	.210	.210	.200	.203	.266	.385
S.D.	.020	.039	.058	.072	.020	.036	.017	.054

The SNK comparison concerning the design in Figure C.5 indicates no significant difference between dynamic frictional coefficients obtained with and without lubrication, for all archwire types except titanium molybdenum alloy archwire. The comparison of dynamic frictional coefficients with and without lubrication did indicate a significant difference with this archwire. The SNK comparison concerning the design in Figure C.6 indicates significant differences between dynamic frictional coefficients determined with and without lubrication for all archwire types except stainless steel. The comparison of dynamic frictional coefficients, both lubricated and unlubricated did not indicate a significant difference with this archwire. One can appreciate that, in all cases of significant differences in the two aforementioned designs, the addition of a lubricant tended to increase the observed frictional coefficient, over the unlubricated condition.

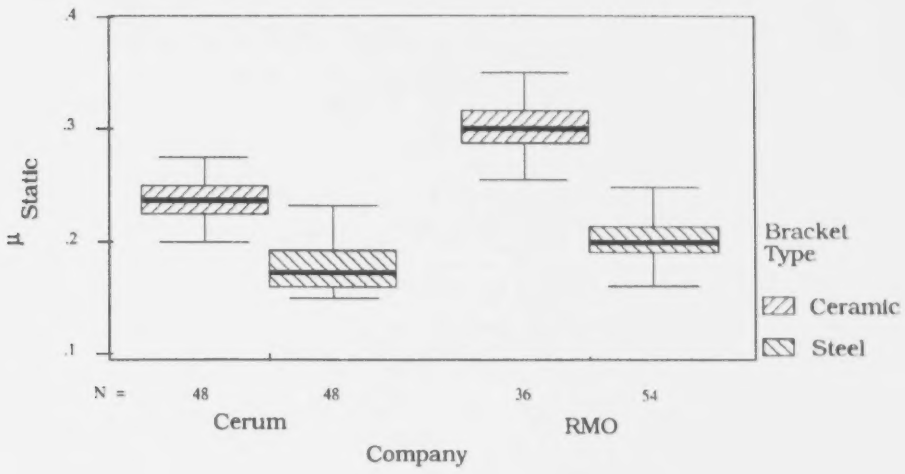

Figure C.7
Boxplot of Static Frictional Coefficient by Company by Bracket Type for Heat Treatable Flat Wire (unlubricated)

Table C.9
Frequencies - Static Frictional Coefficients for Heat Treatable Archwire on Varying Bracket Type (flat archwire, unlubricated)

	Company			
	Cerum		RMO	
	Ceramic Bracket	Steel Bracket	Ceramic Bracket	Steel Bracket
Number	48	48	36	54
Mean	.237	.181	.301	.204
Median	.237	.173	.300	.200
S.D.	.020	.025	.025	.022

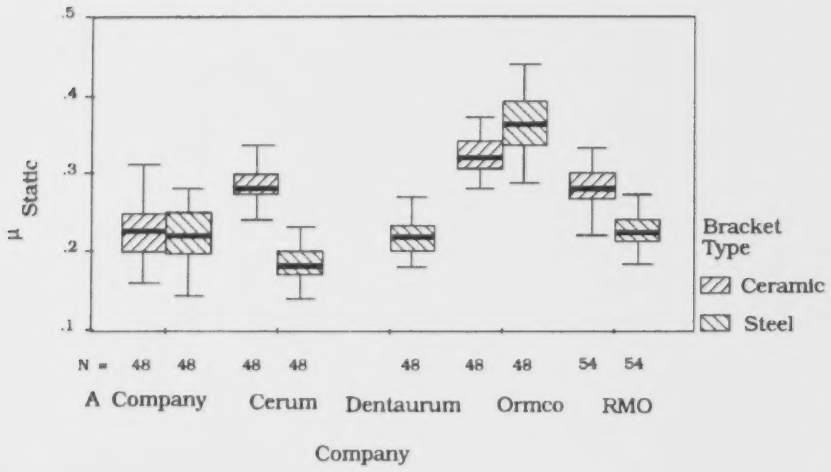

Figure C.8
Boxplot of Static Frictional Coefficients by Company by Bracket Type for NiTi Flat Wire (unlubricated)

Table C.10
Frequencies - Static Frictional Coefficients for NiTi Archwire on Varying Bracket Type (flat wire, unlubricated)

	Company								
	A Co.		Cerum		Dent.	Ormco		RMO	
	Cr.	SS.	Cr.	SS.	SS.	Cr.	SS.	Cr.	SS.
Number	48	48	48	48	48	48	48	54	54
Mean	.225	.220	.287	.185	.219	.320	.364	.285	.228
Median	.227	.220	.280	.182	.218	.327	.338	.280	.224
S.D.	.034	.034	.022	.021	.021	.030	.026	.038	.022

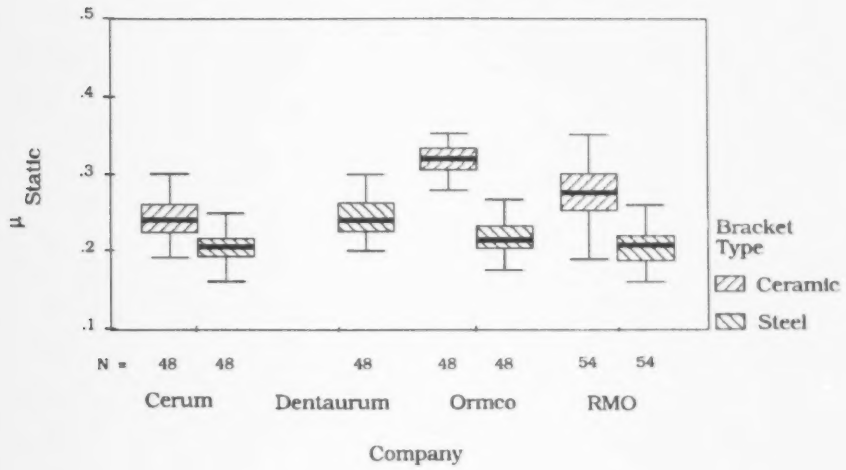

Figure C.9
Boxplot of Static Frictional Coefficients by Company by Bracket Type for Steel Flat Wire (unlubricated)

Table C.11
Frequencies - Static Frictional Coefficients for Steel Archwire on Varying Bracket Type (flat wire, unlubricated)

	Company						
	Cerum		Dentaurum	Ormco		RMO	
	Cr.	SS.	SS.	Cr.	SS.	Cr.	SS.
Number	48	48	48	48	48	54	54
Mean	.243	.208	.243	.321	.219	.282	.207
Median	.240	.207	.240	.320	.215	.277	.207
S.D.	.028	.024	.026	.019	.022	.043	.028

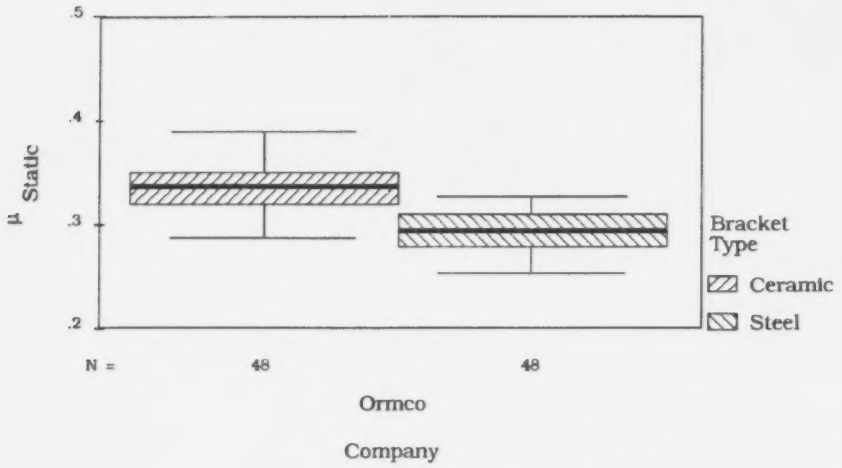

Figure C.10
Boxplot of Static Frictional Coefficient by Company by Bracket Type for TMA Flat Wire (unlubricated)

Table C.12
Frequencies - Static Frictional Coefficients for TMA Archwire on Varying Bracket Type (flat wire, unlubricated)

	Company	
	Ormco	
	Ceramic Bracket	Steel Bracket
Number	48	48
Mean	.338	.293
Median	.336	.295
S.D.	.026	.021

Table C.13
SNK Comparisons of Static Frictional Coefficients for Heat Treatable Archwire against Ceramic and Steel Brackets (flat wire, unlubricated)

		Cerum		RMO	
		Ceramic	Steel	Ceramic	Steel
Cerum	Ceramic		*	*	*
	Steel	*		*	*
RMO	Ceramic	*	*		*
	Steel	*	*	*	

Table C.14
SNK Comparison of Static Frictional Coefficients for NiTi Archwire against Ceramic and Steel Brackets (flat wire, unlubricated)

		Ceramic				Steel				
		A	C	O	R	A	C	D	O	R
Ceramic	A		*	*	*		*		*	
	C	*		*		*	*	*	*	*
	O	*	*		*	*	*	*	*	*
	R	*	*	*		*	*	*	*	*
Steel	A		*	*	*		*		*	
	C	*	*	*	*	*		*	*	*
	D		*	*	*		*		*	
	O	*	*	*	*	*	*	*		*
	R		*	*	*		*		*	

Table C.15
SNK Comparison of Static Frictional Coefficients for Steel Archwire against Ceramic and Steel Brackets (flat wire, unlubricated)

		Ceramic			Steel			
		C	O	R	C	D	O	R
Ceramic	C		*	*	*		*	*
	O	*		*	*	*	*	*
	R	*	*		*	*	*	*
Steel	C	*	*	*		*		
	D		*	*	*		*	*
	O	*	*	*		*		
	R	*	*	*		*		

Table C.16
One-way ANOVA Comparing Static Frictional Coefficients for TMA Archwire against Ceramic and Steel Brackets (flat wire, unlubricated)

Source of Variation	SS	DF	MS	F	Sig of F
between groups	.0485	1	.0485	87.8504	.0000
within groups	.0519	94	.0006		
total	.01004	95			

The SNK comparison matrix in Table C.13 pertains to the design in Figure C.7. The comparison indicates a significant difference between the static frictional coefficients obtained with ceramic brackets and those obtained with stainless steel brackets, for heat treatable archwire.

The SNK comparison matrix in Table C.14 concerns the design in Figure C.8. The comparison shows a significant difference between NiTi-ceramic bracket and Niti-stainless steel bracket static frictional coefficients, for all pairwise comparisons, except for A company. The comparison revealed no significant difference between ceramic and stainless steel brackets, with respect to these static frictional coefficients.

The SNK comparison matrix in Table C.15 concerns the design in Figure C.9. The comparison determined significant differences, for all pairwise associations, for static frictional coefficients derived from ceramic and stainless steel brackets with stainless steel archwires.

The one-way ANOVA table that appears in Table C.16 pertains to the design in Figure C.10. The results indicate a significant difference between the static frictional coefficients obtained with titanium molybdenum alloy archwire against ceramic and stainless steel brackets.

The SNK comparisons for the designs in Figure C.11 and in Figure C.12 indicate no significant differences between the static frictional coefficient obtained with a flat archwire and that obtained with a round archwire. The lack of a significant difference existed with both nickel titanium and stainless steel archwires.

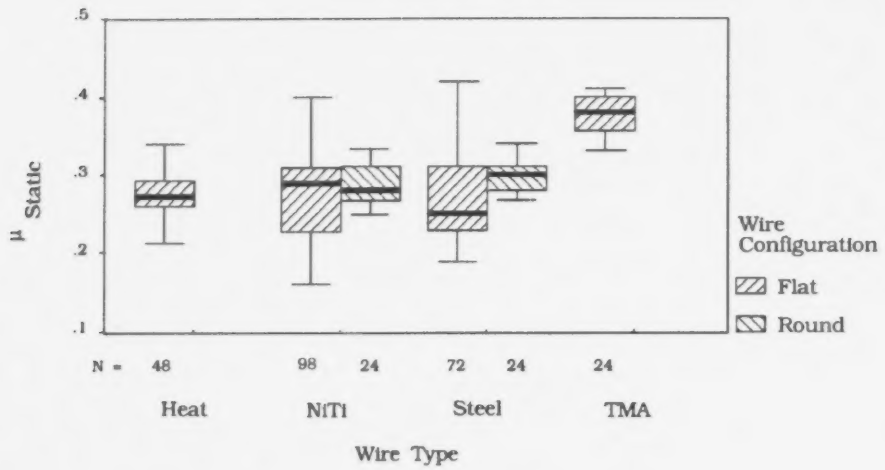

Figure C.11
Boxplot of Static Frictional Coefficient by Wire Type by Wire Configuration for Ceramic Bracket (lubricated)

Table C.17
Frequencies - Static Frictional Coefficients for Various Archwire Types and Configurations (ceramic bracket, lubricated)

	Wire Type					
	Heat Treatable	Nickel Titanium		Stainless Steel		TMA
	Flat	Flat	Round	Flat	Round	Flat
Number	48	96	24	72	24	24
Mean	.273	.272	.285	.272	.295	.377
Median	.273	.288	.280	.252	.300	.380
S.D.	.033	.049	.027	.055	.023	.024

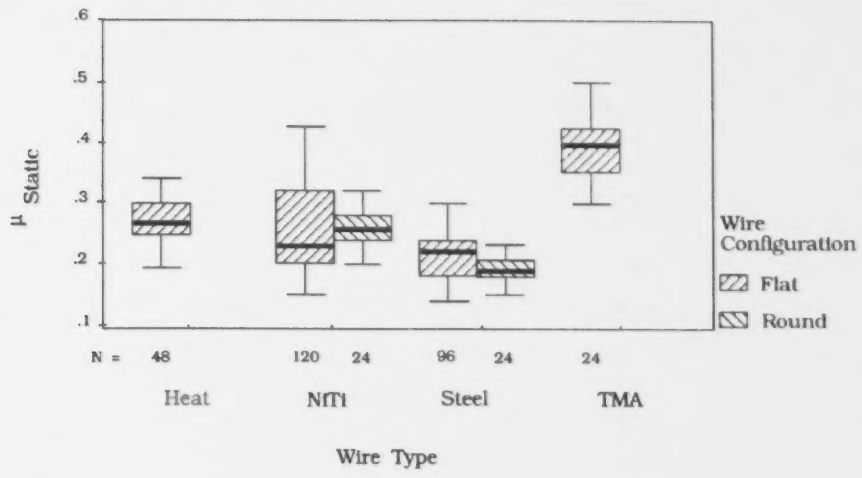

Figure C.12
Boxplot of Static Frictional Coefficient by Wire Type by Wire Configuration for Steel Bracket (lubricated)

Table C.18
Frequencies - Static Frictional Coefficients for Various Archwire types and Configurations (steel bracket, lubricated)

	Wire Type					
	Heat Treatable	Nickel Titanium		Stainless Steel		TMA
	Flat	Flat	Round	Flat	Round	Flat
Number	48	120	24	96	24	24
Mean	.269	.262	.259	.217	.194	.377
Median	.267	.230	.257	.220	.188	.380
S.D.	.039	.075	.031	.042	.029	.024

The final group of experimental designs (C.13-C.22) concern comparisons of five individual company's archwires and brackets. The designs compare static frictional coefficients obtained with each archwire type against ceramic and against stainless steel brackets. These comparisons occur under lubricated and unlubricated conditions. Generally, all of these results appear elsewhere in this thesis, in slightly modified forms. Nonetheless, one may draw some widespread inferences from these comparisons. First, one sees that the frictional coefficients associated with ceramic brackets are often greater than those associated with stainless steel brackets. Second, one appreciates that titanium molybdenum alloy archwires present the highest frictional coefficients and heat treatable the lowest with stainless steel and NiTi archwires presenting intermediate values. Finally, the effect of the lubricant used on the measured frictional coefficients defies simplistic prediction.

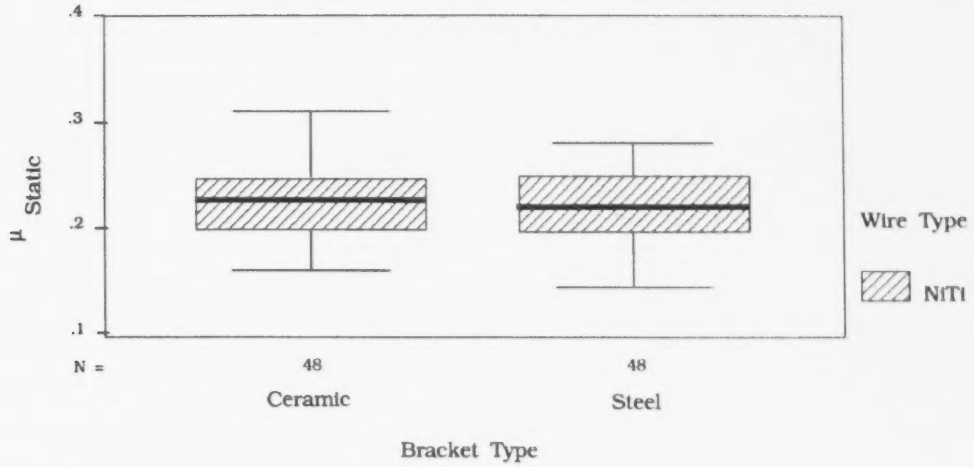

Figure C.13
Boxplot of Static Frictional Coefficient by Bracket Type by Wire Type for A Company (flat wire, unlubricated)

Table C.19
Frequencies - Static Frictional Coefficients for NiTi Archwire against Ceramic and Steel Brackets (flat wire, unlubricated)

	Wire Type	
	Nickel Titanium	
	Ceramic Bracket	Steel Bracket
Number	48	48
Mean	.225	.220
Median	.227	.220
S.D.	.034	.034

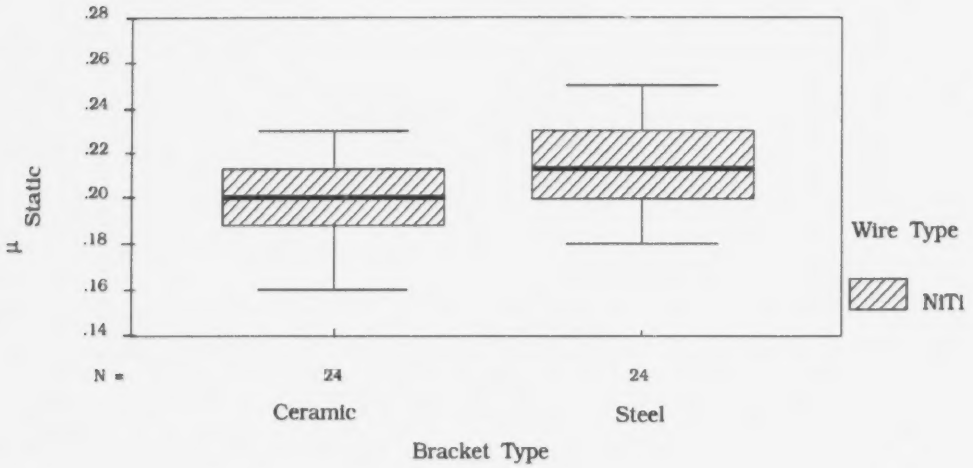

Figure C.14
Boxplot of Static Frictional Coefficient by Bracket Type by Wire Type for A Company (flat wire, lubricated)

Table C.20
Frequencies - Static Frictional Coefficients for NiTi Archwire against Ceramic and Steel Brackets (flat wire, lubricated)

	Wire Type	
	Nickel Titanium	
	Ceramic Bracket	Steel Bracket
Number	24	24
Mean	.203	.216
Median	.200	.213
S.D.	.021	.018

Table C.21
One-way ANOVA of Static Frictional Coefficients for NiTi Archwire against A Company Ceramic and Steel Bracket ((flat wire, unlubricated)

Source of Variation	SS	DF	MS	F	Sig of F
between groups	.0005	1	.0005	.4416	.5058
within groups	.1108	94	.0012		
total	.1113	95			

Table C.22
One-way ANOVA of Static Frictional Coefficients for Niti Archwire against A Company Ceramic and Steel Bracket (flat wire, lubricated)

Source of Variation	SS	DF	MS	F	Sig of F
between groups	.0020	1	.0020	5.0567	.0294
within groups	.0182	46	.0004		
total	.0202	47			

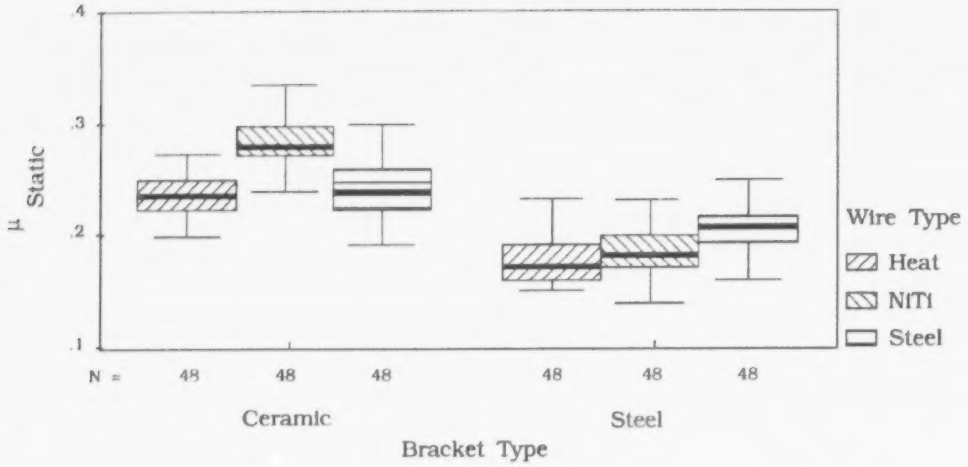

Figure C.15
Boxplot of Static Frictional Coefficient by Bracket Type by Wire Type for Cerum (flat wire, unlubricated)

Table C.23
Frequencies - Static Frictional Coefficients for Various Archwires against Ceramic and Steel Bracket (Cerum, flat wire, unlubricated)

	Bracket Type					
	Ceramic			Stainless Steel		
	Heat	NiTi	Steel	Heat	NiTi	Steel
Number	48	48	48	48	48	48
Mean	.237	.287	.243	.181	.185	.208
Median	.237	.280	.240	.173	.182	.207
S.D.	.020	.022	.028	.025	.021	.024

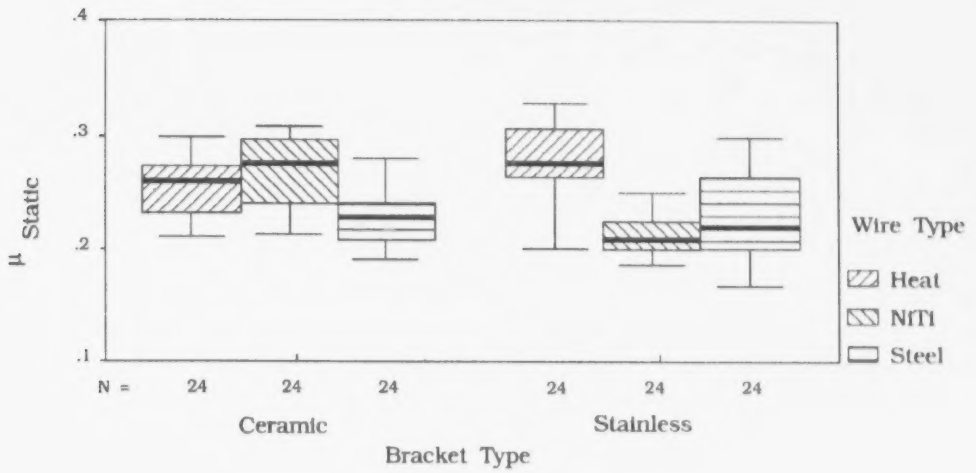

Figure C.16
Boxplot of Static Frictional Coefficient by Bracket Type by Wire Type for Cerum (flat wire, lubricated)

Table C.24
Frequencies - Static Frictional Coefficients for Various Archwires Against Ceramic and Steel Brackets (Cerum, flat wire, lubricated)

	Bracket Type					
	Ceramic			Stainless Steel		
	Heat	NiTi	Steel	Heat	NiTi	Steel
Number	24	24	24	24	24	24
Mean	.258	.268	.227	.281	.214	.224
Median	.260	.277	.228	.277	.208	.220
S.D.	.037	.030	.023	.033	.022	.039

Table C.25
SNK Comparison of Frictional Coefficients for Various Archwires against Ceramic and Steel Brackets (Cerum, flat wire, unlubricated)

		Ceramic			Steel		
		Heat	NiTi	Steel	Heat	NiTi	Steel
Ceramic	Heat		*		*	*	*
	NiTi	*		*	*	*	*
	Steel		*		*	*	*
Steel	Heat	*	*	*			*
	NiTi	*	*	*			*
	Steel	*	*	*	*	*	

Table C.26
SNK Comparisons of Static Frictional Coefficients for Various Archwires against Ceramic and Steel Brackets (Cerum, flat wire, lubricated)

		Ceramic			Steel		
		Heat	NiTi	Steel	Heat	NiTi	Steel
Ceramic	Heat			*	*	*	*
	NiTi			*		*	*
	Steel	*	*		*		
Steel	Heat	*		*		*	*
	NiTi	*	*		*		
	Steel	*	*		*		

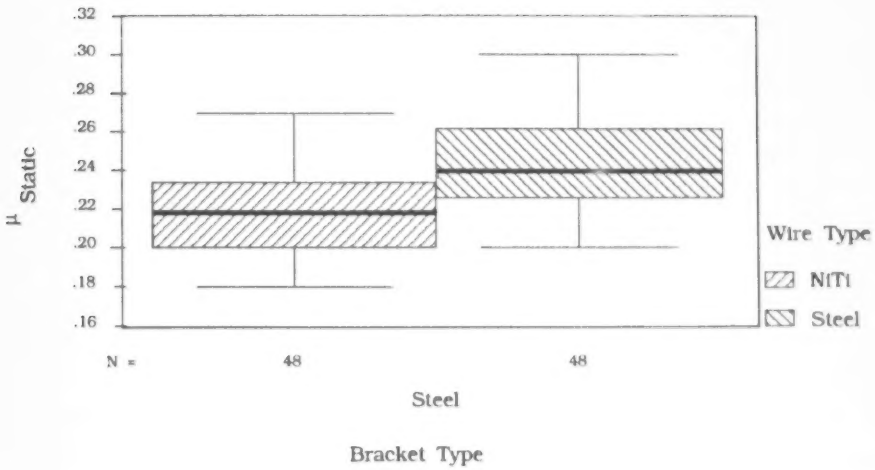

Figure C.17
Boxplot of Static Frictional Coefficient by Bracket Type by Wire Type for Dentaurum (flat wire, unlubricated)

Table C.27
Frequencies - Static Frictional Coefficients for Various Archwires against Steel Bracket (Dentaurum, flat wire, unlubricated)

	Bracket Type	
	Steel	
	NiTi Wire	Steel Wire
Number	48	48
Mean	.219	.243
Median	.218	.240
S.D.	.021	.026

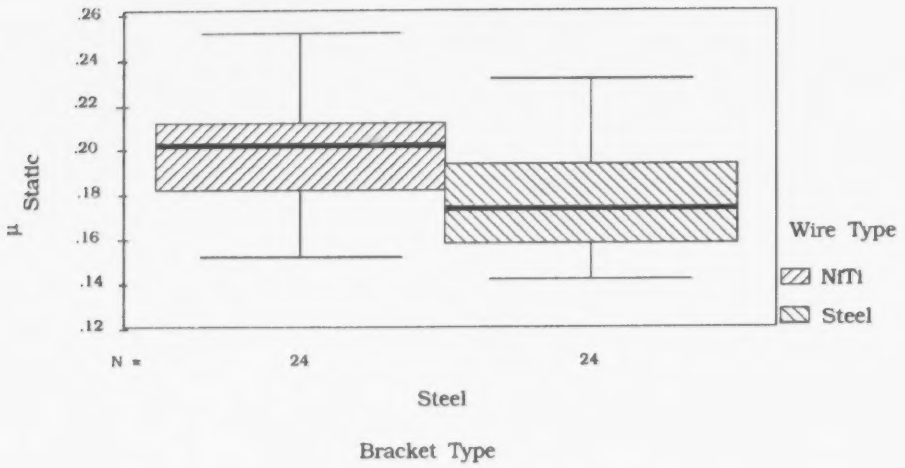

Figure C.18
Boxplot of Static Frictional Coefficient by Bracket Type by Wire Type for Dentaurum (flat wire, lubricated)

Table C.28
Frequencies - Static Frictional Coefficients for Various Archwires against Steel Bracket (Dentaurum, flat wire, lubricated)

	Bracket Type	
	Steel	
	NiTi Wire	Steel Wire
Number	48	48
Mean	.196	.175
Median	.200	.172
S.D.	.025	.024

Table C.29
One-way ANOVA of Static Frictional Coefficients for Dentaurum Steel Bracket against Steel and NiTi Archwires (flat wire, unlubricated)

Source of Variation	SS	DF	MS	F	Sig of F
between groups	.0136	1	.0136	24.6787	.0000
within groups	.0519	94	.0006		
total	.0656	95			

Table C.30
One-way ANOVA of Static Frictional Coefficients for Dentaurum Steel Bracket against NiTi and Steel Archwires (flat wire, lubricated)

Source of Variation	SS	DF	MS	F	Sig of F
between groups	.0053	1	.0053	8.9286	.0045
within groups	.0272	46	.0006		
total	.0325	47			

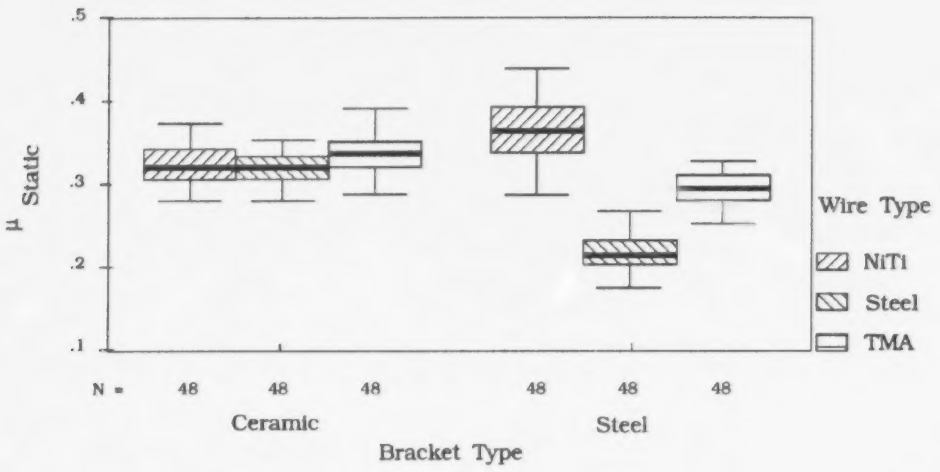

Figure C.19
Boxplot of Static Frictional Coefficient by Bracket Type by Wire Type for Ormco (flat wire, unlubricated)

Table C.31
Frequencies - Static Frictional Coefficients for Various Archwires against Ceramic and Steel Brackets (Ormco, flat wire, unlubricated)

	Bracket Type					
	Ceramic			Stainless Steel		
	NiTi	Steel	TMA	NiTi	Steel	TMA
Number	48	48	48	48	48	48
Mean	.327	.321	.338	.362	.219	.293
Median	.320	.320	.336	.364	.215	.295
S.D.	.030	.019	.026	.034	.022	.021

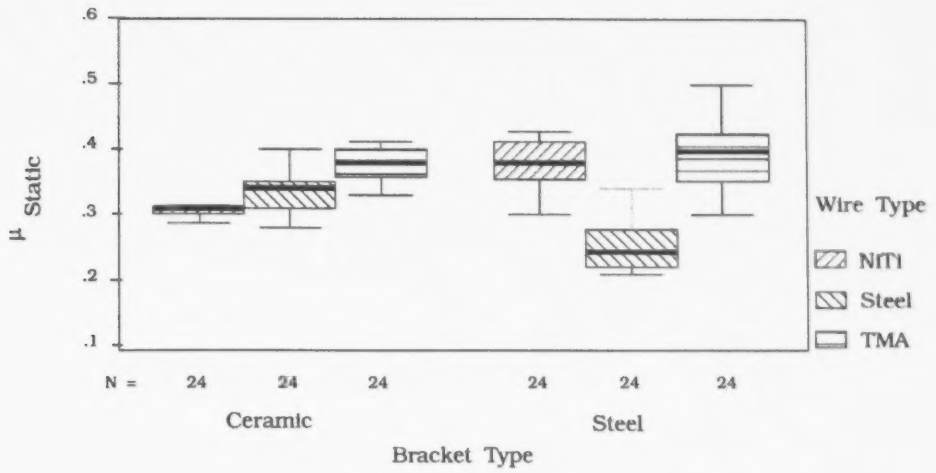

Figure C.20
Boxplot of Static Frictional Coefficient by Bracket Type by Wire Type for Ormco (flat wire, lubricated)

Table C.32
Frequencies - Static Frictional Coefficients for Various Archwire Types against Ceramic and Steel Brackets (Ormco, flat wire, lubricated)

	Bracket Type					
	Ceramic			Stainless Steel		
	NiTi	Steel	TMA	NiTi	Steel	TMA
Number	24	24	24	24	24	24
Mean	.307	.339	.377	.377	.254	.394
Median	.308	.340	.380	.380	.243	.397
S.D.	.016	.036	.024	.035	.036	.053

Table C.33
SNK Comparisons of Frictional Coefficients for Various Archwires against Ceramic and Steel Brackets (Ormco, flat wire, unlubricated)

		Ceramic			Steel		
		NiTi	Steel	TMA	NiTi	Steel	TMA
Ceramic	NiTi			*	*	*	*
	Steel			*	*	*	*
	TMA	*	*		*	*	*
Steel	NiTi	*	*	*		*	*
	Steel	*	*	*	*		*
	TMA	*	*	*	*	*	

Table C.34
SNK Comparison of Static Frictional Coefficients for Ormco Archwires against Ceramic and Steel Brackets (flat wire, lubricated)

		Ceramic			Steel		
		NiTi	Steel	TMA	NiTi	Steel	TMA
Ceramic	NiTi		*	*	*	*	*
	Steel	*		*	*	*	*
	TMA	*	*			*	
Steel	NiTi	*	*			*	
	Steel	*	*	*	*		*
	TMA	*	*			*	

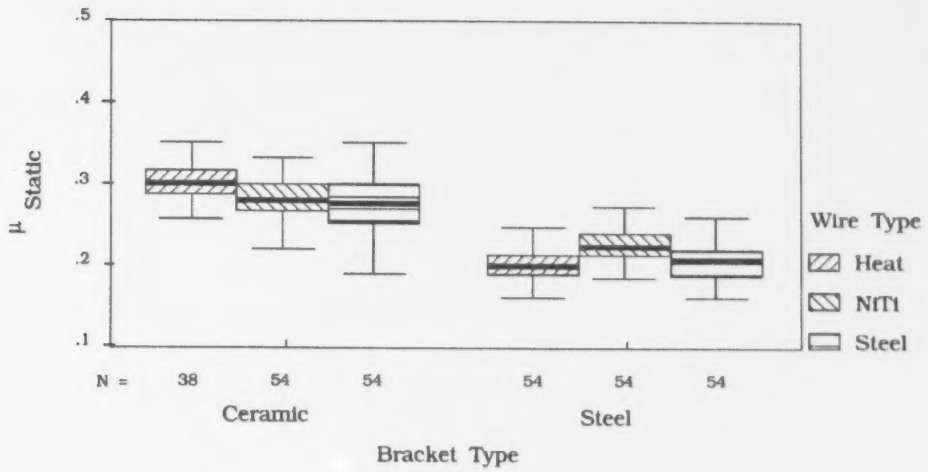

Figure C.21
Boxplot of Static Frictional Coefficient by Bracket Type by Wire Type for RMO (flat wire, unlubricated)

Table C.35
Frequencies - Static Frictional Coefficients for Various Archwire Types against Ceramic and Steel Brackets (RMO, flat wire, unlubricated)

	Bracket Type					
	Ceramic			Stainless Steel		
	Heat	NiTi	Steel	Heat	NiTi	Steel
Number	36	54	54	54	54	54
Mean	.301	.285	.282	.204	.228	.207
Median	.300	.280	.277	.200	.224	.207
S.D.	.025	.038	.043	.022	.022	.028

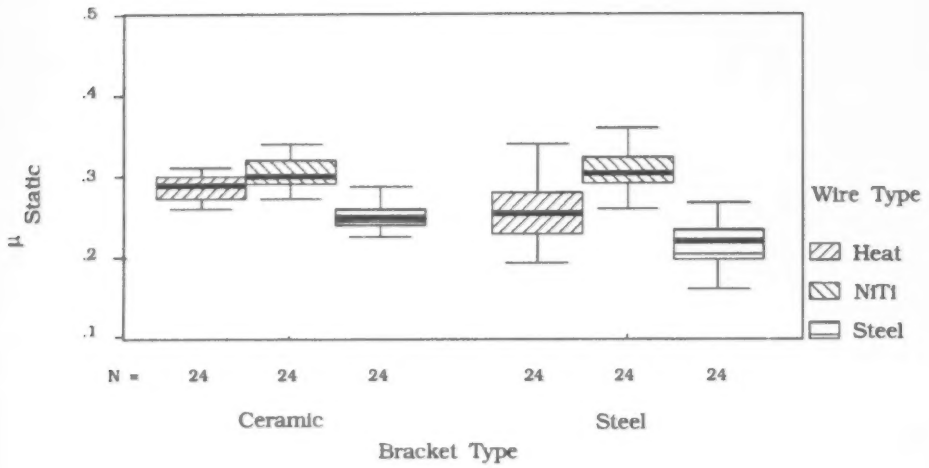

Figure C.22
Boxplot of Static Frictional Coefficient by Bracket Type by Wire Type for RMO (flat wire, lubricated)

Table C.36
Frequencies - Static Frictional Coefficients for Various Archwire Types against Ceramic and Steel Brackets (RMO, flat wire, lubricated)

	Bracket Type					
	Ceramic			Stainless Steel		
	Heat	NiTi	Steel	Heat	NiTi	Steel
Number	24	24	24	24	24	24
Mean	.288	.310	.252	.257	.306	.213
Median	.288	.300	.250	.255	.303	.220
S.D.	.019	.026	.017	.041	.034	.027

Table C.37
SNK Comparisons of Static Frictional Coefficients for RMO Archwires against Ceramic and Steel Brackets (flat wire, unlubricated)

		Ceramic			Steel		
		Heat	NiTi	Steel	Heat	NiTi	Steel
Ceramic	Heat		*	*	*	*	*
	NiTi	*			*	*	*
	Steel	*			*	*	*
Steel	Heat	*	*	*		*	
	NiTi	*	*	*	*		*
	Steel	*	*	*		*	

Table C.38
SNK Comparisons of Static Frictional Coefficients for RMO Archwires against Ceramic and Steel Brackets (flat wire, lubricated)

		Ceramic			Steel		
		Heat	NiTi	Steel	Heat	NiTi	Steel
Ceramic	Heat		*	*	*	*	*
	NiTi	*		*	*		*
	Steel	*	*			*	*
Steel	Heat	*	*			*	*
	NiTi	*		*	*		*
	Steel	*	*	*	*	*	

Appendix D

Frictional Force Calculation

One may expect a hypothetical orthodontic premolar extraction situation to appear as shown in Figure D.1. Prior to a force application, one may envision negligible contact between the archwire and the bracket wings. An applied force intending to produce distal translation of the canine, as indicated by the arrow in Figure D.1, will initially produce some distal crown tip of the canine. This will occur until the archwire reaches maximum contact with the wings of the bracket (Figure D.2). The frictional force also reaches its maximum degree at this position. The following calculations describe this hypothetical situation, and profess to determine the frictional force of archwire against bracket. These calculations have, as their basis, the following assumptions: a stainless steel bracket, a 0.020" round stainless steel archwire, and a value of $E = 28.6 \times 10^6$ lb/in^2 (Young's modulus for stainless steel). The

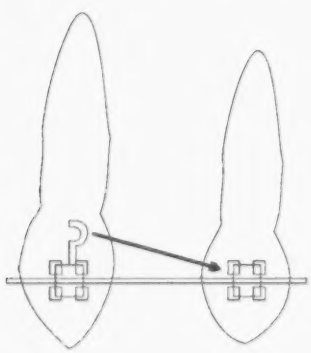

Figure D.1
Situation Before Force Application
in the Case of Premolar Extraction

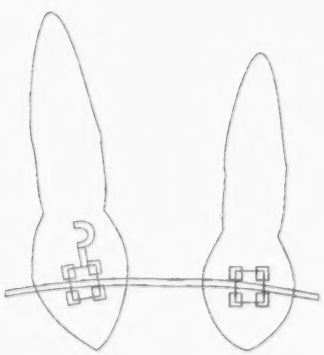

Figure D.2
Situation After Force Application
in the case of Premolar Extraction

calculations neglect the force of friction encountered through archwire-ligature contact, due to the complexity of this interaction.

Once the canine has tipped, the resulting forces produce a moment acting on the canine bracket, a moment acting on the premolar bracket, and a slight deflection of the archwire between the two brackets. This deflection takes the form of a superior bowing of the wire, as shown in Figure D.3. One may consider the arc of curvature as a chord, for the purposes of calculation. In this example, M represents each of the two moments and D indicates the amount of archwire deflection. C represents the width of the chord, or that distance between brackets across the extraction site, and R indicates the radius of the chord. The symbol θ represents the angle formed by the chord. One may express the radius of the chord as follows:

$$R - R\cos\theta = D \qquad (1)$$

Rearranging this expression, one sees:

$$R\cos\theta = R - D \qquad (2)$$

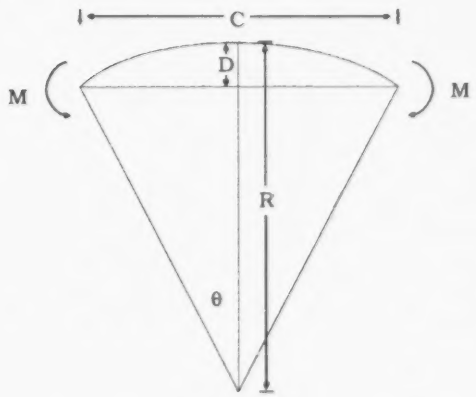

Figure D.3
Schematic Diagram of Archwire Behaviour
During Canine Retraction

One may now square all elements of this equation to yield the following:

$$R^2\cos^2\theta = (R - D)^2 \quad (3)$$

Using elementary trigonometry, one may express dimensions of the chord as follows:

$$\frac{C}{2} = R\sin\theta \quad (4)$$

Squaring all terms of this expression produces:

$$\left(\frac{C}{2}\right)^2 = R^2\sin^2\theta \quad (5)$$

Since one may relate sine and cosine as follows

$$\sin^2\theta + \cos^2\theta = 1 \quad (6)$$

adding equations (3) and (5) produces:

$$(R - D)^2 + \left(\frac{C}{2}\right)^2 = R^2 \quad (7)$$

Expanding the quadratic term of this equation yields

$$R^2 - 2DR + D^2 + \left(\frac{C}{2}\right)^2 = R^2 \quad (8)$$

and clearing the R^2 term nets the following expression:

$$2DR = D^2 + \left(\frac{C}{2}\right)^2 \quad (9)$$

Expressing this in terms of R alone leaves:

$$R = \frac{1}{2}D\left[D^2 + \left(\frac{C}{2}\right)^2\right] \quad (10)$$

One may express the moment, M as follows:

$$M = \frac{EI}{R} \qquad (11)$$

where E indicates Young's modulus for the material and R is the radius of the chord, given by (10), in this example. The following expression produces the term, I, the second moment of area of the cross section about a diameter:

$$I_{xx} = \frac{\pi r^4}{4} \qquad (12)$$

where r indicates the radius of a cross section of the material in question, as indicated in Figure D.4. Substituting this expression for the term I produces the following:

$$M = E\left(\frac{\pi r^4}{4R}\right) \qquad (13)$$

Now, from Figure D.1, an expression exists for R, and M. One may measure the value for C directly, and this example used a value of 14 mm. The use of a suitably prepared typodont, with 0.020" stainless steel archwire material and simulated retraction forces produced a value for D of 0.15 mm. With this information, one may calculate the value for R in this example, as follows:

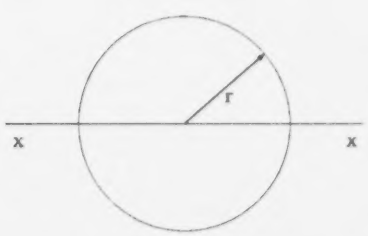

Figure D.4
Cross-section of Hypothetical
Archwire Material

$$R = \frac{1}{2(0.15)}\left[(0.15)^2 + \left(\frac{14}{2}\right)^2\right] \qquad (14)$$

This expression produces a value of 163.4 mm for R. Since other constants in these calculations are in Imperial units, the equivalent value for R is 6.433 inches. Substituting this value into the expression for M, and using Young's modulus for stainless steel, one sees:

$$M = \frac{28.6 \times 10^6 (\pi)(0.01)^4}{4\ (6.433)} \qquad (15)$$

The value for M is 3.49×10^{-2} inch-pounds. Since a moment is the product of a force and a distance, one must divide by the distance in question. Figure D.5 illustrates the situation at the level of the bracket. The distance is approximately 3 mm, so the expression for M would be

$$M = N \times \frac{3}{25.4} \qquad (16)$$

where N represents the normal force, or the force exerted on the archwire by the bracket wing, at each end of the bracket. Again, the expression introduces the value 25.4 (mm/inch) to convert to Imperial measure.

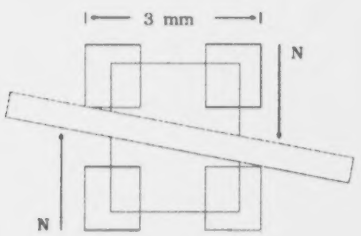

Figure D.5
Forces Experienced by a Bracket During Simulated Canine Retraction

$$N = \frac{3.49 \times 10^{-2}}{\frac{3}{25.4}} \qquad (17)$$

This expression yields a value for N of 0.295 pounds, or 134 grams. In the present example, the following expression gives the frictional force resulting from the sliding of a bracket along the archwire:

$$F_{Friction} = 2\mu N \qquad (18)$$

where μ is the coefficient of friction for stainless steel archwire material on a stainless steel bracket. Experimental data presented in Chapter 3 indicates this value is 0.219, for static friction and without lubrication. Substituting this value into (18) produces:

$$F_{Friction} = 2(0.219)(134) \qquad (19)$$

The value obtained for $F_{Friction}$ is 58.8 grams (0.577 N). One may expect, in the present example, approximately 58.8 grams (0.577 N) of an applied retraction force to be lost to frictional interactions between the bracket and archwire. One may execute these same calculations for various combinations of archwires and brackets. Some results appear in Table 4.1.